EFFECTS OF DOPING ON BEHAVIOUR OF SOL-GEL ENTRAPPED PROTEINS

THE EFFECTS OF DOPING ON THE BEHAVIOR OF SOL-GEL ENTRAPPED PROTEINS

By

MAKEDONKA DONNA GULCEV, B.Sc.

A Thesis

Submitted to the School of Graduate Studies

in Partial Fulfilment of the Requirements

for the Degree

Master of Science

McMaster University

MASTER OF SCIENCE (2003) McMaster University
(Chemistry) Hamilton, Ontario

Title: The Effects of Doping on the Behavior of Sol-gel Entrapped Proteins

Author: Makedonka Donna Gulcev, B.Sc. (McMaster University)

Supervisor: Dr. John D. Brennan

Number of Pages: xiii, 175

Abstract

Research in the field of sol-gel derived materials has evolved dramatically over the past forty years. The developments in the past decade, in the field of bioanalytical chemistry, have revolutionized this field. Early research, as well as that done by our group, has confirmed that the commonly used alkoxysilane precursors (tetraethylorthosilicate – TEOS or tetramethylorthosilicate – TMOS) are not ideal for entrapment of biomolecules. They produce materials that are brittle, often undergo cracking due to hydration stresses and in some cases, can block the accessibility of the analyte to the entrapped biomolecules. My research project therefore focuses on the development of new sol-gel processing methods through the use of an additive – glycerol, which will produce new "second generation" glasses. I have focused on obtaining a basic understanding of glycerol-doped sol-gel derived materials and the effect they have on the entrapped biomolecules. Glycerol-doped sol-gel materials display larger pore size, decreased shrinkage and cracking as compared to the TEOS-based materials. Biocatalysts entrapped in glycerol-doped materials showed significantly smaller decreases in activity over a period of one month relative to enzyme entrapped in TEOS. Also, to gain further insight into the effects of glycerol doping on the properties of entrapped proteins, both steady-state and time-resolved fluorescence of Trp 214 was used to examine the conformation, dynamics, accessibility, thermal/chemical stability and the degree of ligand binding of human serum albumin (HSA) in solution and after entrapment of the protein in glycerol-doped TEOS-based materials.

Acknowledgements

I would like to thank my supervisor, Dr. J.D. Brennan for all the guidance and support over the last three years. I would also like to extend my gratitude to all the "Brennanites" present and past members.

A special thank-you goes to my parents, Minco and Gurgija Gulcev for all of their support, understanding, patience and continued love over the last three years. They have always taught me that hard work will payoff in the end. I would also like to thank my sister Lily, who has been so helpful. I appreciate all your words of wisdom.

Makedonia na Makedoncite!!!

Table of Contents

List of Figures

List of Tables

List of Abbreviations

ABTS – 2-2' azinobis (3-ethylbenzthiazoline-6-sulfonic acid) diammonium salt
a.u. – absorbance units
BET calculation - Brunnauer, Emmett, & Teller calculation
BJH calculation - Barrett, Joyner and Halenda calculation
BSA – Bovine Serum Albumin
CID – Collision Induced Dissociation
$Cr(acac)_3$ – Chromium acetylacetonate
DGS – Diglyceryl Silane
ESI – Electrospray Ionization
ESI-MS – Electrospray Ionization Mass Spectrometry
ESI MS/MS – Tandem Electrospray Mass Ionization Spectrometry
EtOH – Ethyl alcohol
FT-IR – Fourier Transform Infrared Spectroscopy
GOx –Glucose Oxidase
H_2O (d.d) – distilled deionized water
HEPES – 4-(-2hydroxyethyl)-1-piperazineethanesulfonic acid
HRP – Horseradish peroxidase
HSA – Human Serum Albumin
k_{cat} – substrate turnover number
k_{cat}/K_M – catalytic efficiency number
K_M – Michealis Menten Constant (binding constant)
MAS – Magic Angle Spinning
MALDI – Matrix Assisted Laser Desorption Ionization mass spectrometry
ORMOSILs – Organically-Modified Silanes
NiNTA – Nickel nitrilotriacetic acid
NMR – Nuclear Magnetic Resonance
PEG – Polyethylene glycol
PEI – Polyethylene imines
PGS – Polyglyceryl silanes
Phenol red – Phenolsulfonphthalein
pI – isoelectric point
PVA – Polyvinyl alcohol
pyranine – 8-hydroxypyrene-1,3,6-trisulfonic acid, trisodium salt
R 6G – Rhodamine 6G
RNASe T1 – Ribonuclease T1
S_{BET} – surface area calculated using BET calculation
SEM – Scanning Electron Microscopy
SNARF – Semi-naphtharhodofluorophore
SNARF-dex – Semi-naphtharhodofluorophore Dextran
SS-NMR – Solid State Nuclear Magnetic Resonance Spectroscopy
TEOS – Tetraethyl orthosilicate
TGA – Thermal Gravimetric Analysis

TMOS – Tetramethyl orthosilicate
TMS –Tetramethylsilane

Chapter 1

Introduction

1.1. Biomolecule Immobilization

Immobilization can be defined as the confinement of a biomolecule in a distinct phase, which undergoes exchange reactions with, but is separate from, the bulk phase in which substrate or inhibitor molecules are dispersed and monitored.[1] The biomolecule can be restricted in various ways: it can be covalently bonded, adsorbed (through electrostatic or hydrophobic interactions), or physically entrapped. The earliest method of immobilization employed was physical adsorption. In physical adsorption the enzyme is bound to a surface without the use of covalent bonding. A variety of adsorption techniques have been utilized; the binding forces may be ionic, hydrophobic, hydrogen bonding, or Van der Waals' interactions.[1] Unfortunately, the major disadvantages encountered in this technique are the reversible nature of the bonding between the enzyme and the support, which may lead to desorption of the enzyme upon the addition of the substrate, and the inability to control the orientation of the biomolecule, which results in poor overall activity.

Another early method which was extensively used for immobilization of enzymes involved tethering of the enzyme to an organic polymer (such as cellulose or polyacrylamide) or entrapping the enzyme within a porous polymer such as nylon. The disadvantages associated with this method are that it lacks tuneability and compatibility (the biomolecule has to be hydrophobic in nature), the entrapped enzyme may leach, and,

in the presence of an aqueous solvent, there is the potential for preferential partitioning of analytes from the vicinity of the enzyme. [1]

Perhaps the method most extensively used to immobilize enzymes is covalent bonding to activated supports such as polymers. This method involves the formation of bonds to lysine (NH_2), glutamic acid (COOH) or cysteine (SH) residues, and allows for the enzyme to be firmly and irreversibly bound to its support.[1] Covalent immobilization overcomes the desorption problem, but is time-consuming, costly, and may still produce randomly oriented proteins with poor activity. As a result of the negative drawbacks associated with the covalent immobilization method, as described above, many groups now use a process termed 'oriented covalent immobilization'.[2] Oriented immobilization is a generic term encompassing many affinity-based techniques, such as: biotin-avidin interactions, aptamer capture, antibody capture and the use of His_6 tags to bind to NiNTA (nickel nitrilotriacetic acid) - derivatized surfaces. The first method takes advantage of the extraordinarily high affinity constant ($\sim 10^{15}$) between biotin and avidin (streptavidin), which makes this method an efficient one for oriented immobilization using specific biotinylation of the biomolecule.[2] The second method utilizes aptamers (single stranded nucleic acid sequences that can bind to secondary species), which are bound to a surface (often via the biotin interaction) and selectively capture the protein of interest in a controlled orientation.[3] Yet another method of oriented immobilization of proteins is through the use of suitable antibodies which again capture the proteins in a controlled orientation.[2] In the final method site-directed mutagensis is used to place N-terminal hexa-histidine tags into a protein sequence to achieve site-specific binding to NiNTA-

derivatized surfaces.[4] While these methods can control orientation often they require time-consuming steps to produce selective aptamers or antibodies, or require recombinant proteins, restricting their universal application.

1.2. Sol-Gel Processing

A different type of immobilization is based on physical entrapment of enzymes in an inorganic polymer matrix that is formed via the sol-gel process. Encapsulation into the sol-gel-derived silica is perhaps the single most facile and generic immobilization technology available today.[5] Encapsulation involves trapping the biomolecule within a nanoporous silica network where the analyte can diffuse into the matrix while the protein remains entrapped. The polymerization process can be done at low temperature, in an aqueous environment, and thus is highly biocompatible, leading to the formation of a hydrated biogel that contains active enzymes in an aqueous environment.[5] The encapsulation approach confines the biomolecule by size exclusion and therefore orientation of the biomolecule is not an issue.[6]

Interest in sol-gel processing of inorganic ceramic and glass materials began as early as the mid-1800s with Ebelman and Graham's studies on silica gels.[7] Although the utility of sol-gel-derived matrices as hosts for organic and organometallic dopants had been known for quite some time; it was not until 1990 that Avnir and coworkers were able to encapsulate proteins within an inorganic silicate matrix.[8] Since this time, optimization of entrapment protocols has been described by Avnir,[9] Zink[6] and other groups.[5,10]

The standard protocol for the synthesis of sol-gel-derived materials occurs by acid-catalyzed hydrolysis and condensation of alkoxysilane precursors.[5] The alkoxysilane precursor (either TEOS – tetraethylorthosilicate or TMOS – tetramethylorthosilicate) undergoes nucleophilic attack by the oxygen in water causing the alkoxide groups (OR) to be replaced by hydroxyl groups (OH), as shown in the hydrolysis step in Figure 1.1. Subsequently, in the condensation reaction silanol groups (Si-OH) are converted into siloxane bonds (Si-O-Si) plus the by-products water or alcohol are formed, as illustrated in step 2 of Figure 1.1. Under most conditions, condensation commences before hydrolysis is complete. With time the silica fibrils cross-link to form a 3-dimensional network, causing the system to evolve from a sol, where there are individual fibrils more or less weakly interacting with each other, to a gel, which is basically a continuous matrix of interconnected fibrils occupying space. The hydrated gel that initially forms is an interconnected, rigid network with pores of submicrometer dimensions that contain the water/alcohol mixture that is produced by the hydrolysis and condensation reactions.[11,12]

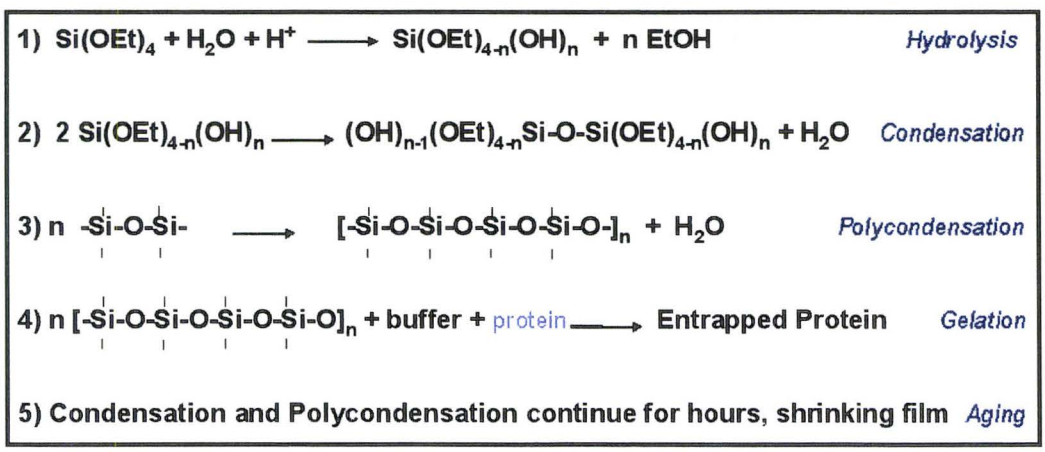

Figure 1.1: The Acid-Catalyzed Sol-gel Processing Method

The properties of a particular sol-gel-derived inorganic network are tunable by varying numerous parameters, such as: hydrolysis, condensation time and pH, H_2O/Si molar ratio (R), the nature of the silane precursor, the presence of polymer additives, catalyst nature and concentration, aging temperature/time, and drying conditions. [11,12,13,14] A dopant such as a biomolecule can be added to the sol-gel material prior to gelation to physically trap the biomolecule in the cross-linked silica network, as shown in Figure 1.2. The biomolecule may act as a template around which the gel solidifies; therefore, the biomolecule is thought to be held in place as a result of size exclusion rather than direct interaction with the silica surface.[6]

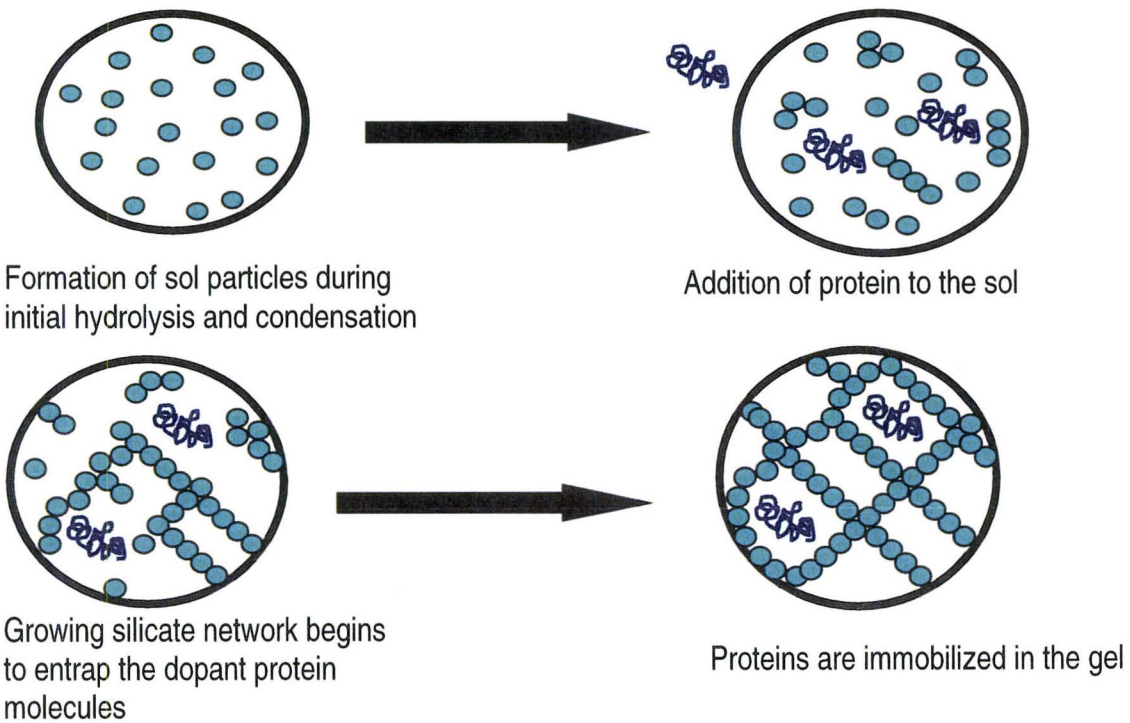

Figure 1.2: Schematic Representation of a Biomolecule Entrapped within a Sol-gel derived Silica Matrix

By far the majority of sol-gel based protein entrapment studies have used TEOS or TMOS as the silane precursor. The advantages of utilizing TMOS and TEOS-based glasses are the following: they allow for some control of the reaction medium and conditions, they prevent bacterial and chemical degradation and they are cost-effective and optically transparent.[6,8,9] The drawbacks, however, associated with this starting material far outweigh the positive aspects, mainly: liberation of alcohol by the precursors can lead to denaturation of the entrapped biomolecules, the silica material formed has small pores (ca. 2-5nm in diameter), which leads to inaccessible sites, the material continues to evolve over many months which can lead to problems with calibration of biosensors, shrinkage of material upon loss of entrapped solvent is significant (up to 80%), and cracking is often observed.[9,15] The above disadvantages of TEOS and TMOS-based glasses have lead to the formation of second-generation sol-gel processing methods which have extended the stability and the activity of the entrapped bioencapsulate.

1.3. Second Generation Sol-gel Processing Methods

As mentioned above, a major drawback of the inorganic materials derived from TEOS or TMOS is that they liberate a significant amount of alcohol during the hydrolysis step, as shown in Figure 1.1, which must be at least partially removed in order to decrease denaturation of the protein upon entrapment. Perhaps the easiest way to alleviate the deleterious effects of alcohol is through its removal upon formation. Levy and colleagues describe vacuum elimination of alcohol by rotavaporation methods in the preparation of TEOS and TMOS sol-gel material.[16] This procedure leads to materials

with larger pores, less shrinkage and higher activity of the entrapped biomolecules. Another way to circumvent the problem is by changing the starting material to sodium silicate,[17] or silicic acid to avoid the production of alcohol during the formation of the sol-gel-derived material. Materials, however, derived from such processes still undergo considerable shrinkage and cracking and tend to be microporous, leading to poor accessibility of entrapped biomolecules.

Another route to improve the material properties is to use Organically-Modified Silanes (ORMOSILs - which have alkyl groups attached directly to Si), which are added to TEOS or TMOS, to provide an additional degree of tunablility in terms of both cross-linking and the hydrophobicity/ hydrophilicity of the sol-gel material.[18] Such precursors, including methyl, dimethyl, propyl and other organo functional silanes, have been noted to improve the stability of hydrophobic proteins such as Lipase.[19] However, one of the disadvantages associated with ORMOSIL-doped sol-gel materials is that the presence of the alkyl groups reduces the degree of cross-linking, leading to a less robust material. Also, the organic functionality can be added only to a certain level before phase separation occurs resulting in poor optical clarity and cracking of the material.[18]

Yet another method of altering the material properties is by adding a dopant to the inorganic matrix (TEOS). Dopants which have been used are: hydrophobic or hydrophilic polymers (i.e. PEG-polyethylene glycol, PVA- polyvinyl alcohol, PEI-polyethylene imides), ionic and zwitterionic surfactants, micelles, liposomes, dyes, redox species, graphite and sugars.[15,20] The materials formed by use of these dopants allow for tunability of polarity, conductivity, morphology and biocompatibility, and the resulting

material can be designed to be rigid, semi-rigid or flexible. Optimization of the dopant level, however, is necessary, and beyond a certain level dopants may lead to phase separation of the material causing a decrease in optical clarity.[15] For further information on the entrapment of proteins and other biological species into a wide range of sol-gel-derived nanocomposite materials and a basic understanding of these materials and their numerous applications including: the development of biosensors, stationary phases for affinity chromatography, biocatalysis, immunosorbent and solid-phase microextraction coatings, refer to recent reviews by Brennan[15] and Gill.[21]

Yet another method that can be used to improve the properties of sol-gel-derived silica is to move away from alkoxysilanes toward more biocompatible precursors that liberate protein stabilizing compounds. This approach was first demonstrated in 1998 by Gill and Ballesteros, who reported the synthesis of glycerated silanes, polyglycerylsilanes (PGS),[20] as a precursor for the formation of protein doped silicate material. The new precursor generated bioglasses that retained high protein activity and displayed large pore sizes and minimal shrinkage. The formation of the polyglycerated material, however, involved a multi-step process involving refluxing and rotovapping steps, which were very difficult to reproduce, and required the presence of catalysts, which were not removed before entrapment of proteins.[20]

Therefore, the focus of this research project was to develop and characterize a simplified method for preparing highly biocompatible glasses wherein glycerol was slowly added at varying levels to provide a biocompatible silane mixture before the addition of proteins. The major impetus of this thesis was to determine an optimal

glycerol level which would impart maximal stability and increased shelf-life for the entrapped enzymes while at the same time minimizing both shrinkage and cracking of the material. A second major goal was to gain insight into the nature of the glycerol-doped material and the properties of entrapped proteins within these materials in order to explain the effects that glycerol doping has on the structure, stability and function of entrapped proteins.

1.4. Overview of Thesis

In the past decade, use of alkoxysilane-based glasses has emerged as a viable method of enzyme immobilization. As described in detail previously, there are many problems associated with TEOS/TMOS-based materials and for this reason there is a need for a new starting material. The research in this thesis focuses on the characterization of glycerol-doped sol-gel materials through the use of traditional techniques such as NMR (nuclear magnetic resonance), IR (infrared spectroscopy), MS (mass spectrometry), SEM (scanning electron microscopy) and fluorescence spectroscopy. The main goal is to determine whether glycerol doping imparts increased stability to the entrapped enzymes as compared to the traditionally used TEOS-based glasses. A related goal is to investigate the environment within the sol-gel matrix into which the biological molecule is encapsulated to gain a clearer picture of how the interior of normal and glycerol-doped matrices affect the structure, conformational flexibility, accessibility, and thermal stability of entrapped biomolecules. To achieve this goal, the behaviour of the biomolecule was further probed through the use of time-resolved

anisotropy techniques, which provide insight into biomolecule dynamics and the presence and extent of biomolecule-silica interactions within doped and undoped materials. Finally, preliminary work was done on the development of a reagentless biosensor prototype for the detection of urea. In this reagentless biosensor prototype the enzyme urease and a pH-sensitive fluorescence probe were co-entrapped within a sol-gel-derived thin film and only the analyte (in this instance the substrate) was needed in order to generate a fluorimetric response.

This chapter provides introductory information on the process utilized for the entrapment of enzymes within sol-gel-derived material. Chapter 2 investigates the development of a biocompatible glycerol-silane precursor and describes the characterization of the sol-gel processed materials used for the entrapment of biomolecules. Chapter 3 examines the activity, stability and catalytic properties of the enzymes urease and glucose oxidase entrapped within the glycerol-doped sol-gel materials. Chapter 4 describes a series of fluorescence-based experiments that are used to assess the factors, which influence the stability of entrapped biomolecules within the glycerol-doped sol-gels, and seeks to determine how such factors (accessibility, dynamics, and stability) control enzyme behaviour in glass. Chapter 5 combines all the information gained from the previous chapters and describes the design of a reagentless biosensor prototype. Finally, Chapter 6 provides conclusions and suggestions for future work.

1.5. References:

1. Trevan, M. D.: in *Immobilized Enzymes: An Introduction and Applications in Biotechnology*; John Wiley and Sons: New York, **1980**, 1.

2. Turkova, J. *Journal of Chromatograpy B.* **1999**. *722*, 11.

3. Cox, C. J.; Hayhurst, A.; Hesselberth, J.; Bayer, T. S.; Georgiou, G; and A.D. Ellington. *Nucleic Acids Research.* **2002**. *30*, e108.

4. Allard, L.; Cheynet, V.; Oriol, G.; Mandrand, B.; Delair, T.; and F. Mallet. *Biotechnology and Bioengineering.* **2002**, *80*, 341.

5. Brennan, J. D. *Applied Spectroscopy.* **1999**, *53*, 106A.

6. Dave, B. C.; Dunn, B.; Valentine, J. S.; and J. I. Zink. *Analytical Chemistry.* **1994**, *66*, 1120A.

7. Hench, L. L. and J. K. West. *Chemical Reviews.* **1990**, *90*, 33.

8. Braun, S.; Rappoport, S.; Zusman, R.; Ottolenghi, M.; and D. Avnir. *Material Letters.* **1990**, *10*, 1.

9. Avnir, D.; Braun, S.; Lev, O.; and M. Ottolenghi. *Chemistry of Materials.* **1994**, *6*, 1605.

10. Narang, U.; Prasad, P. N.; and F. V. Bright. *Chemistry of Materials.* **1994**, *6*, 1596.

11. Brinker, C. J. and G. W. Scherer. *Sol-gel Science: The Physics and Chemistry of Sol-Gel Processing;* Academic Press Inc.: New York, **1990**.

12. Iler, R. K. *The Chemistry of Silica;* John Wiley & Sons: New York, **1979**.

13. Buckley, A. M. and M. Greenblatt. *Journal of Chemical Education.* **1994**, *71*, 599.

14. Liverage, J.; Thibaud, C.; and C.Roux. *Journal of Physics: Condensed Matter.* **2001**, *13*, R673.

15. Jin, W. and J. D. Brennan. *Analytica Chimica Acta.* **2002**, *21959*, 1.

16. Levy, D.; Ferrer, M. L.; and F. del Monte. *Chemistry of Materials.* **2002**, *14*, 3619.

17. Bhatia, R. B.; Gupta, A. K.; Singh, A. P.; and C. J. Brinker. *Chemistry of Materials*. **2000**, *12*, 2434.

18. Brennan, J. D.; Hartman, J. S.; Ilnicki, E.; and M. Rakic. *Chemistry of Materials*. **1999**, *11*, 1853.

19. Reetz, M. T.; Zonta, A.; and J. Simpelkamp. *Angew. Chem. Int. Ed. Engl.* **1995**, *34*, 301.

20. Gill, I. and A. Ballesteros. *Journal of the American Chemical Society*. **1998**, *120*, 8587.

21. Gill, I. *Chemistry of Materials*. **2001**, *13*, 3404.

Chapter 2

Effects of Glycerol Doping on the Structure, Morphology and Physical Properties of Tetraethylorthosilicate-Derived Silica

Glycerol-loaded sol-gel-derived silica materials were prepared by adding varying levels of glycerol into an acid-hydrolyzed, TEOS-derived sol, followed by addition of an aqueous buffer solution to induce gelation. The composition of the glycerol-doped precursor solution was characterized using ^{13}C and ^{29}Si NMR, FT-IR and ESI-MS to assess whether transesterification of TEOS by glycerol had occurred in sols and gels, and by fluorescence spectroscopy of pyranine-doped gels to assess the level of ethanol retained in the glycerol-doped materials. After gelation the morphology and optical transparency of the silica materials were examined via UV-VIS absorbance, SEM (scanning-electron microscopy), and N_2 adsorption porosimetry methods. It was determined that increased levels of glycerol led to a significant improvement in optical clarity, produced reduced shrinkage and cracking and led to larger mesopores in the final material. These material properties provide insight into the potential roles of glycerol in stabilizing entrapped proteins, as will be discussed in subsequent chapters.

2.1. Introduction

In the past decade several reports have appeared describing the encapsulation of biomolecules into monoliths derived from tetraethyl orthosilicate (TEOS) or tetramethyl orthosilicate (TMOS).[1,2,3,4,5] Encapsulation protocols generally involved the hydrolysis of the alkoxysilane precursor in the absence of added alcohol via sonication. A buffer solution containing the protein of interest was then added to the reaction medium to promote gelation. The addition of buffer brings the pH of the system up to biologically acceptable levels and dilutes the alcohol produced during hydrolysis. In most cases, low-temperature aging over a period of several days or weeks resulted in a durable, optically clear biomaterial, which showed good retention of protein activity, as summarized in several recent reviews[6,7,8]

Recently, several groups have published a number of studies which show that adding dopants such as sugars and polyols to TEOS during the hydrolysis stage can produce a composite material that is both mesostructured and biocompatible.[9] Eggers and Valentine have explored the causes of the enhanced stability of entrapped proteins in wet aged glasses that had protein stabilizing dopants, such as sugars and amino acids, added to them after gelation.[10] We also examined how the presence of the osmolytes sorbitol and sarcosine (N-methylglycine) in the buffered protein solution, which were used to form the glass, affects both the thermodynamic stability and activity of enzymes entrapped into TEOS-derived silica. Measurement of the physical properties of osmolytes showed increases in average pore size, which resulted in greater diffusion of analytes into the matrix, and thus higher overall enzymatic activity.[11] Wei and

researchers on the other hand, report on the development of templating the sol-gel material using D-glucose. In this method, D-glucose templates sol-gel material prpepared from tetraalkyl orthosilicate, which resulted in the creation of mesoporous silica.[12,13]

Further studies have extended the concept to include the preparation of specific polyol-silane materials such as PGS (polyglyceryl-silane)[9] and DGS (diglyceryl-silane).[14] Such materials were shown to stabilize various biomolecules which did not remain functional in matrices derived from TEOS.

A key question that has not yet been fully explored is what changes in material properties arise as a function of increased levels of glycerol. Glycerol was chosen on the basis of its solubility and its extensive use as a protein stabilizer. The primary objective of this chapter is to prepare and characterize glycerol-doped composite materials using protocols which are amenable to protein encapsulation. These protocols include sonication of precursors in the absence of added ethanol, addition of a buffer solution to promote gelation, and low-temperature aging.[1-3] We prepared materials by sonicating TEOS and adding 0 to 4.16 mol ratio of Gly:Si.

Composite materials were characterized using fluorescence, nuclear magnetic resonance (NMR), FT-IR spectroscopy, mass spectrometry, scanning electron microscopy and pore size analysis. Many ^{29}Si and ^{13}C NMR studies have appeared recently describing the hydrolysis and condensation of TEOS,[15,16] with sugars and sugar acids.[17,18,19] ^{29}Si NMR was used to study the structural intermediates in TEOS (Si_1:Gly_0)

and glycerol-doped (Si_1:$Gly_{0.60}$ and Si_1:$Gly_{4.16}$) sol-gel precursors. In this work, NMR of both sol and solid (gelled) samples was done using ^{1}H, ^{13}C and ^{29}Si nuclei.

Tandem electrospray ionization mass spectrometry (ESI-MS/MS)[20] studies were used to determine the daughter-ion spectra of peaks obtained from injection of glycerated TEOS sols into the MS. In this process termed CID (collisional induced dissociation), a molecular ion, selected from the first MS, is collisionally fragmented using a gas such as Ar, and the m/z ratio is measured for the resulting daughter fragment ions.[21]

Both the sol and gel synthesized materials were tested using IR spectroscopy. FT-IR can be used to characterize the oligomeric species formed during the hydrolysis-polycondensation reactions of TEOS, right up to the structural evolution of silica gels in the early and later stages (xerogels) of conversion to glasses.[22,23,24,25] This study investigated whether glycerol was incorporated into the silica matrix and whether it influenced the extent of the condensation reaction.

Both nitrogen sorption isotherms BET and SEM were used to determine the pore size and pore morphology of the gel material. The porosity in sol-gel-derived oxides depends on the internal structure of the primary particles, the size and size distribution of the primary particles, how these primary particles aggregate, and how the gel structure responds to the capillary stresses during drying. Both BET and SEM analysis were employed to determine whether glycerol being incorporated into the silica matrix altered the morphology of the material.[26,27,28] Adsorption and desorption isotherms can be obtained by measuring the quantities of gas taken up by or removed from the sample as

the relative pressure is raised and lowered.[29,30] The resulting adsorption and desorption isotherms were examined to provide information about the pore size and shape.[30,31]

Initially, the chemical properties of glycerol-loaded sol-gels were examined by NMR, FT-IR and MS techniques, to determine whether glycerol was incorporated into the silica matrix and the extent to which it influenced the rate of condensation. The altered chemical properties in turn affected the physical properties of the glycerol-doped sol-gels, as shown with SEM and N_2 sorption techniques. Overall, this chapter aims to address the impact glycerol doping has on the sol-gel process.

2.2. Experimental Section

2.2.0. Chemicals:

Tetraethylorthosilicate (TEOS, 99.999%) was obtained from Aldrich Chemical Company (Oakville, ON). Glycerol (99.999%) was ordered from Caledon Chemicals (Georgetown, ON). Pyranine (8-hydroxy-1,3,6-trisulfonated pyrene) was purchased from Molecular Probes (Eugene, Oregon). Water was purified by reverse osmosis and deionized using a 4-stage Milli-Q Synthesis A10 water purification system. All other chemicals and solvents used were of the highest available grade and were used without further purification.

2.2.1. Preparation of Glycerol-Doped Silanes:

Sol preparation: 2.25 mL of TEOS, 0.7 mL of H_2O (d.d) and 0.05 mL of 0.1 N HCl were mixed and sonicated until the mixture became a clear, homogeneous phase (ca. 1 hour). At this point, varying volumes of glycerol were added, at 41 ± 2 °C over an hour, with continual stirring, to prepare solutions with glycerol:TEOS mole ratios, ranging from 0.08:1 to 4.16:1. Upon complete addition of glycerol, the mixture was immediately used for studies of precursor composition or was used to prepare gels as described below.

2.2.2. Preparation of Gels:

Gels were prepared as bulk glasses by combining a 1:1(v:v) ratio of the hydrolyzed silane (TEOS-based or glycerol-doped silanes) and a buffer solution (10 mM sodium phosphate/ 100 mM KCl at pH 7.2) into a methacrylate cuvette and shaking the contents gently to ensure complete mixing of the two solutions. Samples had final volumes of 1 cm x 1 cm x 1.5 cm (blocks) or 0.3 cm x 1 cm x 4.0 cm (slides). Slides were prepared by sealing the cuvettes with Parafilm™ and tipping the cuvettes on their sides prior to gelation. The addition of a buffer for gelation resulted in the R values (H_2O:Si molar ratio) of 11 during gelation of TEOS-based samples. With increasing glycerol content the R values (H_2O:Si molar ratio) increased, for Si_1:$Gly_{0.60}$ an R value of 13 and for Si_1:$Gly_{4.16}$ an R value of 28 were obtained, respectively. Following the mixing of the two components, the cuvettes were capped with Parafilm™ and were allowed to gel at room temperature. After gelation the blocks or slides were either dry aged (by punching five

holes into the Parafilm^{TM}) without washing or washed extensively to remove all the entrapped glycerol. All samples were aged at 4°C over a period of several months.

2.2.3. Characterization of Sol Material:

^{29}Si Solution Nuclear Magnetic Resonance Spectroscopy:

The ^{29}Si solution NMR spectra of 2 mL samples (of Si_1;Gly_0 and Si_1:$Gly_{0.60}$) were obtained on a Bruker DRX 500. Spectra were collected using a 30° pulse with no spinning in a 7 mm zirconium oxide rotor with a spectral width of approximately 14.9 kHz. For each experiment the number of scans collected were 256, each experiment took 4.5 min to run, with a recycle time of 1s over a 2 hour period. In order to obtain high quality spectra, a relaxation reagent $Cr(acac)_3$ was used as described by Fyfe and Aroca.[13] Due to solubility problems encountered with $Cr(acac)_3$ in the glycerol doped sols, the concentration used in this study was 0.008M, or half of the concentration used by Fyfe and Aroca.[15] Lowered solubility of $Cr(acac)_3$ in the Si_1:$Gly_{4.16}$ sample required the collection of a larger number of scans, 1024, per experiment; as a result, each experiment took 18 minutes. All samples were referenced to an external standard, consisting of neat tetramethylsilane (TMS).

IR Spectroscopy of Sol and Gelled Samples:

The gel samples were ground to fine powder and the liquid sol samples were utilized as formed. The FT-IR instrument used was the Bruker Vector 22. One hundred and

fifty scans were obtained for solids, 40 scans for liquids and 20 scans were collected to obtain the background. The data was acquired from 650 to 4000 cm^{-1} with a resolution of 4 cm^{-1}. The acquisition mode employed collected data in transmittance units, which were later converted into Kubelka-Munck absorbance units. These peak intensities were monitored in this study using an integration function, P, available from the IR fitting software.

Electrospray Ionization: Mass Spectroscopy

Samples were tested during the sol phase of precursor formation. Sol samples were tested using electrospray ionization (ESI – both negative and positive modes), on a Waters (Micromass) – Quattro Ultima, triple quadrupole instrument, using a Z-spray atmospheric pressure analyzer as the ESI source. The capillary was set at 3.00 kV at a temperature 80 °C. The cone was set at 30-35 V, with a cone gas flow of 64 (L/Hr). Initially samples were diluted 100-fold (due in part to the viscous nature of the glycerated sols) in 0.2% NH_4OH ACN/H_2O at pH 8 and were analyzed using negative ion ESI. To keep the pH consistent with sol material (which are acidic), negative mode ESI-MS was carried out in an acidic environment by adding formic acid (the sol was diluted fifty-fold) to the solvent prior to analysis. Neat sol samples were also injected into the ESI-MS instrument. The only drawback is that negative ion mode ESI is suppressed in an acidic medium. After finding a peak of interest, the m/z 151, CID, was performed to determine the daughter ion spectra of this $[M-H]^-$ peak.

2.2.4. Characterization of Gelled Material:

Gelation Time Studies:

Gelation studies were performed in sealed cuvettes using 1.5 mL of sample prepared with a buffer consisting of 10 mM phosphate buffer with 100 mM KCl, pH 7.0. The material was considered a gel when it remained completely stationary upon shaking. The determination of the gel point is difficult to track and this measurement is qualitative in nature.

Fluorescence Studies of Internal Environment:

Various percent volumes of EtOH in H_2O or H_2O in glycerol samples were used to determine the amount of ethanol present in the TEOS-based materials and glycerated silanes. Ethanol concentrations ranged from 0-100%. A calibration curve of 5 μM pyranine with varying levels of EtOH:H_2O was constructed and the same was constructed and repeated for glycerol:H_2O samples. Following this, the sol-gel-derived glass was made containing a known amount of glycerol. The ratio of peaks of Gly + EtOH versus the ratio of peaks in glycerol only, gives EtOH ratio. This value is then compared to the standard curve of EtOH to determine the % v/v of EtOH present in the sol-gels.

Solid-State MAS ^{29}Si NMR:

In order to quantitatively determine the relative intensities of the condensation peaks, at different [Gly], ^{29}Si magic angle spinning (MAS) spectra of the solids were obtained

on the Bruker Advance 300 using a 4 mm zirconium oxide rotor at a frequency of 59.62 MHz with proton decoupling during acquisition. For ^{13}C solid samples, cross-polarization magic angle spinning at a frequency of 75.47 MHz with proton decoupling during acquisition was used. Both ^{29}Si and ^{13}C samples were spun at 5 kHz. For ^{29}Si and ^{13}C, 5.5 ms and 1.1 ms contact times were used, respectively. For ^{29}Si the delay between successive pulses was 3 s, using a 2 ms pulse width and spectral width of 14.9 kHz. For ^{13}C SS-NMR multiple scans ranging from 3600 to 17700 were obtained using a spectral window of 273.8 ppm.

Thermal Gravimetric Analysis - TGA:

Both washed and unwashed samples were tested using thermal gravimetric analysis. Samples were washed with 2 mL of buffer at least fifteen times. The instrument used was the NETZCH STA 409 PC. For these studies the temperature ranged from 20 – 600 °C degrees, with a 5 °C/min increase in temperature. To determine the amount of ethyl alcohol or glycerol that was present in the sol-gel, the % sample weight versus temperature was plotted for washed and unwashed samples.

Pore Size Analysis:

Pore-size analysis of completely dried monoliths was performed on a Quantachrome Nova 2200 surface area/pore size analyzer. The monoliths were extensively washed prior to analysis to remove any residual glycerol or ethyl alcohol present in the silica samples and were crushed to a fine powder. Note: attempts to do

BET measurements in the presence of glycerol did not work because the glycerol extracted from the matrix interfered with measurements. The samples were then dried in the oven at 110 °C and subsequently freeze-dried to remove any residual water. Subsequently, the samples were degassed for a day at 125 °C to remove air and bound water from the surface of the powder. The pressure was measured as nitrogen was adsorbed and desorbed at a constant temperature of -196 °C. Using the desorption branch of the resulting isotherms, the average pore size, total pore volume and distribution of sizes was determined using the BJH[32] (Barrett, Joyner and Halenda) calculation. To determine the surface area of the pores, and estimate the total pore volume the Brunauer-Emmett-Teller (BET)[33] analysis (of the amount of N_2 gas adsorbed at various partial pressures, P/P_o, with at least five points, $0.05 < P/P_o < 0.3$) was done using a nitrogen cross sectional area of 16.2 $Å^2$.

Scanning Electron Microscopy (SEM):

The samples used in SEM analysis were prepared in two different ways. The first was through the use of thin films, formed by spin coating of the sol onto glass slides, that were treated for 12 hr in KOH to remove any residue adhered to the glass surface. To each slide a 1:1 ratio of the silane buffer mixture was added and spun at 4000 rpm for 10 s. In the second method utilized, monolithic slides (4 cm x 1cm x 0.3 cm) were imaged. All samples were aged for three days prior to SEM analysis. Monoliths were cut and the fresh surface was coated with a gold film under vacuum to improve

conductivity. Imaging was performed over a range of accelerating voltages from 5-40 kV using a JEOL 840 SEM.

Shrinkage/Cracking Studies:

Shrinkage studies were done on block samples only. The percent shrinkage of the monolithic blocks was monitored by measuring the length, width and height of the blocks to determine the volume for up to 4 months. For cracking studies slides were spin coated with the sol material of interest. This method was used as it provided greater ease for monitoring the effects of the glycerol dopant in the sol-gel film, since films are more susceptible to cracking than are monoliths. The coated slides were imaged before and after hydration using an optical microscope. Cracking of sample slides was also examined on thin film samples using SEM.

Optical Clarity Studies:

For transmittance studies, monolithic blocks were employed to monitor the optical clarity of the sol-gel material. The degree of clarity was determined using percent transmittance at 400 nm. Three precursors were selected for testing: the non-glycerated silanes, Si_1:Gly_0, the mid-range glycerol-doped silanes, Si_1:$Gly_{0.60}$, and the highest doped silanes Si_1:$Gly_{4.16}$. The transmittance studies were performed on a Cary 400 UV-VIS spectrophotometer, using the multi-read option at constant wavelength; all samples were measured in triplicate. The instrument was zeroed using empty polymethacrylate cuvettes in the sample and reference path.

2.3. Results and Discussion

2.3.1 .Characterization of Sol Material

2.3.1.1. Nuclear Magnetic Resonance

The ^{29}Si solution NMR spectra of TEOS and glycerol-doped precursors were obtained after one hour of sonication and one hour of continual stirring, during which time the glycerol was incorporated into the sol. Figures 2.1 and 2.2 show the solution of ^{29}Si NMR of the Si_1:Gly_0 and Si_1:$Gly_{0.60}$ sols as a function of time after addition of glycerol (or one hour of stirring for TEOS). The condensation products are described according to the Q^n terminology of Engelhardt.[34,35,36] The n term is indicative of the number of Si-O-Si linkages. The respective condensation species which show up in the figures below are summarized in Table 2.1. Figures 2.1 and 2.2 showed the relative changes of the condensation species of the sol material as a function of time.

Table 2.1: Respective and Theoretical Condensation Species for the Sol and Gelled Materials

Peak Spectra Shifts (ppm)	**Condensation Peaks Q^n**	**Theoretical Peaks (ppm)** [31]	***Si Linkages***
	Q^0	-74.31 to -81.95	*No Si-O-Si*
-81.13 to -81.21	Q^1	-79.93 to -88.85	*1-(Si-O-Si)*
-83.13 to -83.50	Q^1 (dimer)	-79.93 to -88.85	*1-(Si-O-Si)*
-90.75 to -90.97	Q^2	-91.00 to -95.00	*2-(Si-O-Si)*
-100.12 to -100.43	Q^3	-99.00 to -103.00	*3-(Si-O-Si)*
-109.95 to -110.90	Q^4	*~ -110*	*4-(Si-O-Si)*

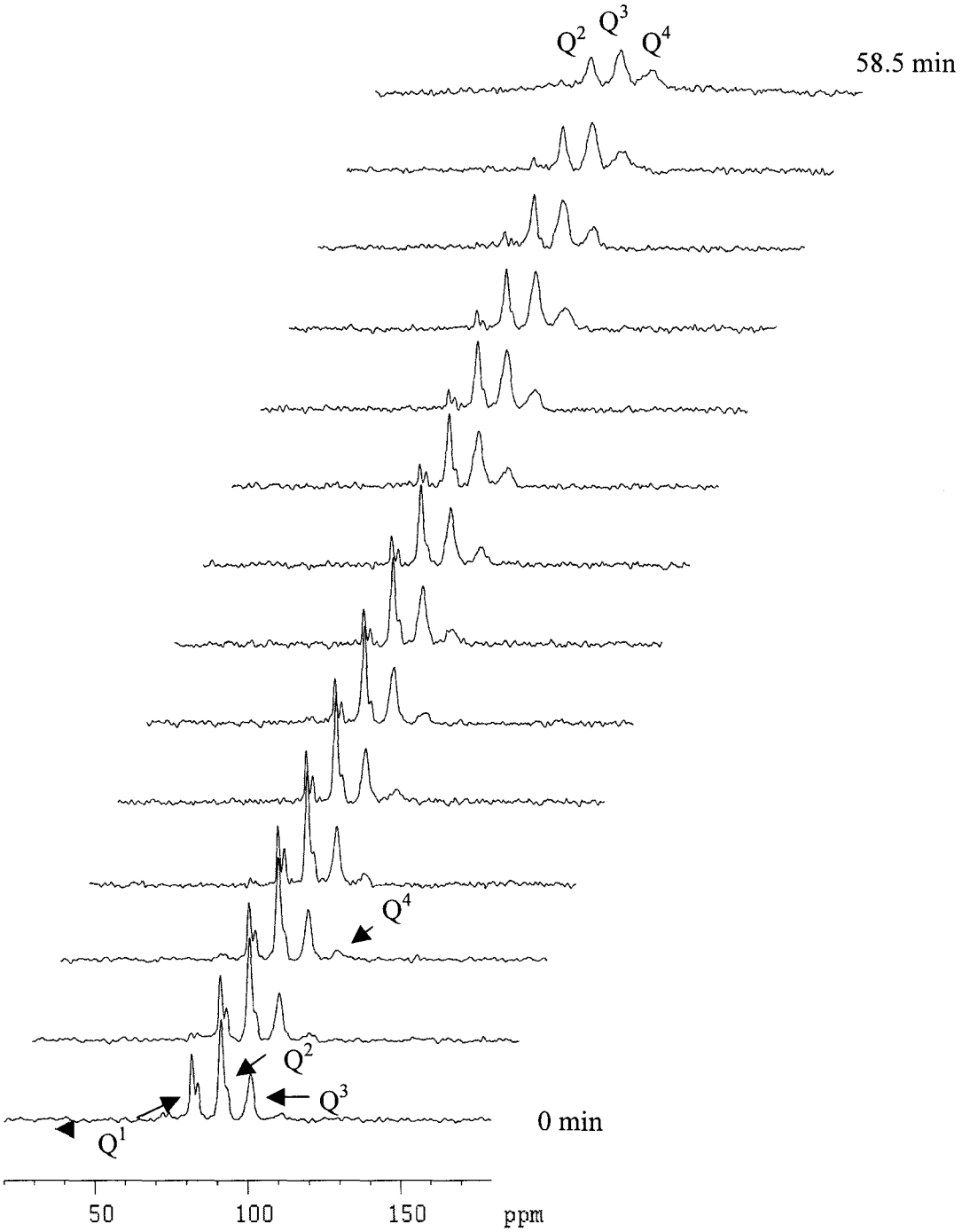

Figure 2.1: ^{29}Si Solution NMR spectra of Si_1:Gly_0 sol evolution with time (time between spectra: 4.5 minutes)

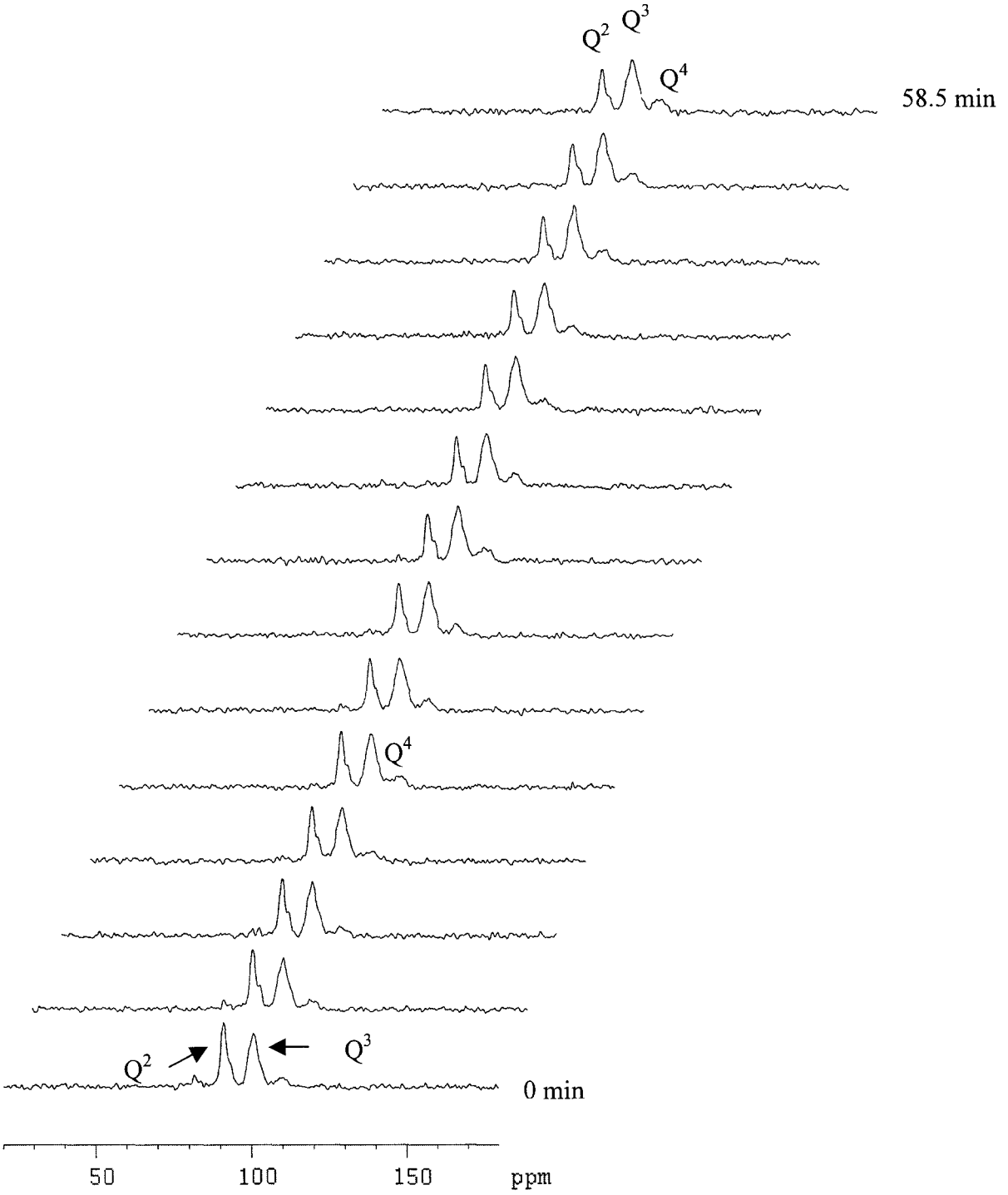

Figure 2.2: ^{29}Si Solution NMR spectra of Si_1:$Gly_{0.60}$ sol evolution with time (time between spectra: 4.5 minutes)

Figures 2.3 and 2.4 illustrate the evolution of each condensation species with time as a function of the total integrated peak intensities. Figures 2.3 and 2.4 clearly show the ratio of the Q^2, Q^3 and Q^4 condensation species for sol samples (Si_1:Gly_0 and Si_1:$Gly_{0.60}$) with time. In Figure 2.3, the Si_1:Gly_0 material shows a gradual increase in the higher condensation species Q^3 and Q^4, with a corresponding decrease in the Q^1 and Q^2 condensation products with time. The Q^3 species appears to plateau at a level of approximately 40%, then decreases slightly, while Q^4 species reach a level of 30%. The Q^3 species in the Si_1:$Gly_{0.60}$ sol is far more abundant than in TEOS-based sols, with up to 60% relative abundance, while the Q^4 species is the least abundant, reaching only 10% relative abundance even after 60 min.

The reason for the lack of Q^1 species in the glycerol doped sols is not known, but may be related to higher pH present in these samples. Nonetheless, the data conclusively demonstrates that glycerol decreases the rate and extent of condensation (as evidenced by the lower Q^4 signal) and may also undergo transesterification with SiOEt species, leading to the larger Q^3 signal. This is beneficial because it allows for EtOH to be removed. This trend was also observed for the Si_1:$Gly_{4.16}$ sol sample (spectra not shown) where the relative amount of Q^4 stays constant at a value on the order of 11% with time. It should be noted that ^{29}Si NMR spectra of the Si_1:$Gly_{4.16}$ were of poor quality and were difficult to analyze quantitatively owing to both peak broadening (due to the increased viscosity of sol) and poor signal-to-noise ratio due to the low solubility of $Cr(acac)_3$ in this sample.

The possibility of transesterification of $Si(OEt)_4$ by glycerol is supported by the work of Kinrade et al. Kinrade and co-workers have shown that the incorporation of

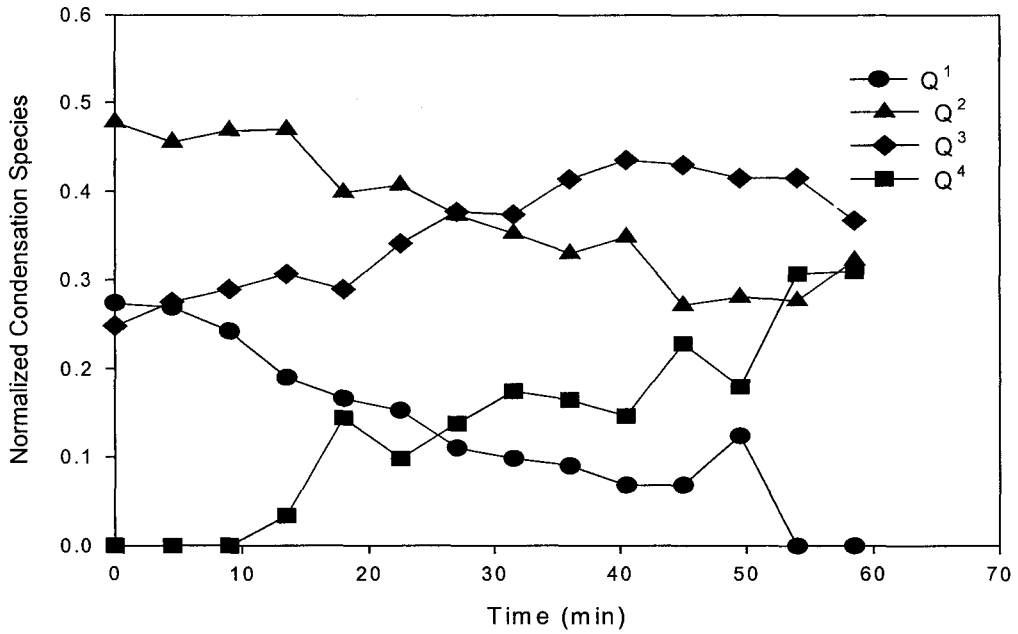

Figure 2.3: Evolution of Condensation Species in Si_1:Gly_0 with time as a function of the total integrated peak intensities

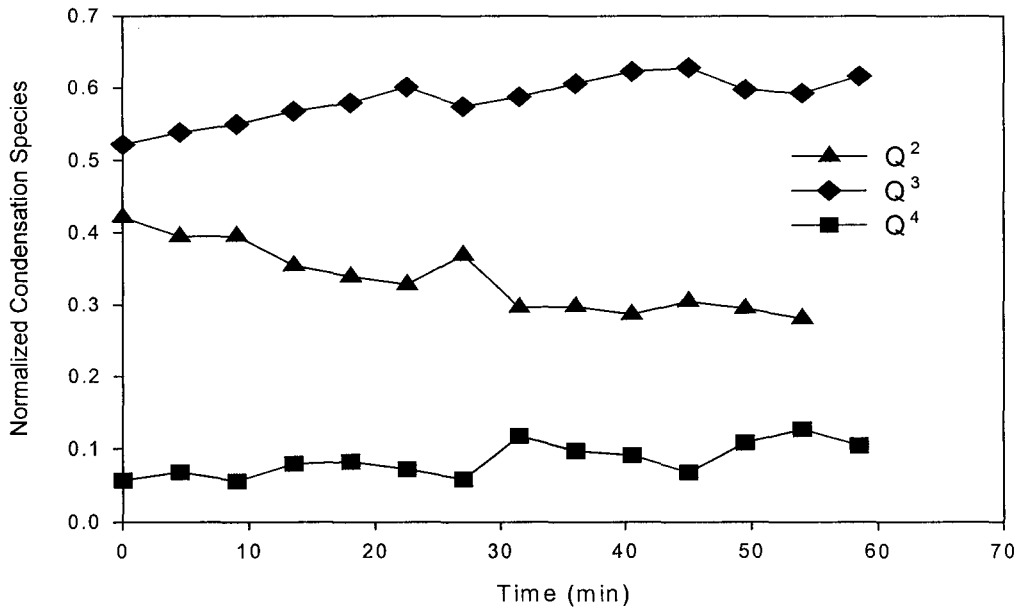

Figure 2.4: Evolution of Condensation peaks in Si_1:$Gly_{0.60}$ with time as function of the total integrated peak intensities

sugar acids is possible and quite common in an aqueous environment. Polyol chains which contain terminal carboxylic groups, "polyol acids", have a higher affinity for a siloxane network than their neutral counterparts. These linkages produce hypervalent complexes; the resulting polyolatosilicate structures are relatively short-lived making them impossible to determine with certainty. The short-lived nature of polyol-silica linkages could be one reason why ^{29}Si NMR peaks corresponding to glycerol-silicon linkages were not observed in this study.[17,18,20] However, as noted below, such species are likely to exist, even in aqueous solution.

2.3.1.2. Characterization of Sol Material using ESI-MS

Mass spectrometry studies were done on both the TEOS-based sol material and glycerated sols ($Si:Gly_0$, $Si:Gly_{0.60}$ and $Si:Gly_{4.16}$) to determine if any Si:Gly transesterification products were present. Both MALDI and electrospray mass spectrometry[21,37] were conducted; MALDI however, provided no conclusive data regarding the incorporation of glycerol into the silica network.

Various types of solvent systems and both positive and negative ESI modes were used in order to obtain information from sols. The most useful data were obtained from the negative ESI mode. During the characterization of the quasimolecular ion peaks, one peak in particular was of interest, which was present in the spectra of $Si_1:Gly_{0.60}$ as shown in panel B and $Si_1:Gly_{4.16}$ panel C of Figure 2.5, the m/z 151 peak; this peak, however, was not visible in the TEOS-based sol material panel A. The quasimolecular ion is most prominent in the most highly doped glycerol silane $Si:Gly_{4.16}$, followed by

$Si:Gly_{0.60}$. To determine the components which comprise this quasimolecular ion, CID (collision induced) MS/MS was performed. In the $Si:Gly_{4.16}$ glycerol-doped precursor, the m/z 151 peak underwent CID and only two daughter peaks were generated at m/z 60 (base peak) and m/z 91. The quasimolecular ion at m/z 91 is generated from deprotonated glycerol $[CH_2OHCHOCH_2OH]^-$ and the quasimolecular basepeak at m/z 60 is $[SiO_2]^-$ as shown in Figure 2.5 (panel D). This data is consistent with the presence of transesterified Si-Gly species within the sol sample. Given that the slightly basic pH would increase the rate of condensation and the presence of ACN would affect the substitution of glycerol into the silica matrix, the sol samples were run under acidic conditions. The sol sample of $Si_1:Gly_{0.60}$ was injected neat into the ESI-MS and the m/z 151 peak was still observed. Also, due to the viscous nature of the $Si_1:Gly_{4.16}$, the sample was run dissolved in a slightly acidic environment. An acidic environment, however, is known to suppress negative ions generated in ESI-MS. Even so, the m/z 151 peak was still present though at a lower level than in basic media. However, it is possible that the m/z 151 peak could have been generated in the gas phase during volatilization of the sample, and thus may not be representative of solution-based species. Neither NMR, nor MS can conclusively determine the incorporation of glycerol into the oligomeric silicas; for this reason, samples were further characterized by FT-IR.

2.3.1.3. Characterization of the Sol Material using IR Spectroscopy

Major difficulties arose in the discrimination of the Si-O-Si and Si-O-C asymmetric stretches because the peaks attributed to these two stretches are in close

Figure 2.5: Panel A - ESI-MS spectra of Si_1:Gly_0 sol sample

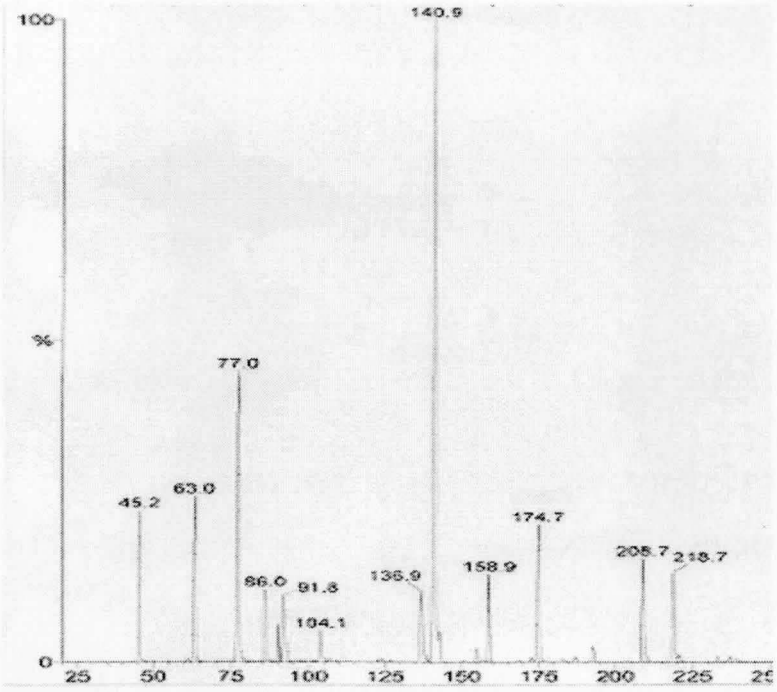

Figure 2.5: Panel B - ESI-MS spectra of Si_1:$Gly_{0.60}$ sol sample

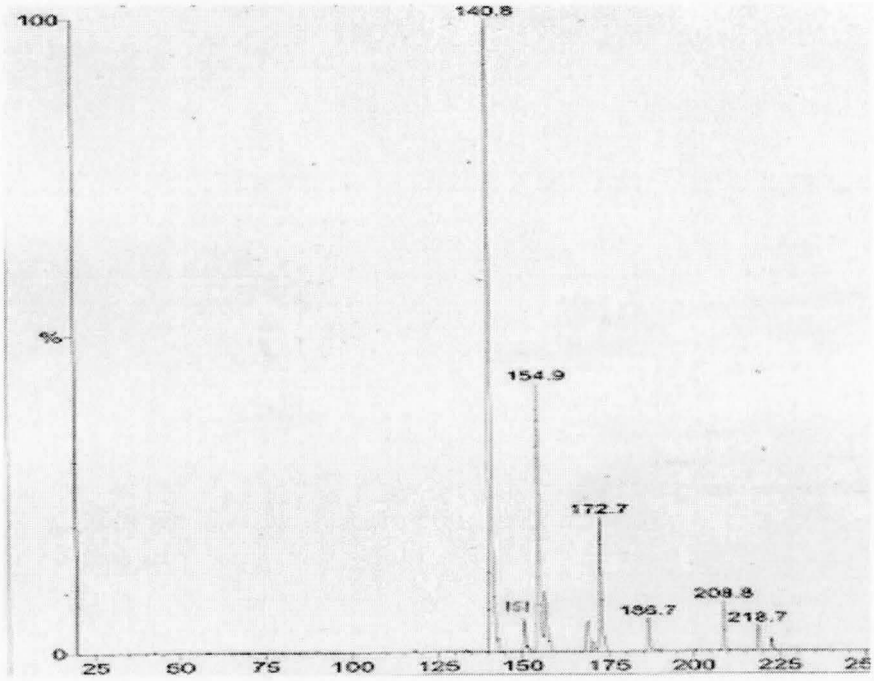

Figure 2.5: Panel C - ESI-MS spectra of Si_1:$Gly_{4.16}$ sol sample

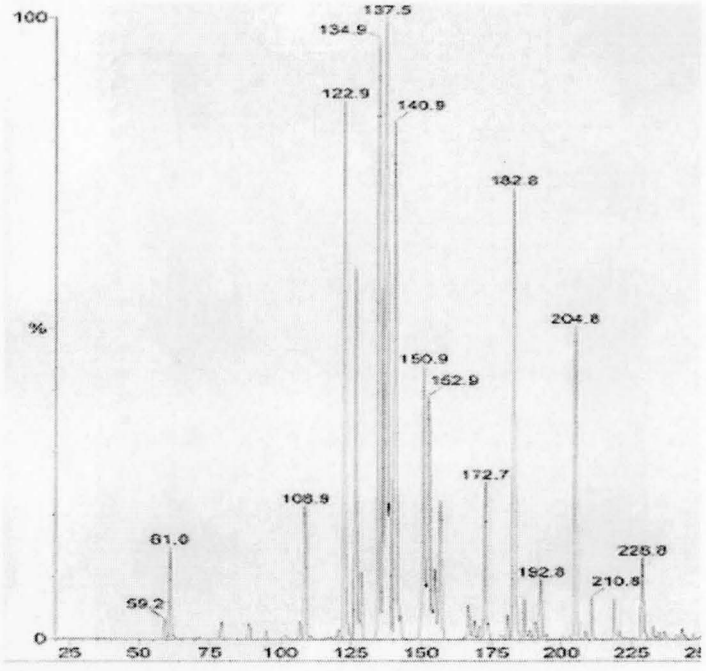

Figure 2.5: Panel D - CID MS/MS of m/z 151 peak in Si_1:$Gly_{4.16}$ sol sample

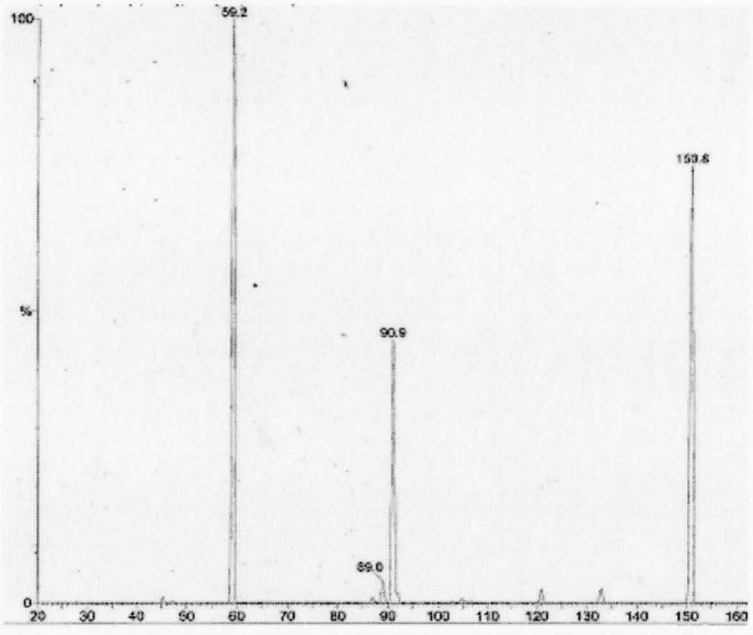

Figure 2.5: Mass Spectra of sol samples Si_1:Gly_0 (panel A), Si_1:$Gly_{0.60}$ (panel B) and Si_1:$Gly_{4.16}$ (panel C) followed by CID MS/MS of m/z 151 in Si_1:$Gly_{4.16}$ (panel D)

proximity and often times their assignments overlap.[23,24] Furthermore, the exact microstructures of the vibrations in the range 1000-1300 cm^{-1} interval were difficult to assign. Table 2.2 provides a list of the solvents used during the hydrolysis and condensation of the sol-gel material, along with the generic classification of the sol material peaks.

Innocenzi used IR spectroscopy to characterize sol-gel derived silica-based film microstructural evolution and showed that certain peak assignments between ethanol and TEOS were indistinguishable and that both had to be taken into account when characterizing the prepared material.[22] The sol-gel materials prepared using our two-step method also had residual EtOH which was still present in the sol and gel material; therefore, care must be taken when assigning peaks to see whether there are overlapping peaks which could be attributed to ethanol.

Table 2.2 shows the characteristic peaks associated with the respective sol materials. These peaks are also present in the aged sol material through the relative intensities vary with time. The TEOS (Si_1:Gly_0) and glycerated (Si_1:$Gly_{0.60}$ and Si_1:$Gly_{4.16}$) sols have similar peaks associated; however, the relative intensities of the peaks vary with the type of sol material generated and the length of time. Representative IR spectra of the sol materials are shown below in Figure 2.6.

As shown in Figure 2.6 the respective peaks of interest are the ~1090cm^{-1}, 950 cm^{-1} and 880 cm^{-1} peaks, corresponding to the ν_{as} Si-O-Si stretch, the ν Si-O_d (Si-OH and Si-O^-) and ν_s Si-O-Si stretching vibration, respectively. The ν_{as} Si-O-Si is in close

Table 2.2: Characterization Using IR Spectroscopy of Sol Material and Solvents Present

EtOH	*Assign*	*Glycerol*	*Assign*	*Si:Gly$_0$*	*Assign.*	*Si:Gly$_{0.60}$*	*Assign*	*SiGly$_{4.16}$*	*Assign.*
3323	νOH	3298	νOH	3325	νOH	3321	νOH	3321	*νOH*
2973	$\nu_a CH_3$	2933	$\nu_a CH_2$	2975	νCH	2975	νCH	2934	*νCH*
1087	ν_a(C-C + C-O)	2879	$\nu_s CH_3$	1084	ν_aSiOSi ν_aSiOC	1081	ν_aSiOSi ν_aSiOC	1417	*CH_2 bend*
1046	δCOH δCCH_3 & ν C-O in alcohol	1414	CH_2 bend	1045	δCOH δCCH_3 & νC-O in alcohol	1044	δCOH δCCH_3 & νC-O in alcohol	1090	*ν_aSiOSi ν_aSiOC*
880	ν_s (C-C + C-O)	1032	C-O stretch in alcohol	952	νSi-O_d	959	νSi-O_d	1040	*δCOH δCCH_3 & C-O stretch in alcohol*
				879	ν_sSiOSi	879	ν_sSiOSi	973	*νSi-O_d*
								879	*ν_sSiOSi*

proximity to the ν_{as} Si-O-C stretch ~1085 cm^{-1} and we have no way of distinguishing between these two stretching vibrations from the peak centered at 1045 cm^{-1}, which is comprised of overlapping peaks.[24,25] Figure 2.7 describes the evolution of the sol material with time. The particular peaks of interest include the Si-O_d (either Si-OH or Si-O^-) and the Si-O-Si/Si-O-C peaks.

Three features merit special attention: 1) with time the ratio of Si-O-X / Si-O_d increased, except for the Si_1:$Gly_{0.60}$ which solidified after 24 hrs, 2) the glycerated sol (Si_1:$Gly_{0.60}$ and Si_1:$Gly_{4.16}$) samples have higher ratios (Si-O-X/Si-O_d), and correspondingly, 3) the sol material with the highest glycerol level of doping, Si_1:$Gly_{4.16}$, had the highest aforementioned ratio. The higher ratio signifies a decrease in the amount of free silanol groups (either Si-OH or Si-O^-) and an increase in Si-O-Si and/or Si-O-C bonds with time. Based on the ^{29}Si solution NMR studies of the glycerol doped sol material, which showed no increase Q^4 and very little increase in Q^3 species with time, therefore the presence of more Si-O-X in the highest doped glycerol sol must signify Si-O-C, showing that transesterification occurs.

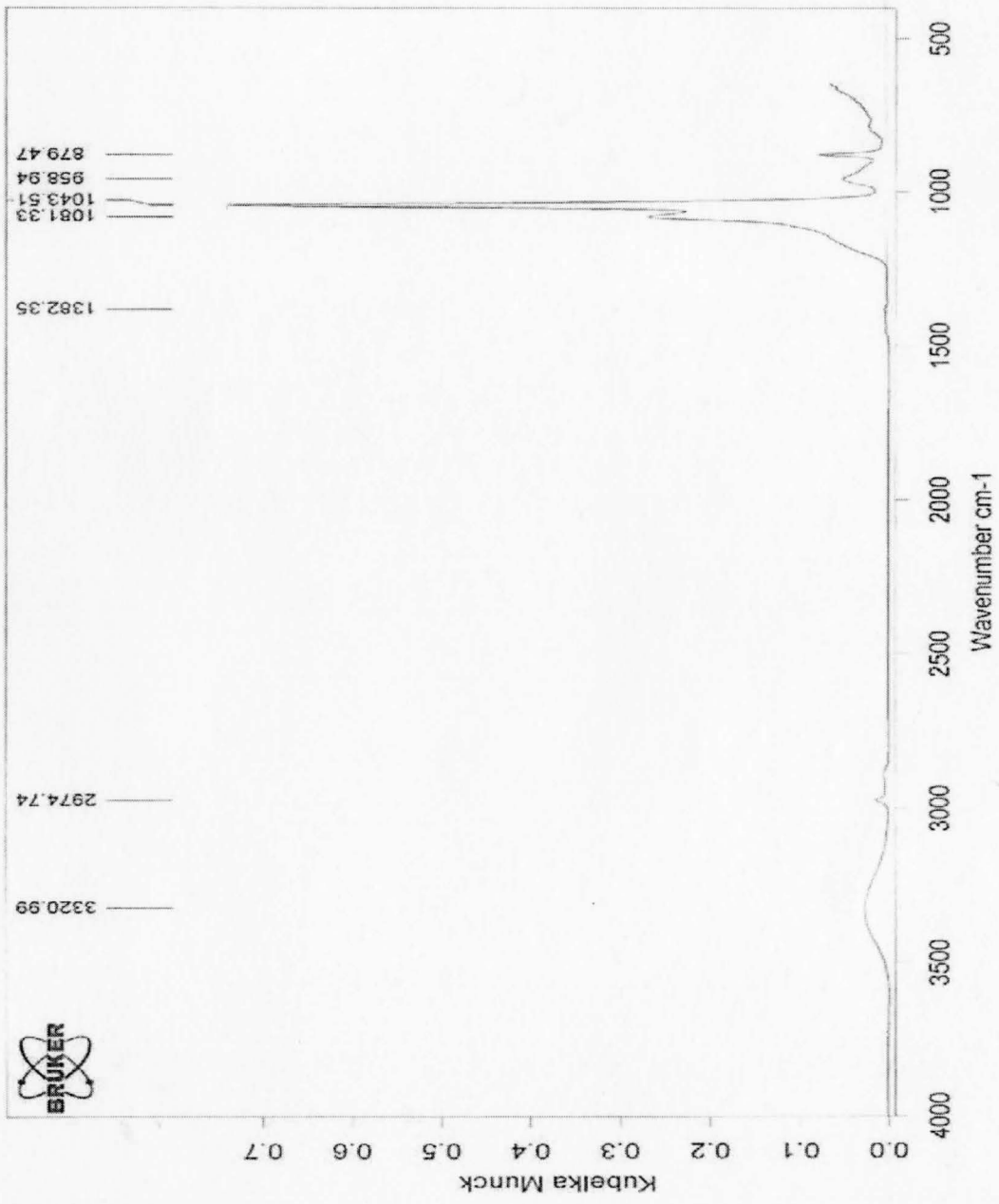

Figure 2.6: FT-IR spectra showing the peaks of interest in the characterization sol-gel material (for both TEOS and glycerol-doped materials) using Kubelka-Munck a.u.

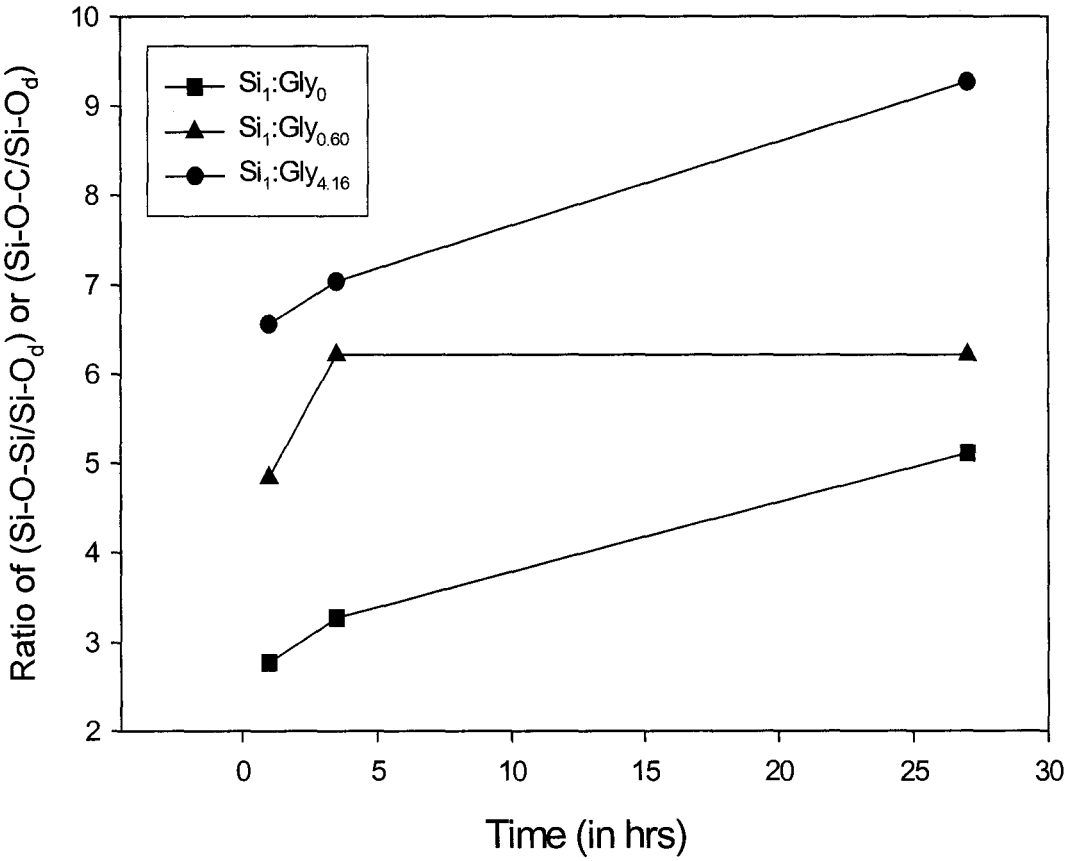

Figure 2.7: FT-IR data showing the evolution of the ratio of the Si-O-X to Si-Od with time for TEOS and glycerol-doped silica sols

2.3.1.5. Summary of the Sol Material

^{29}Si solution NMR data from the sol samples reveal that the glycerol doping increased the extent of the transesterification process, as shown in Figures 2.1 and 2.2. Mass spectrometry analysis of the sol material using negative ESI clearly showed the incorporation of glycerol by the presence of the m/z 151 peak. On performing CID, one of the daughter peaks generated is the m/z 91, which is attributed to a deprotonated glycerol species, and the other was m/z 60. Therefore, negative mode ESI-MS illustrated the incorporation of glycerol by the transesterification process.

Glycerol is a triple alcohol which is capable of interfering in the sol-gel reaction. The presence of glycerol also allows for transesterification reactions to take place, which incorporates the addition of glycerol into the silsequioxane network. In ESI-MS, the products are tested within three hours of formation. This technique allows for the transient species to be detected unlike NMR in which the $(Si\text{-}O\text{-}Gly)_n$ species were not observed.[17,18] FT-IR data of the sol material also showed an increase in the Si-O-X / Si-O_d ratio for the glycerol loaded sols. ^{29}Si solution NMR clearly shows that the Si-O-Si does not increase with higher glycerol doping as illustrated in Figures 2.3 and 2.4. Therefore, the increase of Si-O-X is from Si-O-C, once again suggesting that the extent of the transesterification process increased with glycerol doping.

These findings are consistent with those of the Feldman group, who used dielectric spectroscopy to analyze the internal structures of non-crystalline solids, such as sol-gel derived glassy matrices, with glycerol encaged therein and their mutual interaction.[38] This group group found that glycerol added to the sol-gel derived glass

during preparation was adsorbed and partiallly chemically bound to the ends of the polymer-like siloxane chains, even in aqueous solution.[38]

2.3.2. Characterization of the Gelled Material

2.3.2.1. Gelation of Sol Material

Gelation is the process which results as the sol forms a 3-D network that does not show flow behaviour. The sol-to-gel conversion is a gradual process, which is easily observed qualitatively, but difficult to measure quantitatively. The t_{gel} is not an intrinsic property of the sol.[31] Previous work done by our group and others has demonstrated that gelation is influenced by the size of the container, the solution pH, the nature of the salt, ionic strength, the anion and solvent, the type of initial alkoxy group, and the amount of water. [6,39,40] In this work, the process involving the loss movement upon shaking the cuvette was used to determine t_{gel}. Figure 2.8 illustrates how the gelation times are affected with the addition of glycerol dopant to the silica material.

This figure shows that the gelation time is essentially constant up to a Si_1:$Gly_{0.80}$ ratio (i.e. close to a 1:1 molar ratio of Si:Gly), after which the gelation times increased linearly with increasing glycerol dopant levels. The length of time for the silane to gel, without the addition of buffer, was also examined. The sample Si_1:$Gly_{0.60}$ was the first to gel, within 7 hours on the day it was prepared, the Si_1:Gly_0 took 24 hours to gel, and the Si_1:$Gly_{4.16}$ took the longest to solidify, approximately 75 hours. The increased time of gelation for the highest doped sol material, in the absence of buffer, is consistent with glycerol doping slowing down the rate of condensation and this promoting

transesterification. The Si_1:$Gly_{0.60}$ sol material gelled faster than the Si_1:Gly_0 because of the slight increase in the pH, which resulted from increased levels of the glycerol dopant.

2.3.2.2. Fluorescence Studies of Sol-gel Material

The fluorescent probe used for characterizing the solvent environment in the sol-gel derived materials was pyranine (8-hydroxypyrene-1,3,6-trisulfonic acid, trisodium salt). This probe enabled us to quantify the amount of ethanol present in the pore liquid by examining the ratio of the emission peaks at 515 nm, which is indicative of water, and 438 nm, which is indicative of ethanol.[41] The fluorescence studies (done with pyranine) reveal that there is a 10% decrease in the v/v EtOH that remains in glycerated silane after gelation for the Si_1:$Gly_{4.16}$, as compared to a 35% v/v EtOH in TEOS-based glasses.[42] For Si_1:$Gly_{0.60}$ there was only a 1% decrease v/v EtOH when compared to TEOS.

2.3.2.3. Characterization of the Gelled Material Using Solid State NMR

The gelled material was characterized using ^{29}Si and ^{13}C MAS NMR. The samples analyzed using ^{29}Si solid state NMR had been aged for a month. Figure 2.10 shows the ^{29}Si MAS with the direct excitation of the gelled material. The peaks shown were deconvoluted and integrated. Using direct ^{29}Si excitation it was possible to quantify and compare the relative intensities of species between samples. The chemical shifts obtained for direct excitation of ^{29}Si MAS were similar to literature values, and the Q^2, Q^3, Q^4 were similar to those observed in solution.[31,43] As shown in Figure 2.10 below, Q^2, Q^3, and Q^4 silicon sites predominate, with the majority being in the Q^3 and Q^4 silicon sites. There is a decrease in the Q^2 species for all the gelled materials with progressive

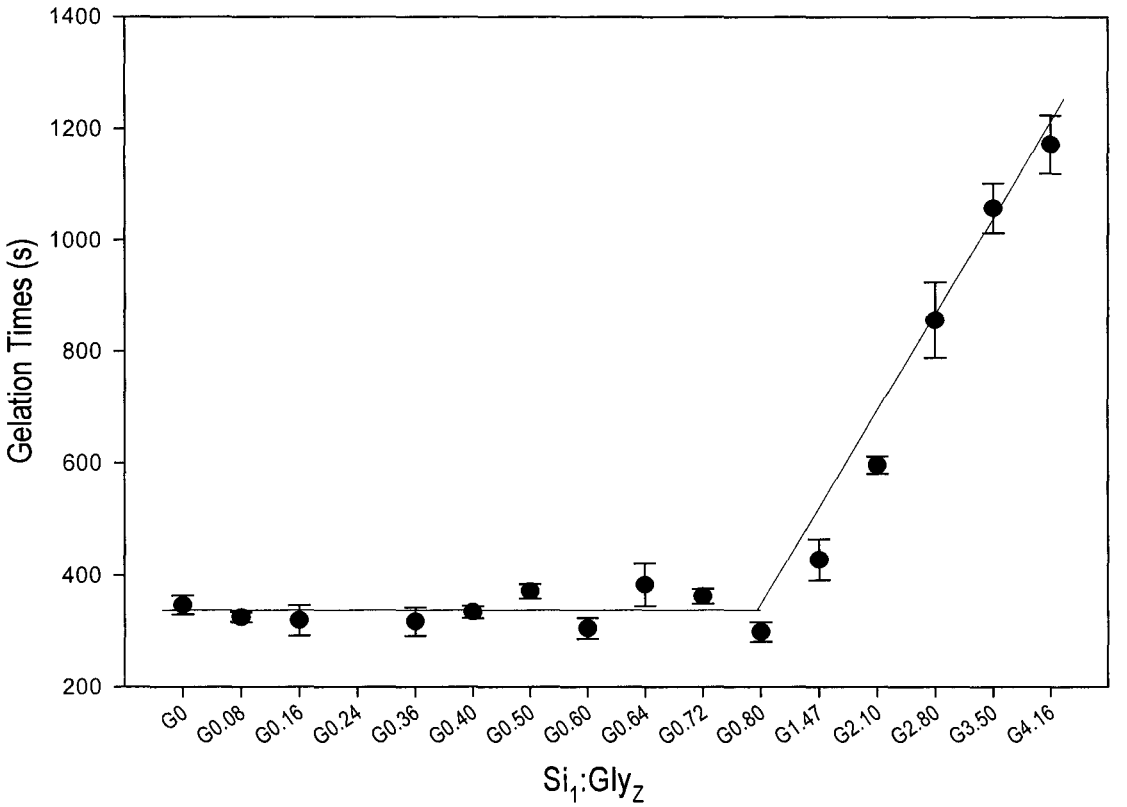

Figure 2.8: Gelation Times versus Sol Material at pH 7.0

shift increase in Q^3 and Q^4 species. However, the ^{29}Si solid spectra look relatively similar with Q^4 being the most abundant followed by Q^3 condensation species, as shown in Figure 2.10.

Figure 2.11 below shows the relative abundance of the condensation species present calculated from the integration of ^{29}Si NMR resonances in the glycerol-doped and undoped (TEOS) sol-gel material. The Q^4 species is most abundant in the $Si_1:Gly_0$ gel sample followed by $Si_1:Gly_{0.60}$ and finally the $Si_1:Gly_{4.16}$ sol-gel. This data is in agreement with previous ^{29}Si solution NMR, and IR sol spectroscopy data which showed that glycerol did not promote condensation. This trend is also observed for the gelled materials in which the Q^4, Q^3 and Q^2 condensation species are most prominent in the $Si_1:Gly_0$ followed by the glycerol doped $Si_1:Gly_{0.60}$ and $Si_1:Gly_{4.16}$ samples, respectively.

For the solid state ^{13}C NMR spectra of samples, which were aged for at least a month, there are obvious differences in the spectra of the TEOS-based gel materials and those of the glycerated silanes. The $Si_1:Gly_0$ gel shows peaks at 15.88 ppm and 58.05 ppm corresponding to CH_3 and CH_2 groups present in TEOS with the EtOH byproduct. This result proves that either there is still some partially unhydrolyzed species present in the gel or that there is a significant amount of ethanol either free or adsorbed within the gel material, as shown in panel A of Figure 2.12. On the other hand, the ^{13}C NMR spectra of the glycerated silanes, $Si_1:Gly_{0.60}$ and $Si_1:Gly_{4.16}$, display the 62.43 ppm and the 72.88 ppm peaks as shown in Figure 2.12 (panel B). These peaks are assigned to the CH_2 group and the –COH groups, respectively. The glycerated gels show no CH_3 groups and none of the CH_2 groups from ethoxy show up either, had they done so they

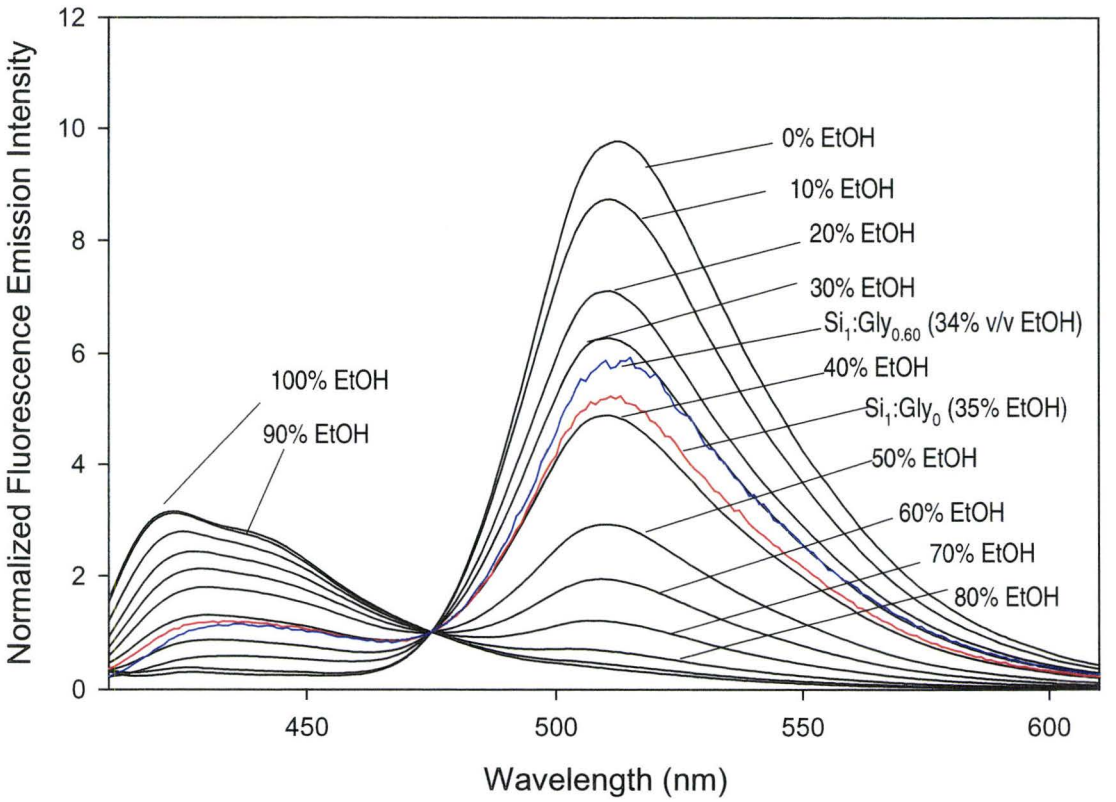

Figure 2.9: Normalized Fluorescence Emission Spectra Si_1:Gly_0 (TEOS-based sol-gels) and glycerol-loaded sol-gel (Si_1:$Gly_{0.60}$) the % v/v EtOH monitored using the 438 nm peak of pyranine

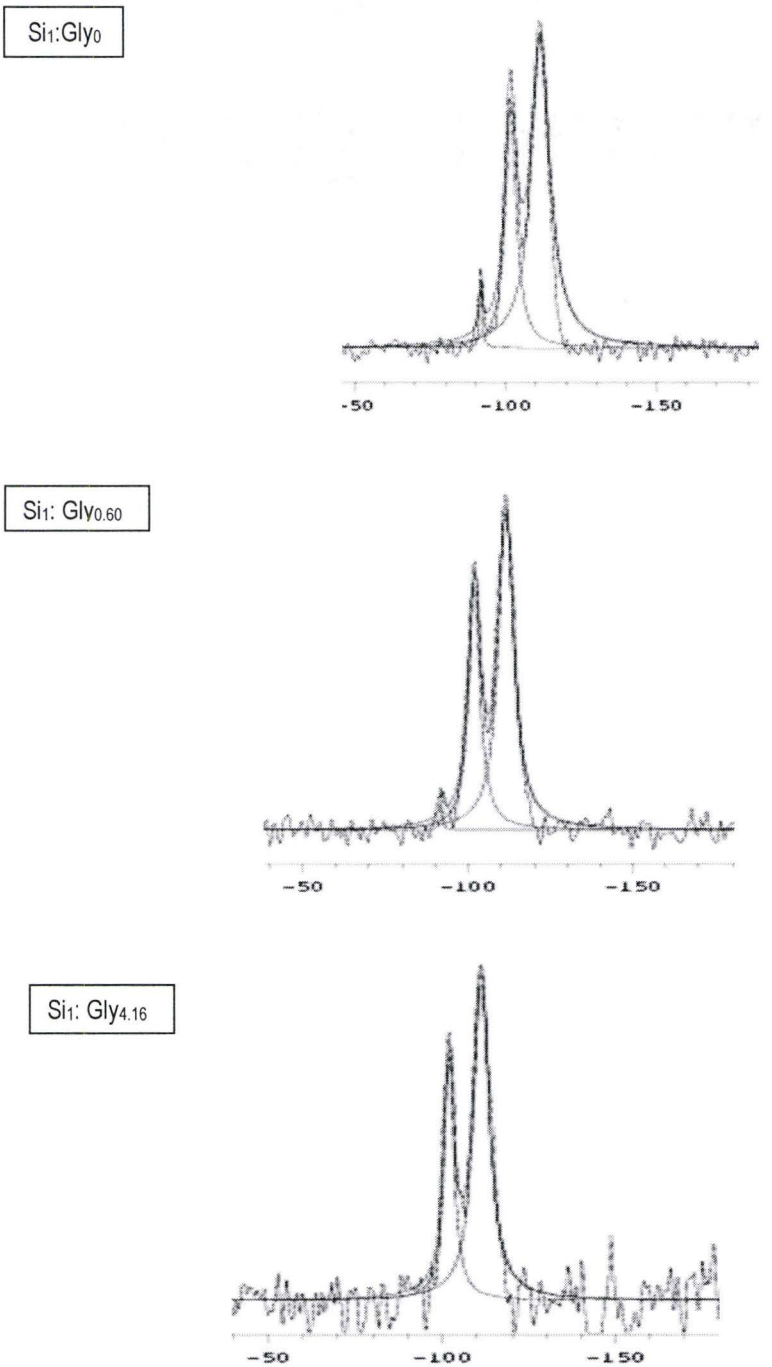

Figure 2.10: Direct Excitation ^{29}Si MAS of the TEOS-based and glycerol-doped gelled samples

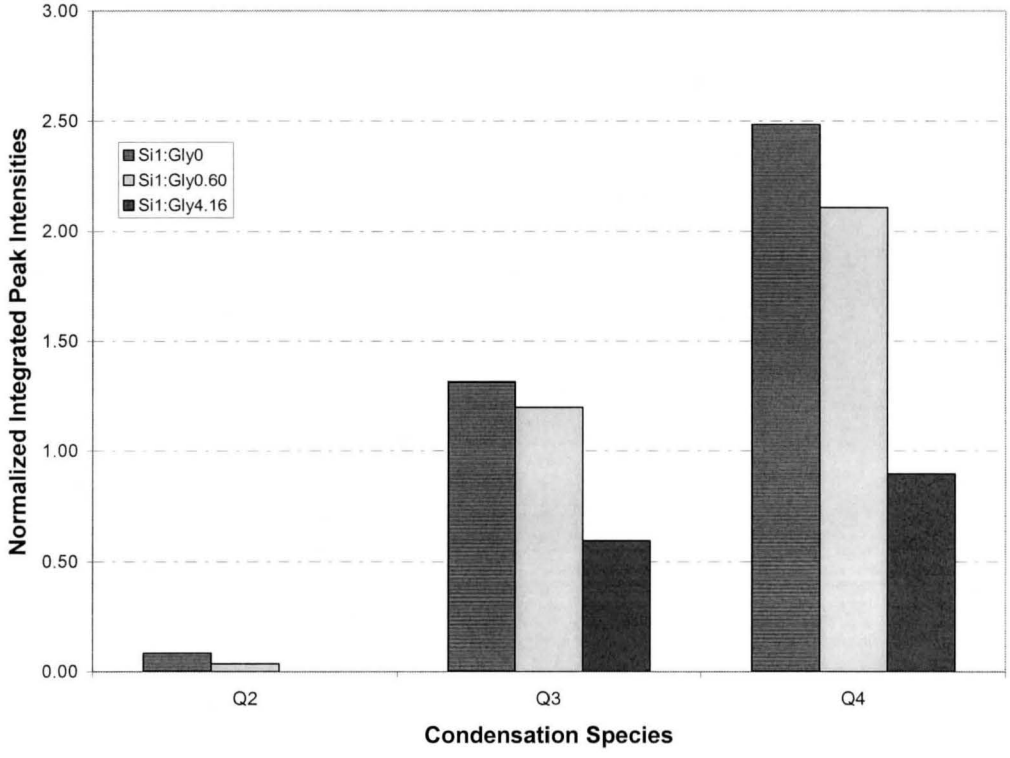

Figure 2.11: ^{29}Si MAS spectral peak intensities normalized to the cumulative peak areas of all the condensation peaks present in the TEOS-based and glycerol-doped sol-gel Materials

would be easily distinguished by the different peaks shifts; this data suggests that there are no unhydrolyzed ethoxy species present and that the level of EtOH present within these gel materials is so small that it is not detectable or ethanol may be invisible to CP due to mobility of the sol. These results are in agreement with decreased initial level of EtOH observed from pyranine studies, and indicate that such materials are likely to be good for protein entrapment.

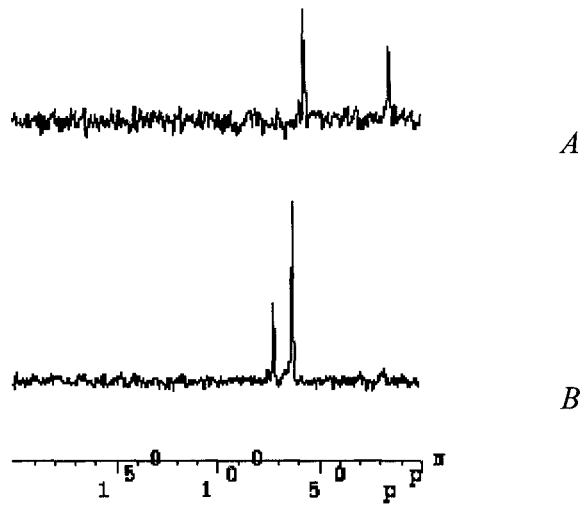

Figure 2.12: ^{13}C CP-MAS NMR spectra of the Gelled TEOS-based and Glycerated Material

2.3.2.4. Characterization of the Gel Material using IR Spectroscopy

In the section above, the sol material was characterized using Infrared Spectroscopy. After gelation of the sol material a gel is formed. By examining the spectra at the various stages of aging predominantly day 1 and 22, the peak at ~1640cm^{-1} shows the presence of water within the sol-gel. The presence of the δ HOH stretch in glycerol-loaded samples at day 22 (not shown) illustrates that more water is retained

relative to TEOS and that glycerol may act as humectant. By day 167, no δ HOH peak is present in Si_1:Gly_0 and glycerol-loaded gels (Si_1:$Gly_{0.60}$ and Si_1:$Gly_{4.16}$). For samples aged 167 days, the ν OH stretch was no longer present in TEOS samples indicating that all of the ethanol had evaporated. Glycerated sol-gel samples (Si_1:$Gly_{0.60}$ and Si_1:$Gly_{4.16}$) however, still had ν OH present which was attributed to glycerol.

2.3.2.5. Shrinkage of the Sol-gel Material

Shrinkage of the gel structure occurs due to the large capillary forces exerted by the pore liquid. Shrinkage studies were performed by determining the volume of the sol-gel on day 1 and following shrinkage in order to calculate the volume by which it had decreased. The changes in volume with aging time are shown in Figure 2.13. The TEOS-based glasses experienced the greatest degree of shrinkage as compared to the glycerol-doped glasses. Even in the early stages of drying the TEOS-based glasses showed a significant amount of shrinkage. By day 102, the Si_1:Gly_0 glasses shrank to <10% of their original volume, while the Si_1:$Gly_{0.60}$ samples shrank to approximately 19% if their original volume. The Si_1:$Gly_{4.16}$ samples had shrunk the least and retained 44% of their original volume. Therefore, the presence of glycerol reduces the amount of shrinkage, as illustrated in Figure 2.13.

This finding is also confirmed by Venkateswara Rao and colleages, who employed glycerol as a DCCA (drying control chemical additive) in the formation of aerogels. The glycerol was shown to actively control the evaporation rate of the solvent from the pores.[44] Hench et. al. also reported the use of drying control chemical additives

in sol-gel chemistry. They observed that the use of DCCAs such as oxalic acid and formamide greatly altered the rates of hydrolysis and condensation reactions and thereby controlled the distribution of pore sizes and solid networks; this modification in turn increased the strength during aging, which caused an increase in the drying rate without promoting cracking.[45] Since large pores tend to shrink more slowly, they are subjected to compressive stresses by the smaller pores. Conversely, the shrinkage of the smaller pores is inhibited by the larger pores, since the former experience tensile stresses. The low percent shrinkage is not unexpected since glycerol is non-volatile and therefore remains inside the matrix, occupying much of the pore volume.

Glycerol may also coat the silicon surface allowing for reesterification to take place as shown in ESI-MS, lengthening the time for the matrix to stiffen and strengthen. Glycerol may also promote the retention of water.[31] This possibility is also in agreement with the δ HOH stretch (of the gelled material) observed in IR studies, which is consistent with retention of internal H_2O. The presence of H_2O in sol-gel material is desirable since it allows for entrapped biomolecules to be preferentially hydrated and retain their native conformation (see Chapters 3 & 4).

2.3.2.6. Optical Clarity

Another characteristic which is of importance for the development of optical biosensors is the percent transmittance of the sol-gel materials. The optical clarity of the sol-gel samples was probed by measuring the percent transmittance at a wavelength of 400 nm, where scattering of visible light would be most pronounced. As shown in

Figure 2.14, the addition of glycerol provides slight improvements in optical transmittance. The higher transmittances for glycerol-doped sol-gels are consistent with a smaller degree of light scattering, which has been shown to improve resolution and linearity of the dynamic response for sol-gel-based sensors.[46,47] Another interesting point which can be drawn from this study is that the glycerol was readily dispersed through the silica matrix, since if phase separation was apparent there would be an increase in scattering and a corresponding decrease in optical clarity. The minor improvement in optical clarity of the glycerated silanes could be a result of a better match between the refractive index of glycerol and silica than the silica, water, ethanol sol-gel mixtures.

2.3.2.7. Pore Size, Structure and Morphology of Gelled Material

The BET surface area and BJH porosity data were extracted from the appropriate isotherms. Figure 2.15 shows the nitrogen adsorption-desorption isotherms of the Si_1:Gly_0, Si_1:$Gly_{0.60}$ and Si_1:$Gly_{4.16}$ samples. Pore morphology can be inferred through the curves of nitrogen sorption hysteresis.[29] Hystersis occurs when the desorption branch does not follow the adsorption branch but gives a distinct loop – the hystersis loop.[27] Following this, sol-gel materials are classified according to types of pore shapes which are determined from the adsorption isotherms and hystersis loops as described by IUPAC standards.[30,31]

In Si_1:Gly_0 glasses, a type I or Langmuir isotherm is observed. Type I physisorption isotherms are usually exhibited by microporous solids having relatively small external surfaces, and a large volume of extremely small pores, as is the case with the TEOS-based materials. The small hystersis loop in the Si_1:Gly_0 sample is generally

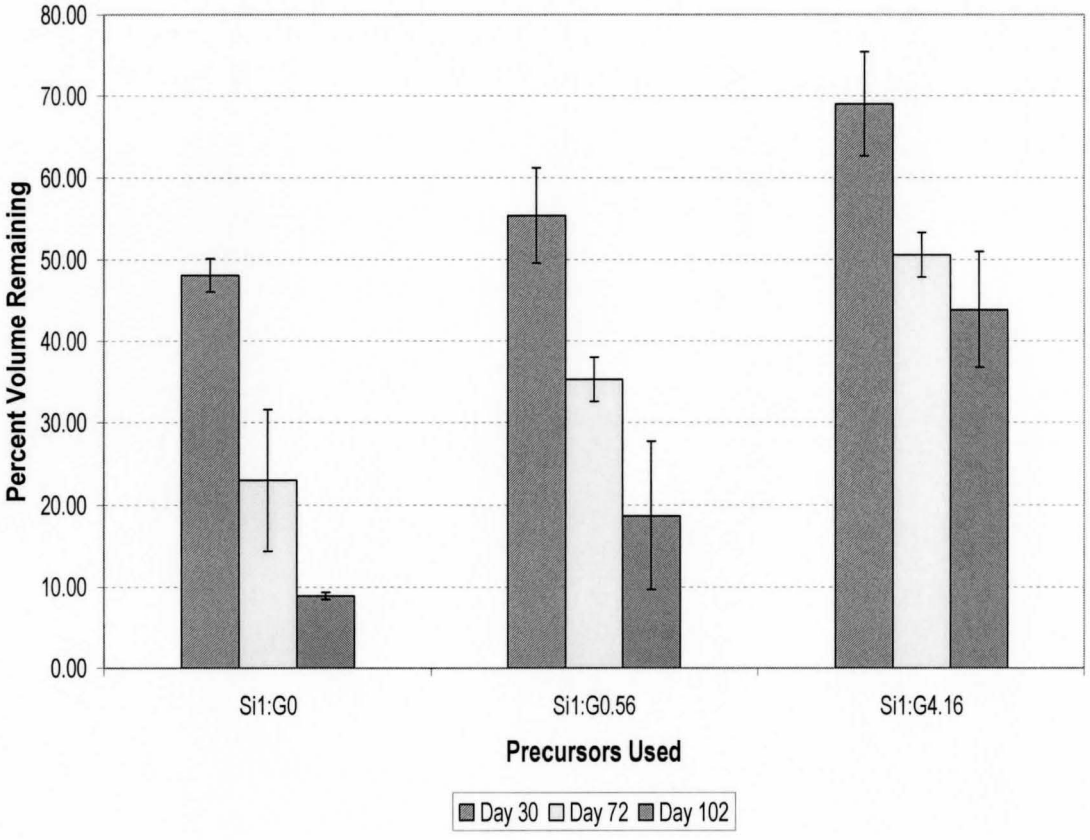

Figure 2.13: Percent Volume Remaining of the TEOS-based and glycerol-doped sol-gels studied

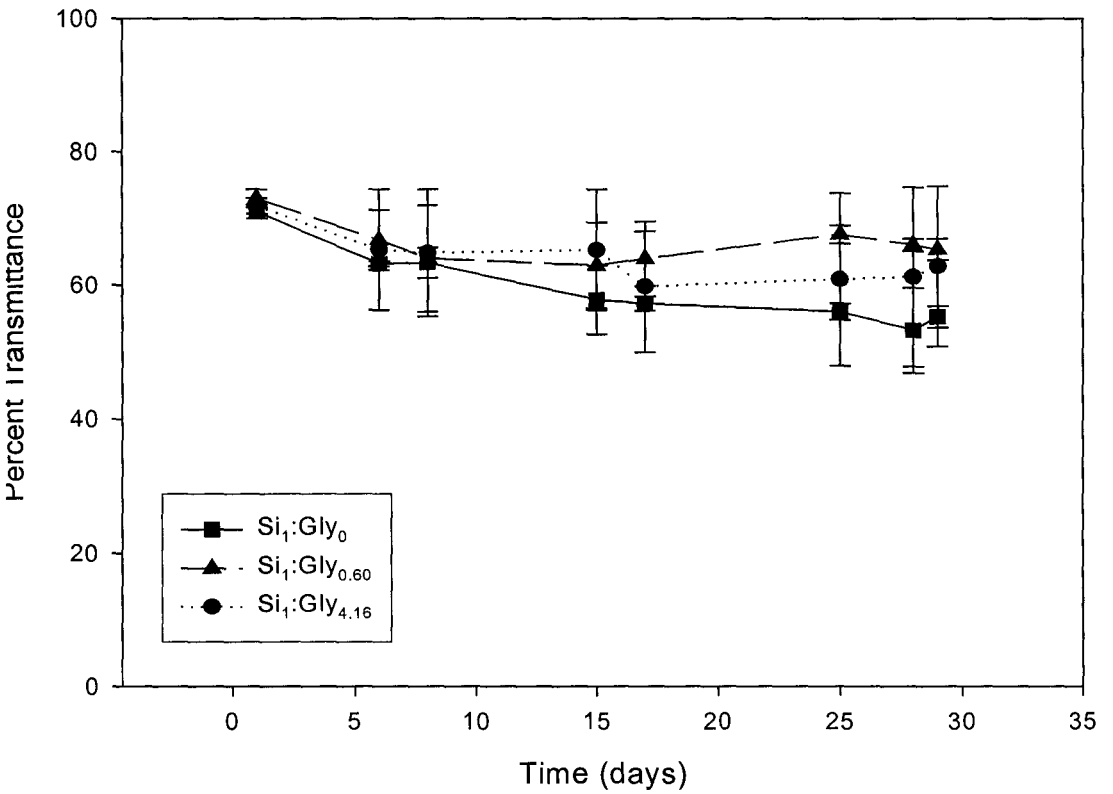

Figure 2.14: Percent Transmittance of sol-gel $Si_1:Gly_0$, $Si_1:Gly_{0.60}$ and $Si_1:Gly_{4.16}$ Samples

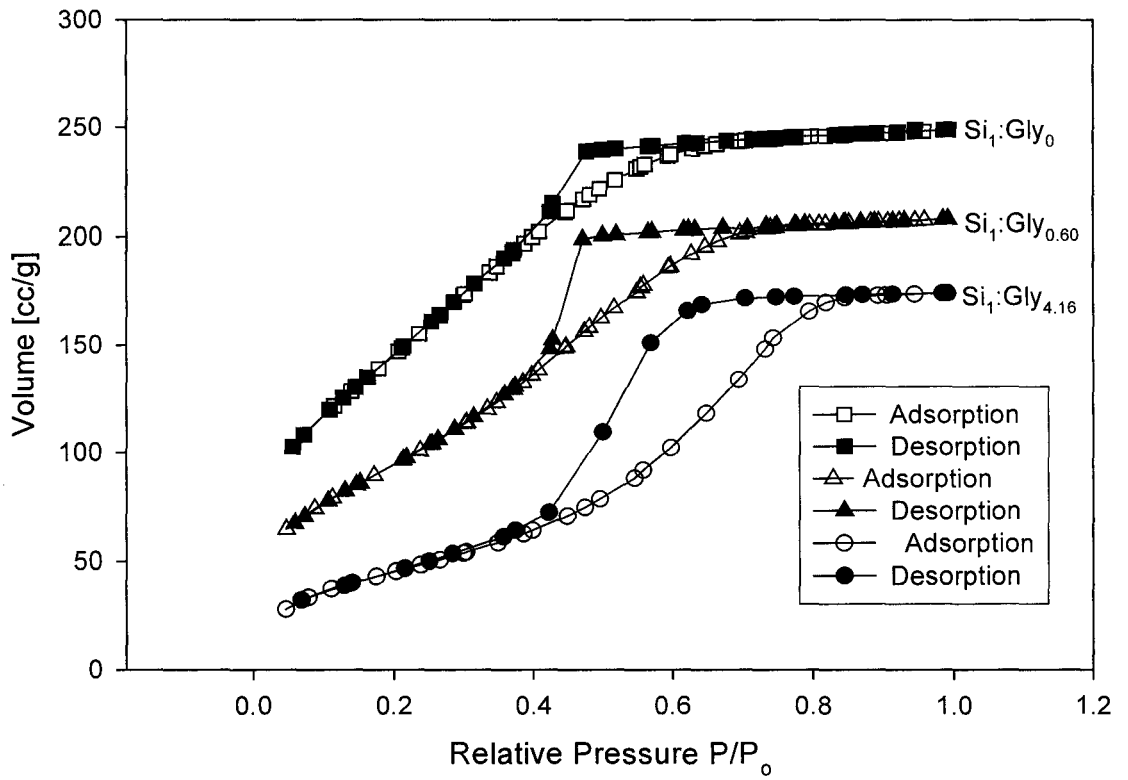

Figure 2.15: Adsorption and Desorption Isotherms of TEOS-based and glycerol-doped sol-gel Materials

interpreted to mean that the pores are smooth and cylindrical. Acid-catalyzed gels formed from TEOS show slit-shaped micropores and have a fibrous or plate-like structure.[30,31] On the other hand Si_1:$Gly_{0.60}$ displays type IV isotherm with H2 hystersis. The hystersis loop is used to assign pore morphology, this type of H2 hystersis displayed in Si_1:$Gly_{0.60}$ is normally attributed to the existence of pore cavities larger in diameter than the openings (throats) leading into them (so called ink-bottle pores). Finally, the adsorption-desorption isotherm for Si_1:$Gly_{4.16}$ resembles that of particulate silica xerogel. For Si_1:$Gly_{4.16}$, with the highest level of glycerol doping, the isotherm is classified as type II with H4 hystersis, which is typical of mesoporous materials that show fewer yet larger pores. The lack of microporosity of Si_1:$Gly_{4.16}$ is further proven by the decrease in specific surface area and pore volume as shown in Table 2.3.

Table 2.3: BET Parameters, Surface Area (S_{BET}), Total Pore Volume (V_P) and Pore Diameter Φ for Gelled Materials

Samples	**S_{BET} (m^2g^{-1})**	**Φ (nm)**	***V_P (cm^3g^{-1})***
Si_1:Gly_0	552.3	2.77	*0.383*
Si_1:$Gly_{0.60}$	357.3	3.58	*0.319*
Si_1:$Gly_{4.16}$	172.3	6.23	*0.268*

This results from the dissolution of small particles (disappearance of small particles and removal of small pores) and the reprecipitation of silica onto larger particles, filling in the

crevices and necks between particles that have negative radii of curvature. Overall, this effect results in a decrease of overall pore volume due to filling in of micropores, and an increase in the proportion of mesopores as shown in Figure 2.16 below. [30]

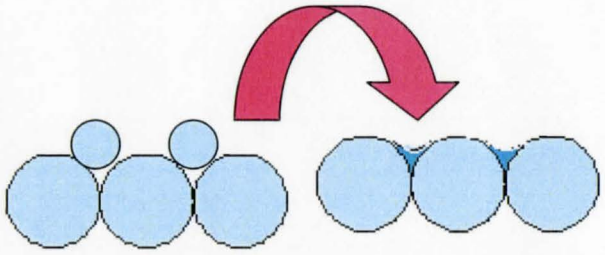

Figure 2.16: Dissolution (of smaller pores) and Reprecipitation of silica into negative crevices (of larger pores)

The corresponding pore size distributions (PSD)s calculated from the desorption isotherm using the Barett-Joyner-Halenda (BJH) alogorithm, assuming cylindrical pores, are presented in Figure 2.17. In Figure 2.17, the shift in the pore size distribution with increasing level of glycerol doping is illustrated. Therefore, using IUPAC-based classification standards, the TEOS-based glasses (Si_1:Gly_0) are microporous in nature (pore diameter < 2 nm). The glycerol-doped samples, both Si_1:$Gly_{0.60}$ and Si_1:$Gly_{4.16}$, are classified as containing mesopores (2-50 nm pore diameter).[30,31] In Figure 2.17, both the Si_1:Gly_0 and Si_1:$Gly_{0.60}$ sol-gel materials display narrower distributions in pore size while

Si_1:$Gly_{4.16}$ glass samples show a wider distribution, between a 27 - 68 Å diameter range, indicating variability in pore size with increased glycerol dopant present.

Braunauer-Emmet-Teller (BET) analysis of the amount of N_2 gas adsorbed at various partial pressures, p/p_o, (at least five points, $0.05 < p/p_o < 0.3$, using nitrogen cross sectional are of $16.2Å^2$) was used to find the specific surface area, S_{BET}, the total pore volume, V_P and the average pore diameter, Φ as shown in Table 2.3.

As indicated in Table 2.3, there is a successive increase in the average pore diameter, with a corresponding decrease in both total pore volume and surface area as levels of glycerol doping are increased. It must be noted that the pore sizes reported in Table 2.3, are those that are present after removal of entrapped water by incubation of samples at 120 °C followed by freeze-drying.[11]

Thermogravimetric analysis (TGA) was performed on the Si_1:$Gly_{0.60}$ and Si_1:$Gly_{4.16}$ samplaes prior to washing and after extensive washing. As a result of the silica network being very stable, the weight loss from the sol-gels arose mainly from ethyl alcohol, water and glycerol decomposition. TGA data shows that with extensive washing the glycerol is completely removed from Si_1:$Gly_{0.60}$; however, for the sample with the most extensive addition of glycerol, Si_1:$Gly_{4.16}$, residual glycerol still remained, which may have coated the surface and therefore decreased the surface area.

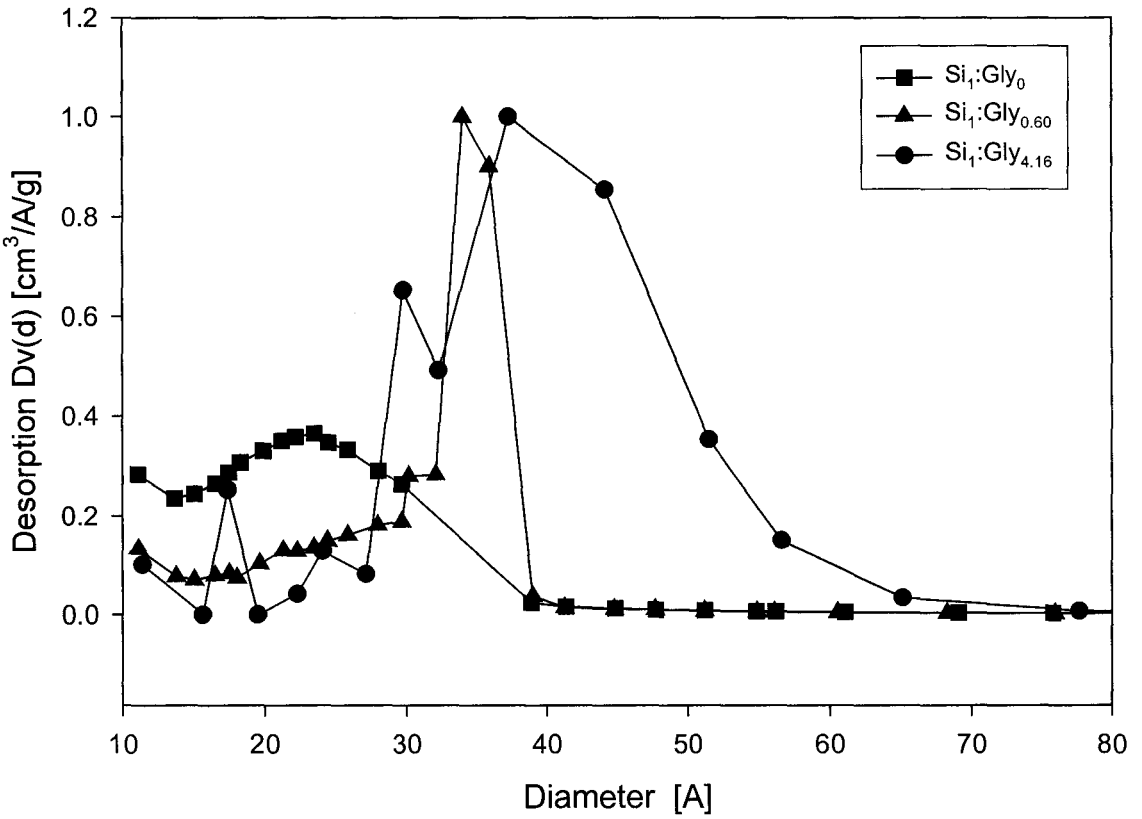

Figure 2.17: BJH Pore Size Distribution of the Sol-gel undoped (TEOS-based) and glycerol doped materials

Contrary to our findings with glycerol, Bright and coworkers noted that PEG-doped materials show no substantial change in geometry and dimensions of the pores. They did observe, however, that there was an overall loss of pore volume and surface area due to the occupation of the otherwise free pore volume by the PEG polymer itself (this group did not wash out the PEG prior to analysis).[48] Therefore, the greater pore size of the glycerol-doped material is likely due to glycerol retaining H_2O and promoting coarsening, which leads to bigger, smoother pores, larger pore volume and lower S_{BET} as observed here. This data is consistent with IR spectroscopy studies performed on the gelled material, which confirm the δ HOH bend (attributed to bending motion of H_2O) present after 22 days of aging.

Following the BET findings, monoliths were made to test whether some macroporsity existed in the Si_1:$Gly_{4.16}$ sol-gels, which could only be observed using SEM analysis, because N_2 sorption is a limiting technique that cannot measure macroporosity (size limit is < 200 nm).[30] Figure 2.18, illustrates that borderline mesopores/macropores exist in the Si_1:$Gly_{4.16}$ gelled sample, relative to the non-porous morphology of Si_1:Gly_0. As can be seen, in part A, of Figure 2.18, the TEOS-based material (Si_1:Gly_0) had a flat surface with no distinctive features (no granular structure). Meanwhile the Si_1:$Gly_{4.16}$ glycerated sol-gel in part B produced a granular image suggesting the presence of mesoporous/macroporous material. Therefore, by adding the glycerol dopant the morphology of the sol-gel material is altered in agreement with the findings of Wei et al.[12,13,44,49]

2.3.2.8. Cracking Studies of Gelled Material

The final parameter determined in the characterization of the sol-gel materials was cracking. The stress that causes cracking is mainly attributed to the internal pressure gradient. As evaporation proceeds, vapor phase and liquid phase exist simultaneously in the pores of the silica gel. If the evaporation rate is relatively high and the gel loses its permeability, an internal pressure gradient will form inside the silica gel and cracking will commence as a result of the flaws at the gel surface in order to reduce this pressure gradient. The flaws at the surface lead to cracks created by way of inhomogeneous capillary forces.[39,50] Figure 2.19 illustrates the bright field images of thin-films of TEOS-based sol-gels and glycerol-doped sol-gel materials.

By looking at the above pictures it becomes clear that with increased glycerol doping there is a corresponding decrease in the degree of cracking of the thin-films. Glycerol-doped silanes of ratios Si_1:$Gly_{0.08}$ to Si_1:$Gly_{0.80}$ display extensive cracking while Si_1:$Gly_{1.47}$ silanes and above show less cracking. This effect is exhibited for thin film samples; for the sol-gel monoliths (be they blocks or discs) with increasing level of dopant, there is a corresponding decrease in the amount of cracking. The Venkateswara Rao group employed additive (glycerol) as a DCCA. This additive was chosen because it actively controls the evaporation rate of the solvent from the pores and therefore reduces cracking. [44]

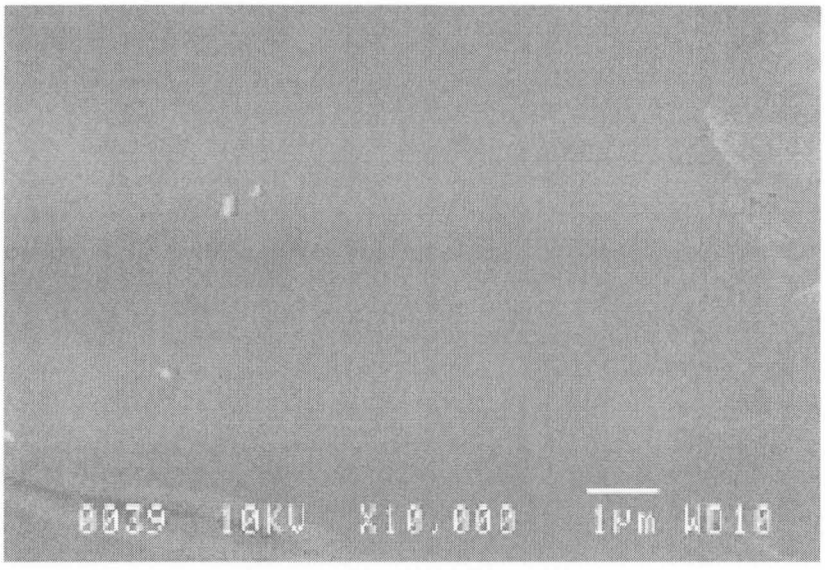

(A) Si_1:Gly_0

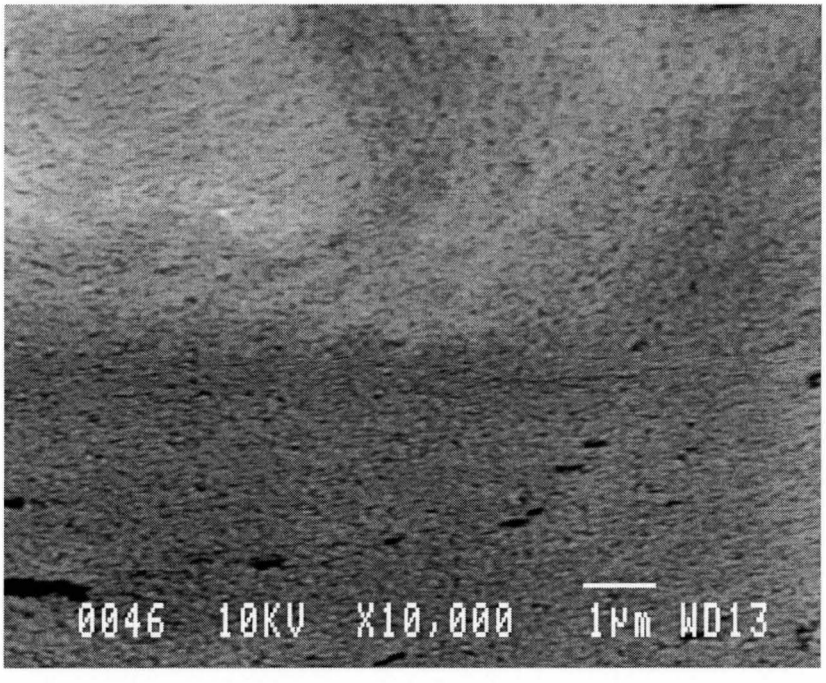

(B) Si_1:$Gly_{4.16}$

Figure 2.18: Morphology of the TEOS (panel A) and Glycerated Materials (panel B)

$Si_1:Gly_0$ - based sol-gel spin cast thin films (Extensive Cracking)

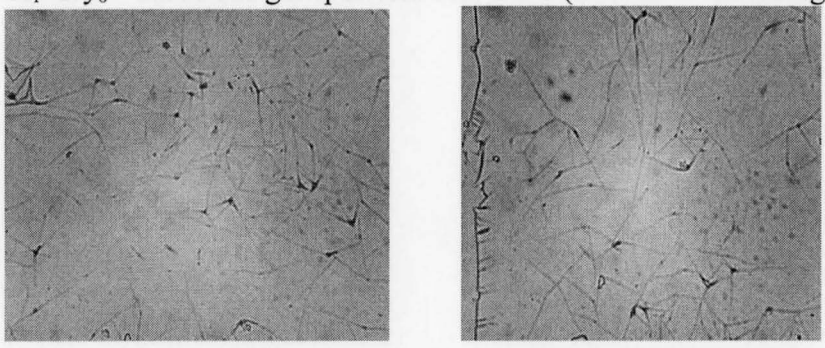

200μm

$Si_1:Gly_{0.60}$ sol-gel thin films

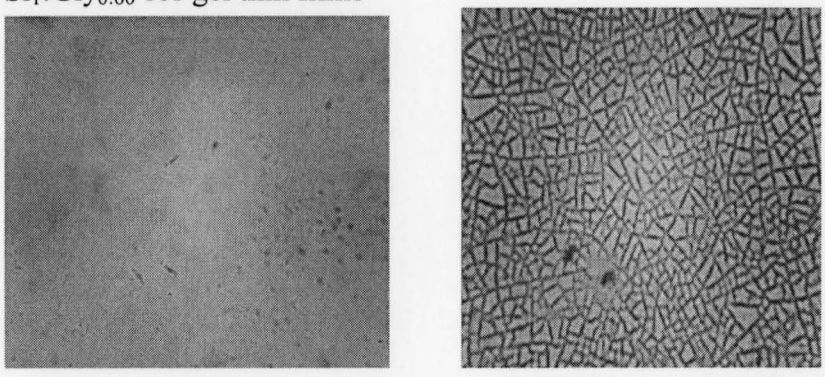

200 μm

$Si_1:Gly_{4.16}$ sol-gel thin films

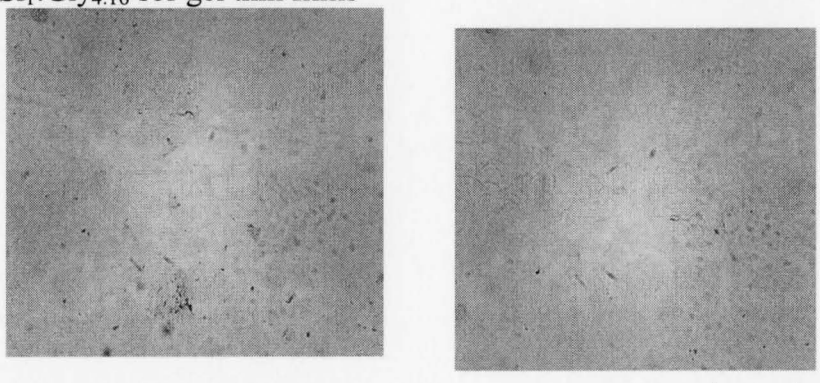

200μm

Figure 2.19: Bright-Field Images used for Cracking Studies of Sol-gel Thin Films Pre-Hydration (left) and Post Hydration (right)

2.3.2.9. *Summary of the Gelled Material*

The ^{29}Si NMR experiments shows that with glycerol doping retards condensation as shown in Figure 2.11. The ^{13}C NMR gelled samples show that in the Si_1:Gly_0 samples there was ethanol present; meanwhile the glycerol-doped gelled materials, Si_1:$Gly_{0.60}$ and Si_1:$Gly_{4.16}$, showed no peaks which were attributable ethanol; only two peaks were observed which are indicative of the presence of glycerol, as is shown in Figure 2.12B. Thermal Gravimetric Analysis (TGA) for both the Si_1:$Gly_{0.60}$ and Si_1:$Gly_{4.16}$ samples showed that glycerol was present in the gelled materials. By classifying the gel material by means of pore size, volume, surface area and morphology, there is an obvious difference between the non-glycerated sample (Si_1:Gly_0) material and the glycerated gels (Si_1:$Gly_{0.60}$ and Si_1:$Gly_{4.16}$). The glycerol-doped gels display larger pore sizes and a change in morphology of the pores with increased levels of glycerol. The traditional characteristics of sol-gels classification are: optical clarity, degree of shrinkage and cracking, all of which showed visible improvements in the glycerol-doped gels (Si_1:$Gly_{0.60}$ and Si_1:$Gly_{4.16}$) as compared to the TEOS-based (Si_1:Gly_0) monolith gels.

2.4. Conclusion

As shown in the above sections, all the methods used to characterize the sol-gel material have shown significant improvement in properties of the glycerol-doped materials relative to the TEOS-based glasses. Through the analysis of the sol and gel material, glycerol has been shown to rapidly transesterify with the silica and remove the ethanol present in the starting sol material. Glycerol then hydrolyzes at pH 7.0 to

generate Si-OH groups which condense rapidly to form condensation products; the following is the most probable model for the incorporation of glycerol in the sol-gel:

$$Si(OEt)_4 + Glycerol + H_2O \rightarrow Si\text{-}(OGly)_n(OH)_{4-n} + nEtOH \qquad (1)$$

Tailoring the porosity of silica-based materials through the use of dopants has emerged as an area of interest. These materials have numerous potential applications in nanotechnology and particular areas of technological interest including cataysis and separation science. Other promising applications including biocatalyst, biosensor, biodiagnostic, and combinatorial biocatalysis arenas exist. The problem of traditional-based biosensors is their length of utility, stability and activity. Traditional biosensor entrapped biomolecules using TEOS suffer extensively from a loss of stability as a result of the denaturing effects of ethanol.[7,8] The materials which are doped with glycerol, a known protein stabilizer, combat the effect of ethanol and extend the longevity of the enzyme under investigation. Indeed, results indicate that, at least for some proteins, the technique may extend the useful stability of biosensors as is explained in Chapter 3.

2.5. References:

1. Narang, U.; Jordan, J. D.; Prasad, P. N.; and F. V. Bright. *Analytical Chemistry.* **1994,** 66, 3139.

2. Ellerby, L. M.; Nishida, C. R.; Nishida, F.; Yamanka, S. S.; Dunn, B.; Valentine, J. S.; and J. I. Zink. *Science.* **1992**, *225*, 1113.

3. Braun, S.; Rapport, S.; Zusman, R.; Avnir, D.; and M. Ottolenghi. *Material Letters.* **1990**, *10*, 1.

4. Edminston, P. L.; Wambolt, C. L.; Smith, M. K.; and S. S. Saavedra. *J. Colloid Interface Science.* **1994**, *163*, 395.

5. Zheng, L.; and J. D. Brennan. *Analyst.* **1998**, *123*, 1735.

6. Avnir, D.; Braun, S.; Lev, O.; and M. Ottolenghi. *Chemistry of Materials.* **1994**, *6*, 1605.

7. Jin, W.; and J. D. Brennan. *Analytica Chimica Acta.* **2002**, *21959*, 1.

8. Gill, I. *Chemistry of Materials.* **2001**, *13*, 3404.

9. Gill, I. and A. Ballesteros. *Journal of the American Chemical Society.* **1998**, *120*, 8587.

10. Eggers, D. K. and J. S. Valentine. *Journal of Molecular Biology.* **2001**, *314*, 911.

11. Brennan, J. D.; Benjamin, D.; DiBattista, E.; and M. D. Gulcev. *Chemistry of Materials.* **2003**, *15*, 737.

12. Wei, Y.; Jin, D.; Ding, T.; Shih, W. H.; Lui, X.; Cheng, S. Z .D.; and Q. Fu. *Advanced Materials –Communication.*

13. Wei, Y.; Xu, J.; Dong, H.; Dong, J. H.; Qui, K.; and S. A. Jansen-Varnum. *Chemistry of Materials.* **1999**. *11*, 2023.

14. Brook, M. A.; Chen, Y.; Guo, K.; Zhang, Z.; and J. D. Brennan. *(Chemistry of Materials - accepted).*

15. Fyfe, C. A. and P. Aroca. *Chemistry of Materials.* **1995**, *7*, 1800.

16. Brennan, J. D.; Hartman, J. S.; Ilnicki, E. I.; and M. Rakic. *Chemistry of Materials.* **1999**, *11*, 1853.

17. Kinrade, S. D.; Hamilton, R. J.; Schach, A. S.; and C. T. G. Knight. *Journal of the Chemical Society – Dalton Transactions.* **2001**, 961.

18. Kinrade, S. D.; Maa, K. J.; Schach, A. S.; Sloan, T. A.; and C. T. G. Knight. *Journal of the Chemical Society – Dalton Transactions.***2001**, 3149.

19. Tacke, R. and M. Muhleisen. *Inorganic Chemistry.* **1994**, *33*, 4191.

20. Hofstadler, S. A.; Bakhatiar, R.; and R. D. Smith. *Journal of Chemical Education.* **1996**, *73*, A82.

21. Cole, R. B., Ed. *Electrospray Ionization Mass Spectrometry: Fundamentals, Instrumentation and Application.* John Wiley & Sons, Inc., New York, **1997**.

22. Innocenzi, P. *Journal of Non-Crystalline Solids.* **2003**, *316*, 309.

23. Whang, C. M.; Yeo, C. S.; and Y. H. Kim. *Bulletin of the Korean Chemical Society.* **2001**, *22*, 1366.

24. Park, O. H.; Eo, Y. J.; Choi, Y. K.; and C. S. Bae. *Journal of Sol-Gel Science and Technology.* **1999**, *16*, 235.

25. Yun, F.; Hinds, B. J.; Hatatani, S.; Oda, W. S.; Zhao, Q. X.; and M. Willander. *Thin Solid Films.* **2000**, *375*, 137.

26. Saito, A. and H. C. Foley. *AIChE Journal.* **1991,** *37,* 429.

27. Sato, S.; Tadahiro, M.; Suzuki, T.; and T. Ohgawara. *Journal of Materials Science.* **1990**, *25*, 4880.

28. Murakata, T.; Sato, S.; Ohgawara, T.; Watanabe, T.; and T. Suzuki. *Journal of Materials Science.* **1992**, *27*, 1567.

29. NOVAWin Operation Manual for Porosimeter.

30. Barton, T. J. et al. *Chemistry of Materials.* **1999**, *11*, 2633.

31. Brinker, C. J. and G. W. Scherer. *Sol-gel Science: The Physics and Chemistry of Sol-Gel Processing;* Academic Press Inc.: New York, **1990**.

32. Barrett, E.; Joyner, L. G.; and P. P. Halenda. *Journal of the American Chemical Society.* **1951**, *73*, 373.

33. Braunauer, S.; Emmett, P. H.; and E. Teller. *Journal of the American Chemical Society*. **1951**, *73*, 373.

34. Engelhardt, G.; Jancke, H.; Hoebbel, D.; and W. Z. Wieker. *Chemistry of Materials*. **1974**, *14*, 109.

35. Magi, M.; Lippmaa, E.; Samson, A.; Engelhardt, G.; and A. R. Grimmer. *Journal of Physical Chemistry*. **1984**, *88*, 1518.

36. Wongcharee, K.; Brungs, M.; Chaplin, R.; Hong, Y. J.; Pillar, R.; and E. Sizgek. *Journal of Sol-Gel Sciences and Technology*. **2002**, *25*, 215.

37. Micromass ESI-MS Manual.

38. Haruvy, Y.; Ryabov, Y.; Arkhipov, V.; Gutina, A.; Axelrod, E.; and Y. Feldman. *Journal of Non-Crystalline Solids*. **2002**, *305*, 226.

39. Wambolt, C. L. and S. S. Saavedra. *Journal of Sol-Gel Science and Technology*. **1996**, *7*, 53.

40. Zheng, L.; Reid, W. R.; and Brennan, J. D. *Analytical Chemistry*. **1997**, *69*, 3940.

41. Dunn, B. and J. I. Zink. *Chemistry of Materials*. **1997**, *9*, 2280.

42. Flora, K. K.; Dabrowski, M. A.; Musson, P. A.; and J. D. Brennan. *Canadian Journal of Chemistry*. **1999**, *77*, 1617.

43. Fyfe, C. *Solid State NMR for Chemists*. C.F.C. Press: Guelph, ON, **1983**.

44. Venkateswara Rao, A.; Pajonk, G. M.; Haranath, D.; and P. B. Wagh. *Microporous Materials*. **1997**, *12*, 63.

45. Hench L. and J. K. West. *Chemical Reviews*. **1990**, *90*, 33.

46. Ulatowska, A.; Kudrawiec, R.; Podbielska, H.; Bryja, L.; and J. Misiewicz. *Optical Materials*. **2001**, *17*, 247.

47. Yuan, X. C.; Yu, W. X.; Cheong, W. C.; and N. Q. Ngo. *Journal of Physics D: Applied Physics*. **2002**, *35*, L81.

48. Baker, G. A.; Jordan, J. D.; and F. V. Bright. *Journal of Sol-Gel Science and Technology*. **1998**, *11*, 43.

49. Wei, Y.; Xu, J.; Dong, H.; Dong, J. H.; Qui, K.; and S. A. Jansen-Varnum. *Chemistry of Materials.* **1999**. *11*, 2023.

50. Haifeng, Y.; Qihui, S.; Bozhi, T.; Songhai, X.; Fuqiang, Z.; Yan, Y.; Bo, T.; and D. Zhao. *Chemistry Materials.* **2003**, *15*, 536.

Chapter 3

Enzyme Viability and Long-term Stability in Glycerol-doped and TEOS-based Sol-gel Materials

A glycerol-loaded, alkoxysilane-based sol was used for the entrapment of highly active biocatalysts into sol-gel-derived silica. Sonication of tetraethylorthosilicate (TEOS) in the presence of water and an acid catalyst at 41 ± 2 °C for one hour afforded a substantially hydrolyzed oligomeric silica product to which glycerol was slowly added over the course of one hour. Addition of buffered aqueous solutions containing the enzymes urease or glucose oxidase resulted in gelation to form a protein-doped nanocomposite silica material. Materials derived from the glycerol-loaded sol provided a major enhancement of enzyme activity as compared to TEOS-derived glasses for the entrapped biocatalysts with optimal activity being highly dependent on the molar ratio of glycerol to silane. Biocatalysts entrapped in glycerol-doped materials showed significantly smaller decreases in activity over a period of one month relative to enzyme entrapped in TEOS. These glycerol-loaded sol-gel materials appear to be well suited for the development of immobilized biocatalysts, biosensors and drug-screening platforms.

3.1. Introduction

The sol-gel process is a low temperature inorganic polymerization method that provides a very convenient route for the immobilization of biomolecules. Sol-gel-derived materials are ideal for the development of bioanalytical devices since they are highly porous, physically rigid, chemically inert, thermally stable, and show little or no leaching of the immobilized species.[1] Furthermore, the matrix often protects the entrapped biomolecule from biodegradation, denaturation, aggregation or precipitation, both during and after entrapment.[2,3]

The majority of sol-gel-derived biocomposites reported to date have utilized alkoxysilane precursors such as TMOS (tetramethylorthosilicate) and TEOS (tetraethylorthosilicate). A major drawback of alkoxysilane-derived materials is that the production of the glass results in the generation of alcohol as a byproduct, which some reports suggest can be as high as 70% (v/v). The alcohol alters the aging of the silica material and, more importantly, can result in significant denaturation of entrapped proteins.[1,2,3] These problems limit the practical utility of such materials for analytical applications such as biosensing. In recent years, modified silica materials have emerged that contain polymer additives, such as PEG (polyethylene glycol) and PVA (polyvinyl alcohol), or polyelectrolytes, such as PEI (polyethyleneimines), which have been reported to improve protein activity; however, these additives do not alter the level of alcohol present in the matrix, and often compromise the optical properties and durability of the resulting material, limiting their application in the development of optical biosensors.[4,5,6]

Recently, Gill and Ballesteros reported on the development of a new class of sol-gel precursors based on polyglycerated silanes (PGS). Their study demonstrated that PGS precursors produced biomaterials that showed superior bioactivity for a wide range of entrapped proteins.[7] However, the synthesis of the PGS precursor was a multi-step process involving several rotory evaporation and refluxing steps, resulting in poor reproducibility and a lack of scalability for industrial applications.

In Chapter 2, the physical and chemical properties of glycerol-doped sol-gels were examined, and it was found that such glasses should be well suited to the entrapment of proteins. In this chapter, the activity of enzymes entrapped in glycerol-doped silica materials is described. Glycerol was chosen primarily due to its well-known stabilizing effects on proteins. This additive also has a relatively small effect on protein structure. Furthermore, it affects the enzyme pKa functional groups minimally.[8,9,10,11] The process involved the incorporation of glycerol into partially hydrolyzed TEOS, followed by addition of an enzyme-loaded aqueous buffer solution to the sol in order to promote gelation and thus entrap the biocatalysts into the resulting silicate materials.[12,13,14] The glycerol:silane ratio in the starting material could be easily adjusted, to optimize the activity of entrapped biocatalysts and to provide Michaelis-Menten and catalytic constants for the entrapped enzymes that were close to those measured in aqueous solution.

Two enzymes of importance for biosensor developments were utilized in this study: glucose oxidase (GOx) and urease. The most prevailing form of urease has a molecular weight of 480 000 Da and consists of two identical, non-covalently linked

enzymatic half units. Each of these half units contains three identical but non-active subunits; as a result, the enzyme is classified as hexameric.[15] The isoelectric point of urease is 4.8 making the enzyme negatively charged at neutral pH.[16] Urease was selected for entrapment within glycerol-doped sol-gels because it has been a relatively difficult enzyme to entrap using traditional sol-gel processing methods.[17,18,19,20] Glucose oxidase catalyses the oxidation of β-D-glucose to D-glucono-1,5-lactone along with the reduction of molecular oxygen to produce hydrogen peroxide. The initial product D-glucono-1,5-lactone hydrolyses spontaneously to gluconic acid.[21,22] Glucose oxidase is a dimeric protein with 583 amino acid residues per subunit and a molecular weight of 160 000 Da.[23] The enzyme consists of two identical polypeptide chain subunits (80 000 Da) covalently linked by disulfide bonds. The isoelectric point (pI) of GOx is 4.2 making it negatively charged at neutral pH.[24] GOx was chosen for the following reasons: 1) wide use for development of glucose sensors based on both electrochemical and optical platforms as reviewed by Gill,[25,26] 2) relatively stable in TEOS-based glasses[27] and therefore provides a useful test case to assess the effects of glycerol-doped glasses on catalytic performance and 3) convenient colorimetric assay. These two enzymes were also chosen since both have neutral analytes which avoid electrostatic effects between analytes and the anionic silica matrix.

Herein, we report on the activity of urease and glucose oxidase in glycerol-doped glasses ([Gly]:Si) and as a function of glycerol doping level and matrix aging. We show that optimal level of glycerol is needed to obtain maximum activity and that under optimum conditions these enzymes retain at least partial activity over a period of one

month, although k_{cat}/K_M does change with time. The results are discussed in light of the properties of the glycerol-doped glasses as discussed in Chapter 2.

3.2. Experimental Section:

3.2.0. Chemicals

Tetraethylorthosilicate (TEOS, 99.999%) was obtained from Aldrich Chemical Company (Oakville, ON). Glycerol (99.999%), and urea (99.9999%) were ordered from Caledon Chemicals (Georgetown, ON). Urease (E.C.1.5.5.1, type IV from Jack Beans, 74, 000 units.g^{-1} solid), Glucose Oxidase (EC 1.1.3.4, type X-S from *Aspergillus niger*, 250,000 units.g^{-1}), Horseradish Peroxidase (EC 1.11.1.7, type VI-A, 1310 units.mg^{-1} solids), hydrogen peroxide (30 % w/v), phenol red (phenolsulfonphtalein), 2-2' azino-bis (3-ethylbenzthiazoline-6-sulfonic acid) diammonium salt (ABTS), rhodamine 6G chloride (R 6G), β-D glucose (minimum 97%) and the Lowry Protein assay kit were purchased from Sigma-Aldrich Chemicals (Mississauga, ON). The Bradford Assay Kit II was purchased from BIO-RAD Laboratories Canada (Mississauga, ON). Water was purified by reverse osmosis and deionized using a 4-stage Milli-Q water purification system. All other chemicals and solvents used were of the highest available grade and were used without further purification.

3.2.1. Preparation of Glycerol-loaded Sol-gels:

The preparation of silane precursor resulted in a final total volume of three milliliters. The total volume was comprised of 2.25 mL of TEOS (99.999%), 0.7 mL of H_2O (d.d)

and 0.05 mL of 0.1 N HCl. The contents of this mixture were sonicated for approximately one hour. After a clear phase was obtained various glycerol:Si mole ratios, ranging from 0.08:1 to 4.16:1, were used to make up the glycerol-loaded sol-gels. Glycerol was added at 41 °C over an hour with continual stirring. Upon complete addition of glycerol, the sol material was ready for use in biomolecule encapsulation.

3.2.2. Determination of Enzyme Concentration:

Glucose oxidase concentration was determined using the $\varepsilon_{280}^{1\%}$=220 800 $M^{-1}cm^{-1}$.[28] For the solution assay, 53 fmol of glucose oxidase was used in a final volume of 0.400 mL. Assays of entrapped glucose oxidase used 70 fmol of enzyme in 0.070 mL sol-gel. Prior to performing a Lowry assay on urease the amount of urease weighted out for solution studies was 0.3 mg, which was dissolved in 10 mL of buffer, to obtain a starting concentration of 0.03 mg/mL; for entrapped samples 20 mg was dissolved in 5 mL of buffer to give a starting concentration of 4 mg/mL. In order to accurately determine the amount of urease present in solution a Lowry assay was performed according to the manufacturer's instruction. After constructing a calibration plot of [BSA] μg/mL versus absorbance, the slope was used to determine the actual concentration of urease in μg/mL prior to entrapment and solution activity studies.[29,30,31]

3.2.3. *Viscosity Studies:*

Rhodamine 6G was used to determine the viscosity of solutions containing varying levels of glycerol. The concentration of R 6G utilized was 2 μM for a 2 mL volume sample. Viscosity was calculated according to the Perrin equation:

$$\eta = \frac{\phi RT}{V} \tag{1}$$

where η is viscosity, T is the temperature (in K), R is the gas constant = 8.3145 J/ K mol and V (expressed in m^3/mol) is the volume of the probe. The probe volume was calculated from the following equation:

$$V = \frac{4}{3}\pi r^3 \tag{2}$$

where r = 5.6 ± 0.1 Å.[32] The solution viscosities were plotted in cP (mPa·s) versus the percent volume of glycerol dopant.

3.2.4. *96-well Plate Assays:*

3.2.4.1. *Solution Assay Activity Studies of Urease and Glucose Oxidase:*

All GOx assays were performed in 96-well plates using the TECAN Safire absorbance/fluorescence platereader operated in absorbance mode. All urease assays were performed in 96-well plates using the Spectra Max absorbance mode. Solution assays of urease were performed by mixing 100 μL of a 0.03 mg/mL solution of the

enzyme in 10 mM HEPES, pH 7.4, with 100 μL of phenol red (30 μg/mL) and 100 μL of the substrate urea (ranging from 0 – 400 mM) dissolved in 10 mM HEPES buffer (either non-glycerated or glycerated) to a final volume of 300 μL. The pH of the urease buffer used was 7.4 because the enzyme activity is known to be dependent upon the pH.[18,33] The absorbance change at 560 nm was then monitored for the next hour in solution using the phenol red indicator. At this wavelength the amount of scattering, as monitored using the 560 nm peak was low in comparison to 400 nm.

Solution assays of GOx activity (100 mM phosphate buffer, pH 7.5) were performed by mixing 134 μL of a solution containing varying concentration of β-D Glucose, with 133 μL of 60.2 mM ABTS/ 1.0μg/mL HRP followed by addition of 133 μL of 0.4 nM GOx. All solutions were present in 100mM phosphate buffer, pH 7.5. The colorimetric response of the probe ABTS (2,2'-Azino-bis(3-ethylbenzothiazoline-6-sulfonic acid) diammonium salt) was monitored at 415 nm for GOx activity studies. Prior to adding either enzyme (urease or GOx) the microtitreplate was stirred for approximately 5 minutes.

3.2.4.2. Urease Activity Sol-gel Discs:

For the 96-well plate sol-gel discs: a volume of 20 μL of the glycerol-doped silane or TEOS sol was added to a volume equivalent of buffer (blank) or enzyme solution (sample – 4 mg/mL prior to dilution). The contents of each microtiter well were mixed thoroughly and a volume total 40 μL of sol-gel was obtained. For these enzymatic assays three different types of precursors were employed: Si_1:Gly_0, Si_1:$Gly_{0.60}$ and

Si_1:$Gly_{4.16}$. Upon gelation, the microtiterplate was covered with Parafilm™ and a hole was punched through the Parafilm™ on top of each well to allow slow drying of the gel to occur. The plates were dry aged and stored at 4 °C until tested. For the urease sol-gel microtitreplate assays, 100 μL of the substrate (0 - 400 mM urea) and a 100 μL of 20.0 μg/mL phenol red indicator were added to the sol-gels. The indicator (phenol red) was added and allowed to equilibrate for (15 - 300 min - longer period of time required for aged gels) and subsequently the substrate was added and the activity of the reaction was monitored using the plate reader. The plates were scanned after one minute intervals and were shaken in between scans.

3.2.4.3. Glucose Oxidase Activity Sol-gel Discs:

A concentration 400 nM of GOx was dissolved in phosphate buffer (100 mM, pH 7.5). In addition to the GOx, a 100 μg/mL, concentration of HRP was co-entrapped with GOx, due to the bi-enzymatic nature of this reaction. Equal volumes of the precursor (35 μL - either TEOS or glycerated silanes) and buffered solution of the enzyme (17.5 μL of GOx and 17.5 μL of HRP) were mixed in a microtiter well (total volume of 70 μL) and allowed to gel. Upon gelation, the microtiterplate was covered with Parafilm™ and a hole was punched through the Parafilm™ on top of each well to allow slow drying of the gel to occur. The plates were dry aged and were stored at 4°C until tested. Assays of GOx prepared with 100 μL ABTS (40 mM) and 100 μL of varying of concentrations of β-D Glucose (0-300 mM), were used. Colorimetric response of the probe ABTS at 415 nm was used to monitor GOx activity.

3.2.5. Enzyme Leaching Studies:

In order to determine whether or not the enzymes had leached out of the sol-gel material, extensive washing (at least 5 times with buffer) of the sol-gel was carried out. Following this, an activity assay was performed on the rinsings to confirm whether or not the enzyme had leached.

3.2.6. Activity Determination of Entrapped Enzyme:

In order to interpret first-order kinetics for a single-substrate enzyme-catalyzed reaction, in which there is one substrate-binding site per enzyme, the Michaelis-Menten Mechanism was used.[34]

The Michealis-Menten equation can be written in its conventional form:[34]

$$v = \frac{V_{\max}[S]}{[S] + K_M} \tag{3}$$

where $V_{\max} = k_{cat}[E]_0$ ($V_{\max}$ is the maximal velocity). Experimental data illustrates that, v, the initial velocity is directly proportional to the concentration of enzyme $[E]_0$ (the total enzyme concentration). However, v, follows 'saturation kinetics' with regards to the concentration of the substrate [S]. The plot of v against [S] is non-linear and thus is not entirely satisfactory for the determination of $V_{\max}$ and K_M (the substate binding constant). This problem was overcome by using a double reciprocal or Lineweaver-Burk plot:[41,34,35,36]

$$\frac{1}{\nu} = \frac{1}{V_{\max}} + \frac{K_M}{V_{\max}[S]} \tag{4}$$

This equation follows the form y = mx + b where y is $1/\nu$ and x is $1/[S]$. For this reason, the Lineweaver-Burk plot of $1/\nu$ against $1/[S]$ is linear with a slope of $K_M/V_{\max}$. Plotting $1/\nu$ against $1/[S]$ gives an intercept of $1/V_{\max}$ on the y-axis when $1/[S]$ equals zero, and an x-intercept of $= -1/K_M$ on the x-axis.[23-28] Therefore, the inverse of the y-intercept gives you the $V_{\max}$ expression. Following this, the K_M value is obtained by multiplying $V_{\max}$ with the slope.

In order to determine the activity of urease and GOx initially the ΔAbs/Δt of the substrate saturated system was divided by ΔAbs/ΔConc term to obtain the ΔConc/Δt value. For GOx the absorbance change of ABTS at 415 nm was monitored for an hour for solution assays and two hours for sol-gel-based assays and was converted to a rate of substrate turnover, ΔAbs/ΔConc, using ε_{max} = 36 000 $M^{-1} \cdot cm^{-1}$. For urease assays a calibration plot of the varying product concentrations (ammonium carbonate), using a constant concentration of indicator (phenol red) was constructed. The linear slope of the absorbance change of the phenol red indicator versus concentration of product gave ΔAbs/ΔConc term. The ΔConc/Δt term (expressed in moles/L/s) was finally converted to Δmoles/Δt term by multiplying by the total volume used. Separately, the moles of urease were determined by converting the mg/mL value into g of solid and then dividing by the molar mass of urease. For GOx the moles were determined by dividing the [GOx] by the total volume. The k_{cat} term for both enzymes (expressed in s^{-1}) was obtained by dividing

Δmoles/Δt term by the number of moles. The catalytic efficiency term was obtained by dividing k_{cat} and K_M.

3.2.7. Optimization of Sol-gel Material used in Enzyme Entrapment:

3.2.7.1. Urease

To find the optimal level of Si_1:Gly_Z doping for urease, crushed glass assays on day 30 sol-gel monolithic blocks were performed. After the monoliths were crushed, approximately 0.02999 g to 0.03100 g of the contents was transferred to cuvettes and spectrophotometric assays, using phenol red as described above in the assays section were carried out. The only difference is the volume added of substrate and indicator which was 1 mL of each as opposed to 100 μL. The optimization assays were conducted in methacrylate cuvettes using the Cary 400 UV-VIS.

3.2.7.2. Glucose Oxidase

GOx was also optimized using varying levels of Si_1:Gly_Z doped materials, instead of running time consuming crushed glass assays, the optimal glycerol doping level was determined using a titremetric plate (where each column corresponds to varying glycerol doped precursor). The sol-gel discs were aged for 5 days as opposed to 30 days for the urease crushed glass assays. A shorter length of time was used due to the decreased volume of the sol-gel discs and the more rapid aging of the sol-gel discs.

3.3. Results and Discussion:

3.3.1. Enzyme Activity Reactions:

3.3.1.0. Urease

Urease catalyzes the hydrolysis of urea to ammonia and carbon dioxide via the intermediate formation of carbamate:

$$(NH_2)_2CO + H_2O \longrightarrow NH_3 + H_2NCOOH \quad (5)$$

$$\longrightarrow 2NH_3 + CO_2 \quad (6)$$

Carbamate is unstable and spontaneously decomposes to yield a second molecule of ammonia and carbonic acid. In aqueous solution ammonia and carbon dioxide generates a net increase in pH.[37,38,39]

The urease assay used phenol red, monitored at a fixed wavelength of 560 nm. Upon the generation of ammonium carbonate as the by-product of the enzyme catalysis, there is an increase in pH which was monitored by the phenol red indicator, which underwent a colour change.

3.3.1.1. Glucose Oxidase

The chromogen used in the colorimetric assay for the determination of β-D glucose was 2,2'-azino-bis(3-ethylbenzothiazoline-6-sulfonate) – ABTS.[40] This assay is a coupled enzyme reaction, where the enzyme glucose oxidase breaks down β-D-glucose to form gluconic acid and hydrogen peroxide. In turn, horseradish peroxidase utilizes the hydrogen peroxide and the chromophore ABTS (reduced form) to produce the oxidized

form of ABTS as well as molecular hydrogen and oxygen, which are by-products of the reaction.[41]

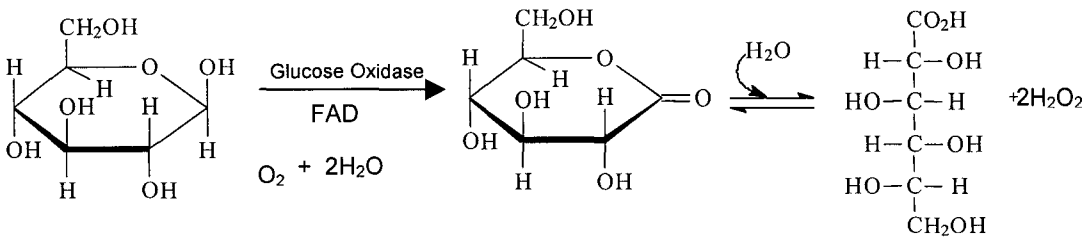

(7)

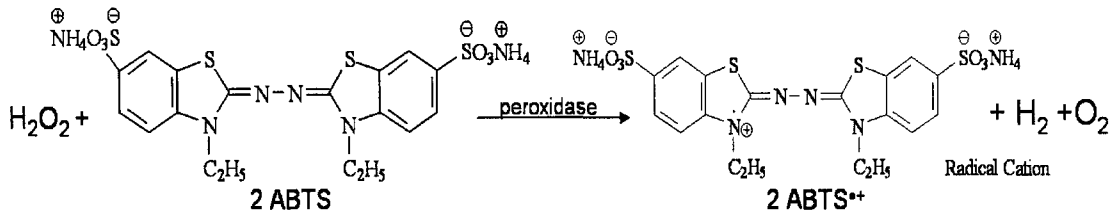

(8)

The colour of the solution gradually becomes green; indicating *ABTS*$^{\bullet+}$ (oxidized product) formation followed by UV-VIS spectroscopy at a fixed wavelength of 415 nm. The reasons for selecting this assay over others included the following: (1) specificity for peroxidase, (2) stability with a well-defined visible absorption spectrum, and (3) inherent chemical stability and (4) is non-toxic.[40]

3.3.2. Preliminary Activity Studies:

Urease was entrapped within a sol-gel using the traditionally employed method (Si_1:Gly_0) and randomly chosen glycerol-loaded sol-gels (Si_1:Gly_Z) in order to determine whether an enhancement in activity would be observed as a result of the glycerol additive. As Figure 3.1 illustrates, urease, within the glycerol doped sol-gel material

Si_1:$Gly_{0.60}$, is highly active, requiring approximately ten minutes to reach saturation. Meanwhile, Si_1:Gly_0 has yet to experience any substantial rise.

Following our initial confirmation that the glycerated sol-gels did in fact enhance the stability of entrapped urease, as illustrated in Figure 3.1, we proceeded to see if an optimal level of glycerol doping exists for urease and GOx.

3.3.3. Leaching Studies

Leaching studies were performed on the entrapped enzymes by extensively washing the sol-gel discs and/or the crushed monolithic glasses. Afterwards, activity assays were run on the rinsings in order to determine if the biomolecules had leached out. No detectable leaching of either enzyme from the sol-gel matrices was observed during the time course of the aging study. Therefore, all changes in activity are due to alterations in the catalytic efficiency of the entrapped enzyme. It is thought that the lack of leaching is a consequence of biomolecule-directed templating of the developing sol-gel matrix, or the development of extensive protein-silica interactions, or the simple embedding into the inorganic framework.[7]

3.3.4. Optimization of Glycerol Loaded Sol-gels:

Subsequently, both urease and GOx were entrapped in varying levels of Si_1:Gly_Z (where z is representative of the varying glycerol mole ratio with respect to TEOS), to

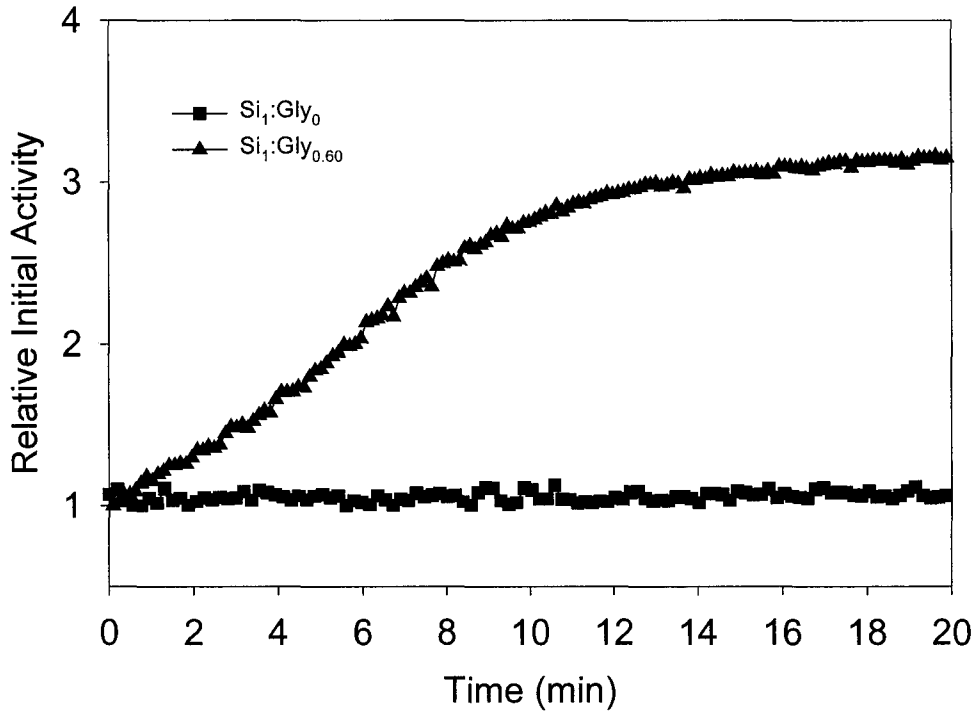

Figure 3.1: Urease Crushed Glass Activity Assay for TEOS and glycerol doped sol-gel after 30 days of aging using the colourimetric pH response of phenol red

determine if an optimal level of glycerol doping existed for the biomolecule under investigation. The urease-doped sol-gel monoliths were crushed because we wanted to ensure that the rate of diffusion was not limiting. If the dimensions of the matrix are large or if there are a large number of very small pores, the enzyme molecules buried inside the matrix encounter a substrate concentration significantly lower than that at the surface. If the substrate diffusion is sufficiently slow compared to enzymatic catalysis, the enzyme molecules close to the surface can consume most of the substrate molecules entering the matrix, effectively making the substrate concentration zero in the interior of the matrix.[42,43] Figure 3.2 illustrates that an optimal level of Si_1:Gly_z exists for urease. The crushed urease glycerol-doped sol-gels retained 75 - 80% of their activity (optimal level of Si_1:$Gly_{0.60}$) when compared to TEOS which is equal to 1% activity. Optimizations of glycerol-doped sol-gels on GOx were also performed, as shown in Figure 3.2. GOx being the more rigorous protein did not exhibit as great an enhancement in protein activity as urease experienced. However, this enzyme also experienced an optimal level of glycerol-doping of Si_1:$Gly_{0.80}$ as shown in Figure 3.3.

3.3.5. Activity Assays of Urease and Glucose Oxidase:

Both solution and sol-gel enzyme activity assays were done in 96-well titremetric plates. For solution with no glycerol added, the activity constants obtained for both urease and GOx are in agreement with literature values as illustrated in Tables 3.1 and 3.2. For urease the catalytic efficiency value of our assay was ~ 2-fold lower then the

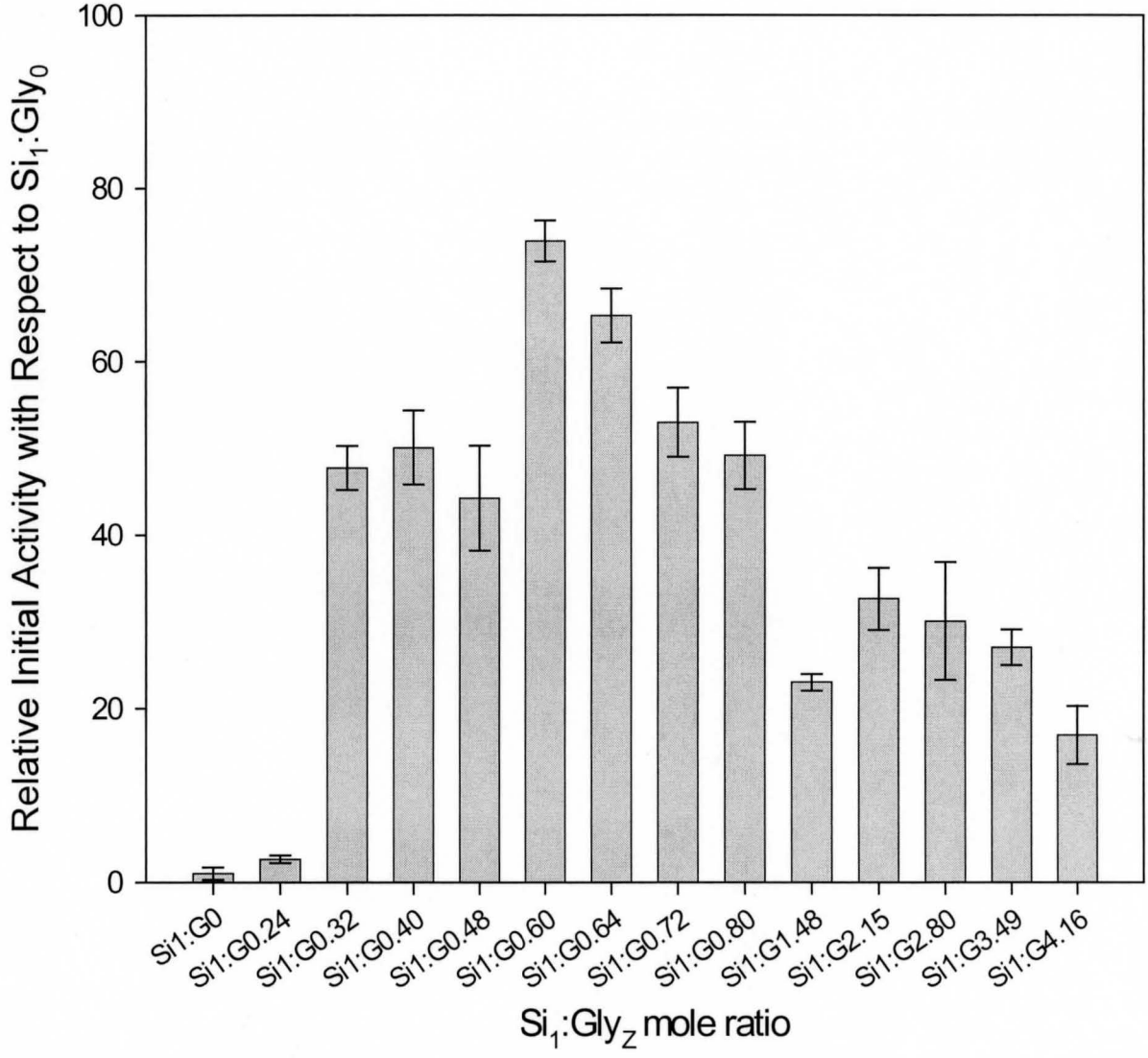

Figure 3.2: Optimized Glycerol-Doped Sol-gels for Entrapped Urease relative initial activity normalized with respect to the activity of the TEOS-based material

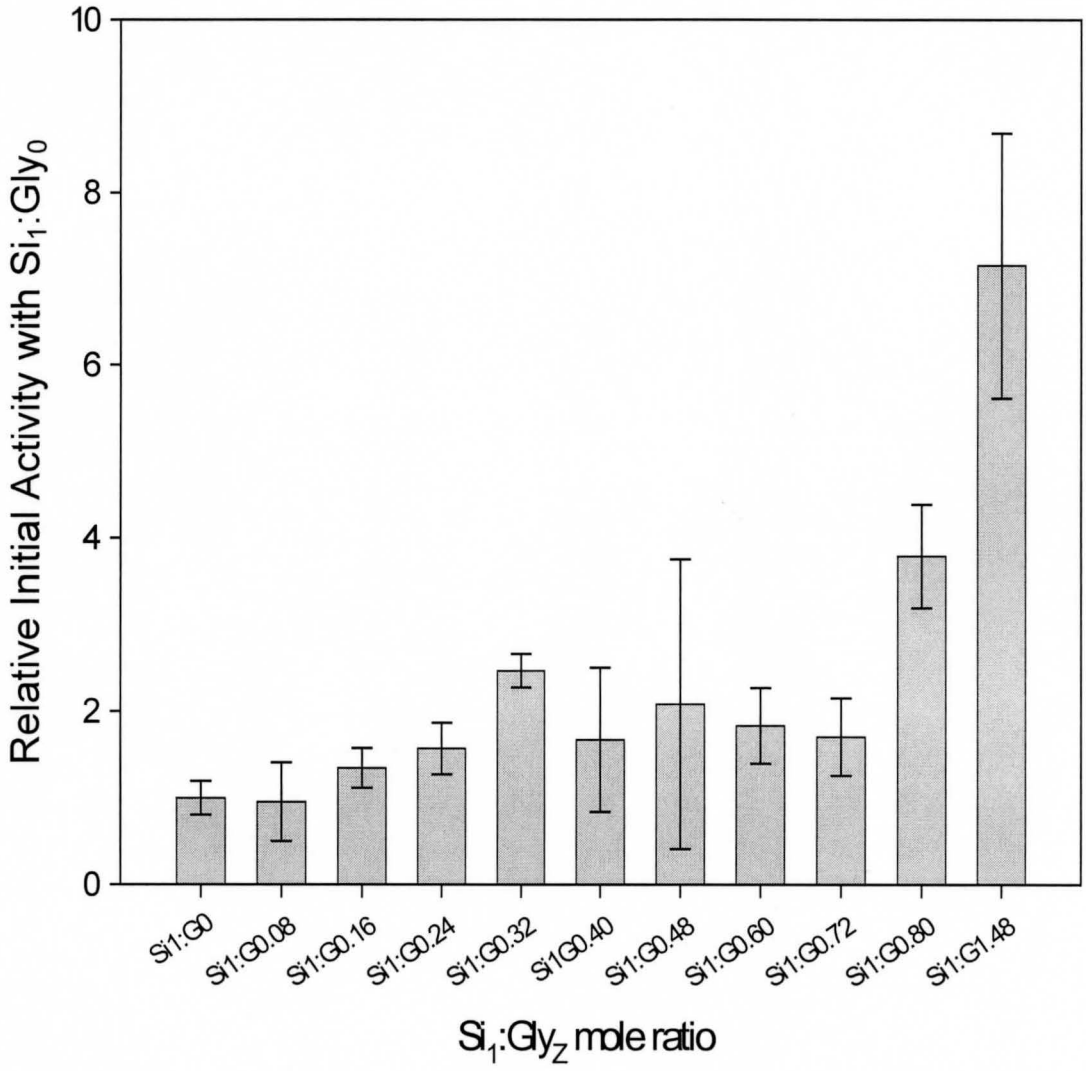

Figure 3.3: Optimized Glycerol-Doped Sol-gels for Entrapped GOx normalized with respect to the initial activity of TEOS-based material

Table 3.1: Urease Enzyme Activity Parameters determined from an average of five measurements

	K_M (mM)	k_{cat} (s^{-1})	k_{cat}/K_M ($M^{-1}s^{-1}$)
Solution			
Literature[38]	3.3	23 400	7.2×10^6
No glycerol	6.3	23 700	3.8×10^6
8.5% v/v glycerol	9.7	9011	780 746
30.1% v/v glycerol	11.8	12 809	919 546
Entrapped			
Day 1			
Si_1:Gly_0	78.8	154.8	1964
Si_1:$Gly_{0.60}$	26.5	187	7060
Si_1:$Gly_{4.16}$	34.1	805	23575
Day 15			
Si_1:Gly_0	Inactive	Inactive	Inactive
Si_1:$Gly_{0.60}$	14.6	3.90	267
Si_1:$Gly_{4.16}$	33.6	51.6	1540
Day 29			
Si_1:Gly_0	Inactive	Inactive	Inactive
Si_1:$Gly_{0.60}$	10.0	2.1	209
Si_1:$Gly_{4.16}$	74.5	27.1	363

Table 3.2: Glucose Oxidase Activity Assay Parameters obtained from an average of five measurements

	K_M (mM)	k_{cat} (s^{-1})	k_{cat}/K_M (M^{-1} s^{-1})
Solution			
Literature[44]	26.0	293	*11 269*
No glycerol	16.0	237	*13 500*
11% glycerol	37.1	341	*9191*
30.1% glycerol	67.9	231	*3460*
Entrapped Day 1			
Si_1:Gly_0	25.6	226	*8820*
Si_1:$Gly_{0.80}$	45.4	263	*5750*
Si_1:$Gly_{4.16}$	51.2	216	*4230*
Day 7			
Si_1:Gly_0	49.3	288	*5840*
Si_1:$Gly_{0.80}$	32.1	247	*7680*
Si_1:$Gly_{4.16}$	35.9	174	*4840*
Day 15			
Si_1:Gly_0	133.3	54.4	*408*
Si_1:$Gly_{0.80}$	29.6	210	*7087*
Si_1:$Gly_{4.16}$	41.3	151	*4020*
Day 30			
Si_1:Gly_0	inactive	inactive	*inactive*
Si_1:$Gly_{0.80}$	85.4	172	*2015*
Si_1:$Gly_{4.16}$	44.5	113	*2540*

literature value.[38] On the other hand, our GOx solution studies, those with no glycerol dopant added, showed a ca. 1.2 fold increase as compared to the literature.[44]Therefore, the activity of GOx used in this study is consistent with literature reported value.

Sol-gel enzyme activity studies were also done in 96-well titremetric plates because crushed glass assays were extremely time-consuming even though they provided more surface area for the interaction of the enzyme with the substrate. In all cases, the enzymatic reactions followed Michaelis-Menten kinetics, allowing for the extraction of kinetic data. The values obtained for our GOx entrapped in a sol-gel environment are in good agreement to those reported by Zink[22,44] and Bright[27,45]. Bright and coworkers only mention $K_M^{'}$ for their sandwich films, which they reported being 15 mM. Zink and coworkers entrapped GOx in TMOS-derived sol-gels and reported its activity using the turnover number k_{cat} and binding constant K_M. The activities of sol-gel entrapped GOx displays similar activity to solution (turnover number: k_{cat} = 250 s^{-1}; substrate binding value: K_M = 50 mM; and a catalytic efficiency value: k_{cat}/K_M = 5000 M^{-1} s^{-1} for aged samples). Our GOx entrapped in TEOS-derived sol-gels, after 7 days of aging, are quite similar to those found by Zink for entrapped and solution samples (k_{cat} = 288 s^{-1}, K_M = 49.3 mM and k_{cat}/K_M = 5840 M^{-1} s^{-1}). Entrapped urease on the other hand, has substantially lower activity constants as compared to solution-based studies. For entrapped urease the literature available only discusses the relative activity, detection limit, dynamic range and long-term stability.[17,18,19] The lower activity could be explained by stating that the entrapped urease is kinetically limited by substrate transport.

As shown in Table 3.1 and 3.2 the entrapment into a sol-gel-derived glass reduced the k_{cat} value of the enzymes, which can be related to a reduced rate of delivery of substrate to the enzyme. This result is expected based on the complicated path that must be taken to allow diffusion of small molecules through the porous network of silica, along with possible substrate silica interaction.[46] For urease, the turnover number, k_{cat}, decreased upon entrapment.

The strength of substrate binding, as reflected by the K_M values, was altered significantly upon entrapment as shown in Table 3.1 and 3.2 for both urease and GOx. Entrapped urease shows a substantial increase in the K_M value. In general, the K_M values of entrapped enzymes increased relative to solution, indicative of weaker binding of substrates to the enzyme. This result is expected owing to the reduction in the rate of transport of the substrates to the enzyme, and is consistent with the reduced k_{cat} values. Since K_M is defined as $\left(k_2 + k_{-1}/k_1^{'}\right)$ for the reaction $E + S \underset{k_{-1}}{\overset{k_1'}{\rightleftharpoons}} ES \xrightarrow{k_2} E + P$ restrictions in mass transport would not affect off-rates (k_{-1} and k_2) but would be expected to lower the k_o value (slower on-rate) which is a component of the $k_1^{'}$ term (where $k_1^{'} = k_1 + k_o$), causing the value of K_M to increase relative to the solution values, as was observed.[47,48]

Overall, the combined effects of K_M and k_{cat} in each of the precursors used resulted in a decrease in efficiency of urease when entrapped, as shown in Table 3.1. Similarly, GOx experienced a decrease in the catalytic efficiency, as revealed in Table

3.2, but not to the extent exhibited by urease. For example, the day after entrapment, TEOS-derived sol-gels doped with GOx (K_M = 25.6 mM, k_{cat} = 226 s^{-1}) showed a ~2-fold lower efficiency than in solution (no glycerol). Meanwhile, the day after entrapment for the urease-doped TEOS sol-gels (K_M = 78.8 mM and k_{cat} = 155 s^{-1}) there was a ~1900 fold decrease in catalytic efficiency when compared to solution (no glycerol present). The substantial decline in the catalytic efficiency of urease can also be due to the denaturing effect of EtOH. Urease is more sensitive to the denaturing effects of ethanol (a by-product generated by TEOS) than GOx and may already be substantially denatured prior to performing day 1 activity assays. The increase in k_{cat} and k_{cat}/K_M terms for the glycerol-doped sol-gels, the day after entrapment, may be due to the decreased levels of % v/v EtOH in the sol-gels as illustrated in chapter 2.

3.3.5. Viscosity Effects

The changes in K_M and k_{cat} are predominantly due to slower diffusion, which results in mass transport limitations of the substrate within the microporous material, suggesting that increases in porosity may be one route to increase the catalytic efficiency of entrapped enzymes. The larger protein, urease, presumably is more restricted by the silica framework and/or experiences a higher trapped solvent viscosity for these materials. Studies done with a fluorescent probe R 6G in solution clearly show that with increased levels of glycerol there is a corresponding increase in viscosity, as illustrated below in Figure 3.4.

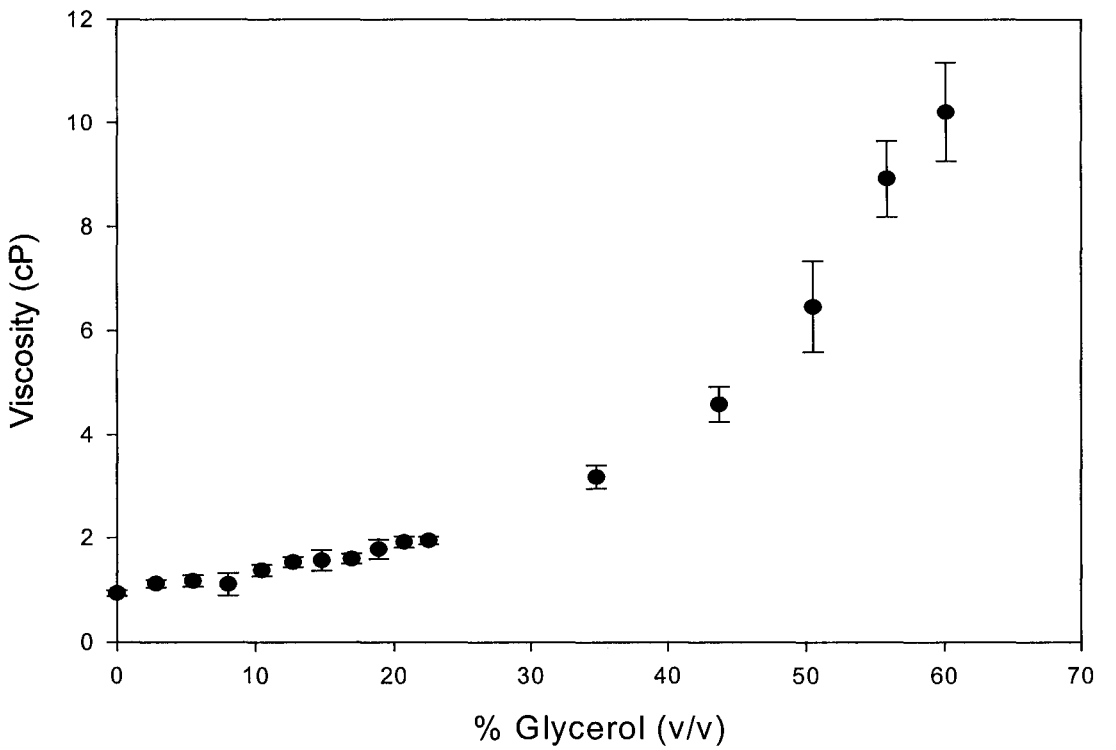

Figure 3.4: Calculated Viscosity measurements (expressed in cP) determined using the fluorescent probe R 6G (using the perrin equation)

M.M. Werber and B. Cavish studied the effects of viscosity on the rate of catalysis of carboxypeptidase A. It was shown that the K_M value increased slightly as a fraction of the organic solvent increased (either methanol or glycerol) k_{cat} on the other hand increased with increasing methanol concentration, but decreased with increasing glycerol concentration.[49]

Indeed, examination of enzyme kinetics in solutions containing glycerol (in which glycerol increases the viscosity and slows down diffusion) confirmed that k_{cat} values were lowered and K_M values increased in the presence of glycerol. For example, GOx in solution has a catalytic efficiency of k_{cat}/K_M = 13 500 M^{-1} s^{-1} (where k_{cat} = 237, K_M = 16.0 mM) however, with increasing % v/v glycerol doping there is a corresponding decrease in GOx catalytic efficiency. For example, 11.0 % v/v glycerol solution (k_{cat} = 263 s^{-1}, K_M = 16.0 mM and k_{cat}/K_M = 9191 M^{-1} s^{-1}) showed ~1.5 fold decrease in catalytic efficiency as compared to non-glycerated solution; likewise 30.1 % v/v glycerol solution (k_{cat} = 231 s^{-1}, K_M = 67.9 mM and k_{cat}/K_M = 9191 M^{-1} s^{-1}) displayed a 4-fold decrease in efficiency. For GOx, k_{cat} value decreases correlate with increased viscosity (increased % v/v glycerol dopant) as shown in Figure 3.2. This trend was not observed for urease, even though there was a decrease in k_{cat} and an increase in K_M on going from non-glycerated to glycerated solutions. The level of % v/v glycerol added affected the K_M value in the usual way, however, the enzyme did not display a slower turnover number, k_{cat}.[47,50]

For urease these results confirm that the presence of glycerol in glycerol-loaded sol-gel materials, coupled with the inherently slow diffusion of material through such matrices, likely contributed to the decrease in catalytic efficiency of the enzymes upon entrapment due to mass transport limitations, but at the same time provided improved stability, thereby resulting in an overall improvement in enzyme performance relative to TEOS-based glasses.

Another potential factor which could influence the altered K_M value is the partitioning of the substrate between the solution and the silica matrix. Silica is both anionic and polar therefore partitioning of charged analytes is likely to occur (increased partitioning for cations and exclusion of anions). Substrate-silica interactions (electrostatic interactions) did not occur for either urea or β-D glucose because both of these substrates used were neutral in charge therefore partitioning was not relevant. However, the GOx assay is a bi-enzymatic reaction as shown above in equations 7 and 8. In the second half of the reaction, the H_2O_2 generated by GOx and a negatively charged substrate, ABTS, interacts Horseradish Peroxidase (HRP) through a redox reaction to determine the activity of GOx indirectly. Therefore, the difference in the enzymatic rate constants between Si_1:Gly_0 and glycerol-doped sol-gels (Si_1:$Gly_{0.60}$ and Si_1:$Gly_{4.16}$) may be due to the electrostatic interactions between ABTS and the negatively charged surface of the silica matrix.[40] ABTS may be excluded from the matrix; as a result, the K_M value increased, so that more substrate is needed for the reaction to continue (k_{cat} and V_{max} are

unaffected by partitioning). However, the partial charge screening likely plays a role in offsetting this effect, leading to K_M values similar to the glycerol-doped sol-gels.

3.3.6. Long-Term Stability Studies

Having proved the general utility of glycerol-loaded silicate-derived bioencapsulates using initial activity values, we then examined their performance with respect to aging time. All samples (urease and GOx sol-gels) were dry aged at 4 °C until tested. One reason for the variability in the activity constants with aging is almost certainly due to the inter-sample variability that is present within all test systems to a certain degree.

It was found that the biosensor response gradually decreased over the elapsed time as shown in Figures 3.5 and 3.6. The urease activity parameters clearly illustrate that enzyme stability and durability is extended through the use of glycerol as an additive. In all the days tested the TEOS-based material had a lower activity than glycerol-doped materials. In our studies TEOS-based materials displayed no activity by day 15. Meanwhile, Lee and coworkers show a urease electrode using an alkoxysilane precursor (TMOS), retaining its activity after 25 days of storage.[18,19] However, there was visible difference in the preparation of the urease sol-gels by our two groups which would explain the extended shelf-life of their biosensor. Lee and coworkers stored their sol-gel in 5.0 mM imidazole-HCl buffer at 4 °C when it was not used, we on the other hand dry-aged our samples at 4 °C. Also, when preparing the precursor for sol-gel preparation, we used it immediately after sonication, while they refrigerated their sol for a day (decrease

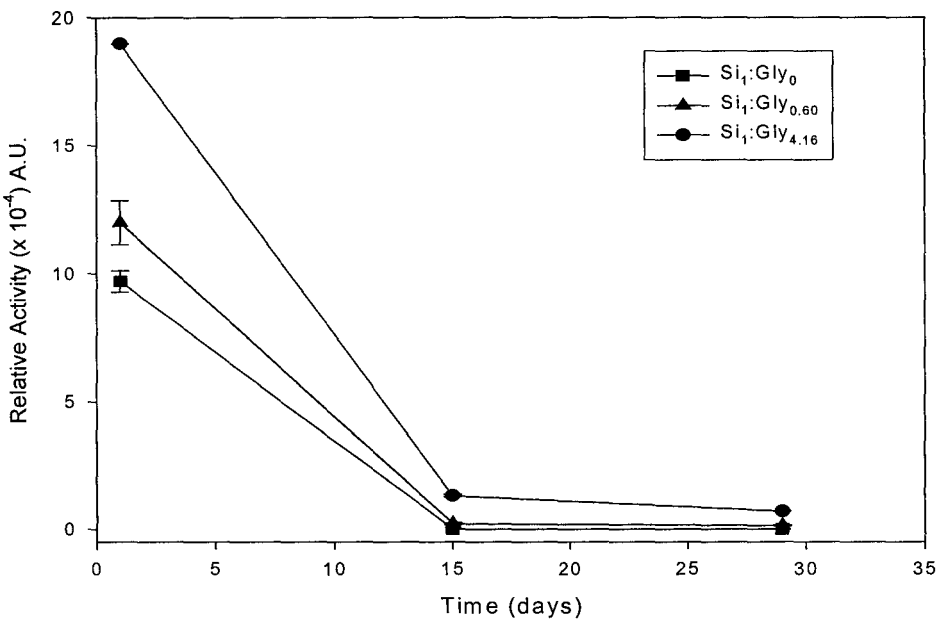

Figure 3.5: Relative Initial Activity of Urease with time data averaged over five samples

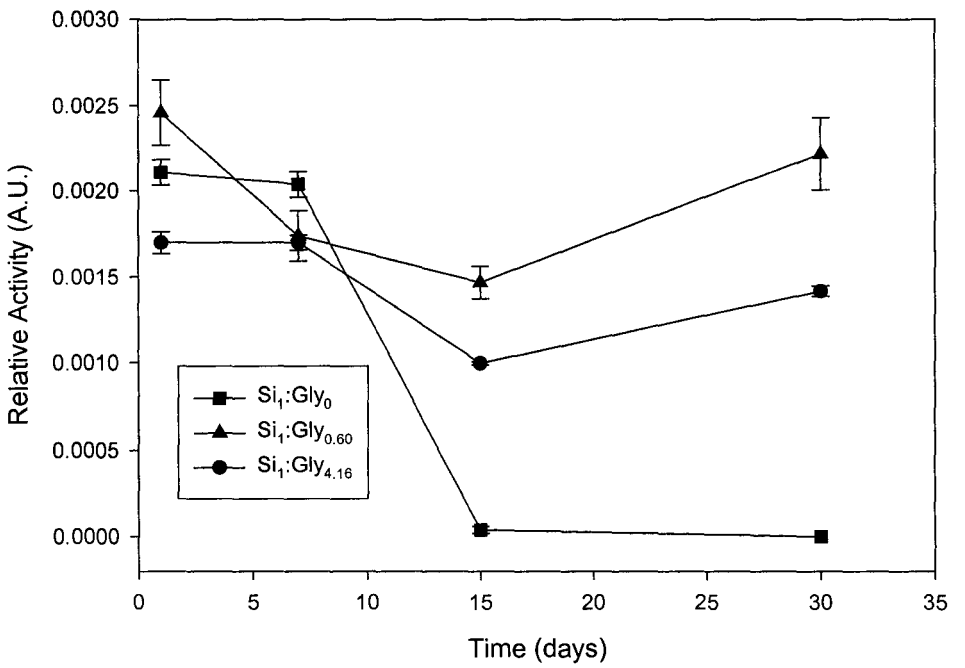

Figure 3.6: Relative Initial Activity of GOx with time data averaged over five samples

in % v/v EtOH) and entrapped urease the following day.

Glucose Oxidase has been shown to be stable in TEOS-based materials and was used in this study to see whether glycerol-doping improved the activity of GOx. Results in Table 3.2 show that with increased time of aging glycerol did indeed impart stability to the entrapped GOx. For the activity of day 1, TEOS-entrapped GOx samples showed higher activity than their glycerol-doped counterparts; this trend, however, was reversed with the aging of the sol-gel material, as illustrated in Table 3.2 and Figure 3.4. By day 30 GOx entrapped in TEOS was no longer active, while the glycerated sol-gels still retained significant activity. The decrease in the TEOS-entrapped GOx is due to the denaturation of HRP which was co-immoblized. Partial loss in the HRP activity (up to ~ 25%) has been reported when using the regular sol-gel encapsulation process. TEOS-derived glasses generate alcohol as a byproduct of the hydrolysis and condensation reaction of the sol-gel process. Bright and coworkers report an activity for their TMOS sol-gel:GOx:sol-gel sandwich films of ~ 2 months.[27] This activity time is a month longer than our fininding for the TEOS-derived sol-discs. The response of the physisorbed GOx-based sandwich sol-gel thin films was recorded by immersing each film in a solution containing the dye, HRP and 10% β-D Glucose, whereas HRP was co-immobilized with GOx in our sol-gels. Therefore, one can safely conclude that glycerated silanes retained their activity, and that the presence of glycerol extends the shelf-life of the entrapped enzyme.

3.4. Conclusions and Future Outlook:

These findings suggest that the enzymes are accessible to externally added reagents. It appears that variations in K_M values between solution and entrapped enzymes are likely to be based on mass transport limitations (K_M) between the solution and glass (increasing K_M). Specific interactions of substrate with the silica matrix only affected the GOx activity assays due to the bi-enyzmatic nature of this assay. First, GOx catalyzes the oxidation of β-D glucose by dioxygen to give D-gluconic acid and H_2O_2. Peroxidase then catalyzes the reaction of the negatively charged dye precursor ABTS with H_2O_2 to produce coloured dyes. This reaction is a commonly employed method for quantitation of glucose in solution.[27,44] Mass transport also alters the K_M values and it is clear that materials with greater porosity should be used to maximize diffusion rates.

Overall, the long-term stability studies showed that all enzymes had improved activity in glycerol-doped materials relative to TEOS-derived materials. This conclusion is not surprising since TEOS-derived materials may contain up to 35% ethanol immediately after gelation,[51] which is likely to promote denaturation of entrapped enzymes. On the other hand, glycerated sol-gels contain glycerol, a known stabilizer of proteins, which may cause the protein to adopt a more compact and rigid conformation due to preferential hydration, and thus decrease the specific volume of the protein.[52,53] Glycerol may also act as a humectant, providing greater retention of entrapped water, and may coat the walls of the pores within the silica material thereby reducing direct contact of the protein with the sol-gel matrix. In conclusion, glycerol-doped materials are more

suitable precursors for sol-gel matrices than TEOS with respect to the encapsulation of enzymes.

Biosensor devices where the biological recognition is carried out by enzymes, antibodies, or some other relatively unstable material can be deactivated by the surrounding environment and have a limited lifetime. Second generation materials that have surfaces modified to be either neutral or zwitterionic, and possess larger pores may also prove advantageous for biosensor development as these materials would eliminate both the mass transport and electrostatic partitioning effects.

3.5. References:

1. Ellerby, L. M.; Nishida, C. R.; Nishida, F.; Yamanaka, S. A.; Dunn, B.; Valentine, J. S.; and J. I. Zink. *Science.* **1992**, *255*, 1113.

2. Jin, W. and J. D. Brennan. *Analytica Chimica Acta.* **2002**, *21959*, 1.

3. Gill, I. *Chemistry of Materials.* **2001**, *13*, 3404.

4. Bakul, D. C.; Dunn, B.; Valentine, J. S.; and J. I. Zink. *Analytical Chemistry.* **1994**, *66*, 1120A.

5. Livage, Jacques. *C. R. Acad.Sci. Paris.* **1996**, *322,* Serie II b, 416.

6. Avnir, D.; Braun, S.; Lev, O.; and M. Ottolenghi. *Chemistry of Materials.* **1994**, *6*, 1605.

7. Gill, I. and A. Ballesteros. *Journal of the American Chemical Society.* **1998**, *120*, 8587.

8. Monsan, P. and D. Combes. *Methods in Enzymology.* **1998**, *137*, 584.

9. Timasheff, S. N. and K. Gekko. *Biochemistry.* **1981**, *20*, 4667.

10. Bolen, D. W. and Y. Liu. *Biochemistry.* **1995**, *34*, 12884.

11. Bolen, D. W. and A. Wang. *Biochemistry.* **1997**, *36*, 9101.

12. Eggers, D. K. and J. S. Valentine. *J. Mol. Biol.* **2001**, *314*, 911.

13. Eggers, D. K. and J. S. Valentine. *Protein Science.* **2001**, *10*, 250.

14. Strambini, G. B. and M. Gonnelli. *Biophysical Journal.* **1993**, *65*, 131.

15. Sakaguchi, K.; Mitsui, K.; Nakai, N. and K. Kobashi. *Journal of Biochemistry.* **1984**, *96*, 73.

16. Contaxis, C. C. and F. J. Reithel. *Nature.* **1971**, *246*, 321.

17. Narang, U.; Prasad, P. N.; and F. V. Bright. *Chemistry of Materials.* **1994**, *6*, 1596.

18. Lee, W. Y.; Kim, S. R.; Kim, T. H.; Lee, K. S.; Shin, M. C. and J. K. Park. *Analytica Chimica Acta.* **2000**, *404*, 195.

19. Lee, W. Y.; Lee, K. S.; Kim, T. H.; Shin, M. C.; and J. K. Park. Electroanalysis. 2000, 12, 78.

20. Ogura, K.; Nakaoka, K.; Nakayama, M.; Kobayashi, M. and A. Fujii. *Analytica Chimica Acta.* **1999**, *384*, 219.

21. Allard, L.; Cheynet, V.; Oriol, G.; Mandrand, B.; Delair, T.; and F. Mallet. B*iotechnology and Bioengineering.* **2002**, *80*, 341.

22. Zink, J. I. et al. *Analytical Chemitry.* **1994**, *66*, 1120A.

23. Tsuge, H., Natusaki, O. and K. Ohashi. *Biochemistry Japan.* **1975**, *78*, 835.

24. O'Malley, J. and J. Weaver. *Biochemistry.* **1972**, *11*, 3527.

25. Wang, J. *Electroanalysis.* **2001**, *13*, 983.

26. Reach, G. and G. S. Wilson. *Analytical Chemistry.* **1992**, *64*, 381A.

27. Bright, F. et al. *Analytical Chemistry.* **1994**, *66*, 3139.

28. Swoboda, B. E. P. and V. Massey. *Journal of Biological Chemistry.* **1965**, *240*, 2209.

29. Lowry, O. .H.; Rosenbrough, N. J.; Farr, L. and R. J. Randall. *Journal of Biological* Chemistry. **1951**, *193*, 265.

30. Peterson, G. L. *Analytical Biochemistry.* **1977**, *83*, 346.

31. Bensadoun, A. and D. Weinstein. *Analytical Biochemistry.* **1976**, *70*, 241.

32. Baker, G. A.; Jordan, J. D.; and F. V. Bright. *Journal of Sol-Gel Science and Technology.* **1998**, *11*, 43.

33. Krajewska, B. and W. Zaborska. *Journal of Molecular: Catalysis B: Enzymatic.* **1999**, *6*, 75.

34. Engel, P. C. *Enzyme Kinetics: The Steady-state Approach*; John Wiley & Sons: New York, **1977**, 1.

35. Fersht, A. *Enzyme Structure and Mechanism, 2nd Ed.*; W. H. Freeman and Company: New York, **1985**, 89.

36. Bernard, S. A. *The Structure, Function and Enzymes*; W.A. Benjamin: California, **1968**, 73.

37. Dixon, N. E.; Riddles, P. W.; Gazzola, C.; Blakeley, R. L.; and B. Zerner. *Canadian Journal of Biochemistry.* **1980**, *58*, 1335.

38. Blakeley, R. L.; Webb, E. C.; and B. Zerner. *Biochemistry.* **1969**, *8*, 1984.

39. Hausinger, R. P. et al. *Protein Science.* **1995**, *4*, 2234.

40. Kadnikova, E. N. and N. M. Kostic. *Journal of Molecular Catalysis B: Enzymatic.* **2002**, *18*, 39.

41. Childs, R. E. and W. G. Bardsley. *Biochemistry Journal.* **1975**, *145*, 93.

42. Bhatia, R. B. et al. *Chemistry of Materials.* **2000**, *5*, A.

43. Ballesteros, A. and I. Gill. *TIBTECH*, **2000**, *18*, 282.

44. Zink, J.I. et.al. *Chemistry of Materials.* **1992**, *4*, 495.

45. Hartnett, A. M.; Ingersoll, C. M.; Baker, G. A. and F. V. Bright. *Analytical Chemistry.* **1999**, *71*, 1215.

46. Zheng, L.; Reid, W. R.; and J. D. Brennan. *Analytical Chemistry.* **1997**, 69, 3940.

47. Trevan, M. D. *Immobilized Enzymes*: *An Introduction and Applications in Biotechnology.* John Wiley and Sons: New York, **1980**.

48. Katakis, I. and E. Dominguez. *Trends in Analytical Chemistry.* **1995,** *14*, 310.

49. Cavish, B. and M. M. Werber. *Biochemistry.* **1979**, *18*, 1269.

50. Besanger, T. R.; et. al. *Analytical Chemistry.* **2003**, *75*, 2382.

51. Flora, K. K.; Dabrowski, M. A.; Musson, P. A. and J. D. Brennan. *Canadian Journal of Chemistry.* **1999**, *77*, 1617.

52. Priev, A.; Almagor, A.; Yedgar, S.; and B. Gavish. *Biochemistry.* **1996**, *35*, 2061.

53. Timasheff, S. N. and T. Arakawa. *Journal of Crystal Growth*. **1988**, *90*, 39.

Chapter 4

Effects of Glycerol on the Behaviour of Human Serum Albumin in Solution and in Sol-Gel Derived Glasses

The steady-state and time-resolved fluorescence of Trp-214 was used to examine the conformation, dynamics, accessibility, thermal stability, chemical stability and the degree of ligand binding of human serum albumin (HSA) in solution and after entrapment of the protein in tetraethylorthosilicate derived glasses doped with varying levels of glycerol. Significant changes were observed in the thermal and chemical stability of the glycerol-doped solution samples relative to those that were entrapped. Entrapped HSA showed full accessibility to the neutral quencher over a months time period at all glycerol levels. The ligand binding ability of salicylate to HSA was not affected by the presence of glycerol dopant which indicated that the conformation of HSA is not altered. The time-resolved anisotropy of HSA in glycerol-doped sol-gels shows predominantly segmental and local motion of HSA biomolecule.

4.1. Introduction

In the past few years, several groups have reported on the development of analytical devices utilizing biological components that were encapsulated in an inorganic silicate matrix formed by a low temperature sol-gel process.[1,2,3,4] An important finding with regard to the implementation of these materials for sensor development was that the entrapped biomolecules within these sol-gel materials retained a substantial fraction of their initial activity.[5] These findings resulted in several studies which were directed towards understanding the structure and dynamics of entrapped proteins,[6,7,8] the internal environment of sol-gel-derived matrices,[9] and the overall basis for the enhancement in long-term protein stability.[2,3,10] In spite of the amount of work done, the structure and environment of entrapped proteins and the overall effect of additives on entrapped protein properties are still not well understood.

The measurement of fluorescence emission from tryptophan residues within biomolecules can be utilized to monitor several parameters; including: protein function,[11] structure,[12,13,14] dynamics[15,16] folding and unfolding phenomena[17] and initial[9,13] and long-term stability[9,13] of entrapped proteins. A standard method of examining protein stability in solution is to measure the changes in the fluorescence from intrinsic tryptophan residues as a function of temperature and chemical denaturant concentration.[9,13] Proteins which contain a single Trp residue are generally used for such studies since they allow for unambiguous investigation of the region being probed, provide a simple system for examining fluorescence lifetimes (which becomes extremely complicated if two or more

intrinsic fluorophores are present) and also provide a simpler system for probing rotational anisotropy or exposure of Trp to quenchers. Tryptophan fluorescence has also been used to examine the kinetics of reactions involving proteins[12], which were either in solution or entrapped in a sol-gel-derived matrix and has recently been used to examine conformational motions and accessibility of entrapped proteins,[12,13] including HSA.[16] Given the intimate relationship between the local microenvironment and the conformation and function of a protein, one might expect the inclusion of additives which change the internal polarity, morphology or charge to produce dramatic changes in the behaviour of an entrapped protein.[7]

In this chapter, steady-state and time resolved fluorescence of Trp 214 are used to examine the conformation, ligand binding ability, dynamics, and accessibility of free and entrapped HSA as a function of glycerol doping. Human serum albumin (HSA) was chosen as the model protein because it is relatively large and complex (MW of 60 kDa with 3 major domains)[18] but yet contains only a single Trp residue within the protein at position 214 in domain II, allowing for detailed fluorescence studies.[19] HSA was also chosen because it's behaviour has been well characterized in solution,[20,21,22,23,24,25] and because it allows comparisons with previous studies of entrapped HSA and BSA.[14,15,26] The two other biomolecules studied were chosen because they had no domains (component parts), and therefore no segmental motion would be observed for their time-resolved anisotropies. Another reason was because both contain a single tryptophan amino acid which can be used to determine the degree of protein-silica interactions. RNASeT1 has a buried tryptophan and therefore we are more likely to see the global

motion of the entire biomolecule. [27,28,29,] On the other hand, Melittin is a polypeptide in which two types of motion could be observed (one was the segmental motion of the fluorophore with respect to polypeptide backbone and the other was the rotation of the fluorophore). Also both biomolecules[30] were smaller in size and therefore the tumbling motions of the both RNASeT1 and Melittin could be more easily observed.[27-30]

The changes in these properties of entrapped HSA and preliminary studies on RNASeT1 and Melittin were monitored as a function of aging time and level of dopant used in the sol-gel materials, and the results provide insights into the effects of glycerol on enzyme activity, as reported in Chapter 3.

4.2. Experimental Section

4.2.1. Chemicals

Human serum albumin (HSA, essentially fatty acid free), salicylic acid and polymethacrylate fluorimeter cuvettes (transmittance curve C) were obtained from Sigma (St. Louis, MO). Tetraethylorthosilicate (TEOS, 99.999+%), potassium iodide (99.9%) and acrylamide (99+%) were supplied by Aldrich (Milwaukee, Wisconsin). Guanidine hydrochloride (GdHCl, Sequanol grade) was obtained from Pierce (Rockford, IL). Sephadex G-25 fine powder was supplied by Pharmacia Biotech (Uppsala, Sweden). All water was twice distilled and deionized to a specific resistance of at least 18 MΩ.cm. All other chemicals were of analytical grade and were used without further purification.

4.2.2. Entrapment of HSA:

HSA was first purified as described elsewhere[7] and diluted into phosphate buffered saline (10 mM phosphate buffer/ 100 mM KCl, pH 7.2) to a concentration of 2 μM in solution and 20 μM in sol-gels, as determined using the extinction coefficient ε_{277} = 36 000 $M^{-1}cm^{-1}$ for HSA.[7] Melittin was diluted (10 mM PIPES/ 100 mM KCl buffer at pH 7.0) to 10 μM concentration for preparation of both solution and sol-gel samples, as determined by the ε_{280} = 5470.[31] RNASeT1 was diluted (5 mM $NaHPO_4$/ 50 mM KCl buffer at pH 7.5) to 5 μM concentration for preparation of solution and sol-gel samples, as determined by absorbance measurements using ε_{280} = 20 900.[32] Sol-gels were prepared in the form of blocks (1.5 cm x 1 cm x 1 cm) by mixing 0.75 mL of the sol with 0.75 mL of the protein solution. Blocks were utilized in the current study to eliminate scattering artifacts and to allow studies of samples at very early aging times, and as the sol-gel block evolved. All samples were aged in air and stored in the dark at 4 °C.

4.2.3. Steady-State Fluorescence Measurements:

Fluorescence measurements were performed using a SLM 8100 spectrofluorimeter (Spectronic Instruments, Rochester, NY), as described elsewhere.[9] HSA emission spectra were excited wavelength of 295 nm with emission collected from 305 nm to 450 nm. All spectra were collected in 1 nm increments using 4 nm bandpasses on the excitation and emission monochromators and an integration time of 0.3 s per point. Appropriate blanks

were subtracted from each sample and the spectra were corrected for deviations in emission monochromator throughput and detector response.

Steady-state fluorescence anisotropy measurements were performed in the L-format using Glan-Taylor prism polarizers in the excitation and emission paths, as described previously.[7,11,12,13] The emission maxima for both HSA and RNASeT1 were 335 and 325 nm, using an excitation at 295 nm. Steady-state anisotropy measurements for Melittin were made using the maximum emission wavelength of 345 nm and an excitation wavelength of 295 nm. Bandpasses of 4 nm were used in the excitation and emission paths, with the signal integrated for 3 s. All fluorescence anisotropy values were corrected for the instrumental G factor (I_{HV}/I_{HH}) to account for any polarization bias in the monochromators. All fluorescence anisotropy values reported were the average of 5 measurements each on 3 different samples. Steady-state anisotropy measurements were converted to average rotational reorientation times (ϕ_{SS}) using the following equation:

$$r = \frac{r_o}{1 + \left(\langle\tau\rangle / \phi_{SS}\right)} \tag{1}$$

where r is the measured fluorescence anisotropy, r_0 is the limiting anisotropy, and $\langle\tau\rangle$ is the intensity-weighted mean fluorescence lifetime of the sample as determined using eqn. (4) below. A limiting anisotropy of 0.310 ± 0.003 (λ_{ex} = 295 nm) was used for the tryptophan of HSA.[27] For RNASeT1 a limiting anisotropy of 0.210 ± 0.001 was used for samples run at pH 7.4. or 0.240 ± 0.001 for samples run at pH 5.5.[27-29] For Melittin, the limiting anisotropy ranges from 0.210 (0 M NaCl) to 0.240 (2 M NaCl) at 20°C.[30] A value of 0.21 was used in this study, which utilized 0.1 M KCl in all buffers.

4.2.4. Time-Resolved Fluorescence:

Time-resolved fluorescence intensity decay data was acquired in the time-domain using a PTI laserstrobe fluorimeter (Photon Technologies Incorporated, London, ON), as described elsewhere.[33,34] Samples were excited at 295 nm with emission collected under magic angle polarization conditions (54.7°), and passed through a monochromator using a 10 nm bandpass set at 335 nm. The intensity data was collected into 25 ps time windows, starting 2 ns before the laser pulse arrived (to establish a pre-pulse baseline) and covering a 40 ns range. The instrument response function was collected by measuring the Rayleigh scattering of the laser pulse from water, and was used to deconvolute the instrument response profile from the experimentally determined decay trace. Appropriate baseline offset and time-shift parameters were obtained by allowing these to be floating parameters in the fit.

The function describing the fluorescence intensity decay was fit using a global analysis method to both discrete and distributed fitting models, with goodness-of-fit evaluated using the reduced chi-squared parameter, residual plots and autocorrelation plots.[35] In all cases, the best fit to the decay data was obtained using a sum of discrete exponential components, given by:

$$I(t) = \sum_i \alpha_i \exp(-t/\tau_i) \tag{2}$$

where τ_i is the decay time and α_i is the pre-exponential factor of the ith decay component. The fractional fluorescence of component i (f_i) was calculated from:

$$f_i = \alpha_i \tau_i \Big/ \sum_i \alpha_i \tau_i \tag{3}$$

Using global analysis, the lifetime components were linked for each sample and thus remained fixed as a function of aging, while the fractional proportion of each lifetime component was allowed to vary as the samples aged. Fractional fluorescence values were also used to calculate the intensity-weighted mean lifetime values from the following equation:

$$\langle \tau \rangle = \sum_i f_i \tau_i \tag{4}$$

Time-resolved decays of fluorescence anisotropy were constructed from intensity decays that were obtained using vertically polarized excitation and vertically polarized emission (I_{VV}) or horizontally polarized emission (I_{VH}), and were corrected for the instrument response profile and the instrumental *G*-factor, as described in detail elsewhere.[27] The anisotropy decay was fit to a two-component hindered rotor model according to the following equation:

$$r(t) = (r_0 - r_\infty)[\beta_1 \exp(-t/\phi_1) + \beta_2 \exp(-t/\phi_2)] + r_\infty \tag{5}$$

where ϕ_1 reflects slow rotational motions associated rotation of the entire protein (global motion), ϕ_2 reflects rapid rotational reorientation of Trp residues around its bond axis (local motion), and r_4 is the residual anisotropy of the protein at long times that reflects hindered rotation of the protein. The terms β_1 and β_2 represent the fractional contributions to the total anisotropy decay from the slow and fast motions, respectively ($\Sigma\beta_i=1$).[27] The goodness-of-fit was evaluated by minimizing the sum-of-squares of residuals (SSR) between the line-of-best-fit and the experimental decay trace and by the randomness of

residual plots and autocorrelation plots. The SSR was typically less than 1×10^{-5} for satisfactory fits.

4.2.5. Thermal Denaturation Studies:

A volume of 1.5 mL of 2.0 μM protein (solution studies) was placed in a quartz fluorimeter cuvette which was N_2 purged. The temperature was raised in ~ 5 °C increments, starting at 20 °C and going to 80 °C. A fluorescence spectrum was collected from the sample and from an appropriate blank at each temperature. The temperature of the solution in the cuvette was measured directly with a thermistor probe (Hanna Instruments model 9043A) to account for loss of heat through the Tygon tubing connecting the sample holder and the water bath. The samples were allowed to equilibrate for at least 25 minutes at each temperature before readings were taken. This equilibration time was found to be sufficient as the signal did not change when using longer equilibration times. Emission spectra were obtained as a function of temperature and the integrated emission intensity was plotted against sample temperature. The midpoint of the resulting unfolding curve was determined by non-linear fitting to extract unfolding temperatures (T_{un}). Cooling the samples indicated that the unfolding transition was not reversible (in agreement with studies of HSA denaturation in solution),[7] thus thermodynamic parameters related to the protein unfolding event could not be obtained for sol-gels.[1,7]

4.2.6. Chemical Denaturation Studies:

Chemical denaturation studies were carried out with 1.5 mL of 2.0 μM HSA in solution. Samples were titrated with 6.0 M GdHCl (in glycerated or non-glycerated buffer) with constant stirring, and a minimum of 20 minutes was allowed for equilibration. A fluorescence spectrum was collected at each point for both the sample and a blank containing an identical concentration of GdHCl. The spectra were corrected for contributions from the blank and instrument factors as well as for dilution. Data obtained from this experiment is analyzed by plotting the Normalized Fluorescence Intensity versus the [GdHCl]. For the entrapped samples a 2 mL volume of [GdHCl] = 6.0 M was added to each sample after entrapment to denature the HSA.

4.2.7. Quenching Studies:

Acrylamide was used to quench the Trp residue in HSA because it is a neutral quencher and mimics the behaviour of both substrates used in enzyme kinetics (see Chapter 3). Samples were placed in a quartz cuvette containing 1.5 mL of PBS and the sample was titrated with 8.0 M acrylamide in PBS (either glycerated or non glycerated) and allowed to equilibrate 20 minutes in solution and for 1 day in sol-gel blocks before measurements were done. Longer equilibration times did not produce any further quenching of the samples. A fluorescence emission spectrum was collected from the sample and an appropriate blank after each addition of quencher. Spectra were corrected for sample dilution and were integrated from 310 nm to 450 nm. Fluorescence lifetimes were also collected in the presence of varying levels of acrylamide, and were converted to intensity weighted mean lifetimes using eqn. (4). Owing to complications arising from

static quenching contributions to the intensity data, the quenching data was fit to the lifetime data using a modified version of the Stern-Volmer equation which accounted for the possibility of there being a fraction of protein that was not accessible to the quencher (f_i):[36,37,38]

$$\frac{\langle\tau\rangle_0(1-f_i)}{\langle\tau\rangle - f_i\langle\tau\rangle_0} = 1 + K_{SV}[Q] = 1 + k_q\langle\tau\rangle_0[Q] \qquad (6)$$

where $\langle\tau\rangle_0$ is the intensity-weighted mean lifetime in absence of quencher, $\langle\tau\rangle$ is the intensity-weighted mean lifetime in the presence of quencher, [Q] is the molar concentration of the quencher, K_{SV} is the Stern Volmer quenching constant for the collisional process (M^{-1}) and k_q is the bimolecular quenching constant ($M^{-1} \cdot s^{-1}$).

4.2.8. Salicylate Titrations of HSA:

A solution of 5 μM HSA in 10 mM phosphate buffer or glycerol-loaded buffer was titrated with 50 μM salicylate (dissolved in non-glycerated or glycerated buffer). Spectra were collected for salicylate in both the presence and absence of HSA. A 40 nm window centred about the emission maximum at 408 was integrated to provide the intensity values for the ligand at each salicylate concentration, and this value was corrected for dilution factors and for the fluorescence blank. After each addition of salicylate to HSA (in solution) it was allowed to equilibrate for 15-20 minutes. The data was plotted as a ratio of the [408 nm (salicylate)/335 nm (HSA peak)] normalized integrated peaks versus

concentration of salicylate added and fit by linear regression to obtain a relative ligand binding efficiency.[16]

4.3. Results and Discussion

4.3.1. Fluorescence Measurements from Entrapped Proteins:

In all cases, high quality emission spectra of the entrapped proteins could be obtained with little or no scattering background from the silica matrix, making for accurate comparisons to the emission spectra of free HSA. The data clearly show that the unfolding of the entrapped HSA can be followed using Trp emission spectra, and further indicate that the entrapped HSA can undergo substantial conformational changes.

Figure 4.1 shows emission spectra of free HSA (A) and NATA (B) in solution (shown in black). In the solution studies there is no significant shift in the non-glycerated versus the 8.5% and 30.1% v/v glycerol doped solution. However, upon entrapment HSA (in red) shows a blue-shift in the emission spectra in both TEOS and glycerol-doped materials. The blue-shift is more pronounced in the emission spectra of the HSA than for the NATA samples. The larger blue-shift noted in the spectra of entrapped HSA may reflect a conformational change in the protein, such as compaction, that produces the blue-shift. Alternatively, the residual EtOH may create a less polar environment, which causes the blue-shift. It is also possible that HSA partially denatures to an expanded state,[7] leading to the blue-shifted emission. Unfolding experiments described below support the latter possibility, although it is not possible to conclusively prove the existence of the expanded form in the absence of energy transfer data.[16]

Spectra show no effect of glycerol on λ_{em}, only entrapment alters the λ_{em}. Glycerol has no effect even after entrapment. Another possible explanation for the blue shift observed upon entrapment is that entrapment may alter the hydration creating a tendency for the protein to minimize its surface without inducing conformational changes.[39,40] Priev and coworkers proposed that the glycerol induces a release of the so-called "lubricant" water, which maintains conformational flexibility by keeping apart neighbouring segments o f the polypeptide chain. This is expected to lead to collapsing of the voids containing this water as well as increase intramolecular bonding which may explain the observed effect.[41] Such an effect may also be present upon entrapment,[42] causing the blue-shift which results in the compaction of the protein.

Figure 4.2 below shows the emission spectra of entrapped HSA as a function of time (for day 1 and 26 of aging) in dry-aged blocks. Figure 4.2.A. illustrates that the emission spectra of HSA after one day of aging do not red-shift, which would be indicative of denaturation of the biomolecule, as is seen above for the entrapped HSA exposed to 6.0 M GdHCl denaturant (addition of 6M GdHCl after a day of aging). Another thing of interest to note is that the HSA entrapped in sol-gel does not red-shift as extensively as the solution samples. The smaller red-shift in the entrapped samples could result from the chemical denaturant not being able to diffuse into the pores and interact with HSA (GdHCl added after entrapment, sol-gel still contains many solvents), or HSA may have adopted a compact structure which results in minimal interaction with GdHCl or pores are too small to accommodate fully the unfolded protein.

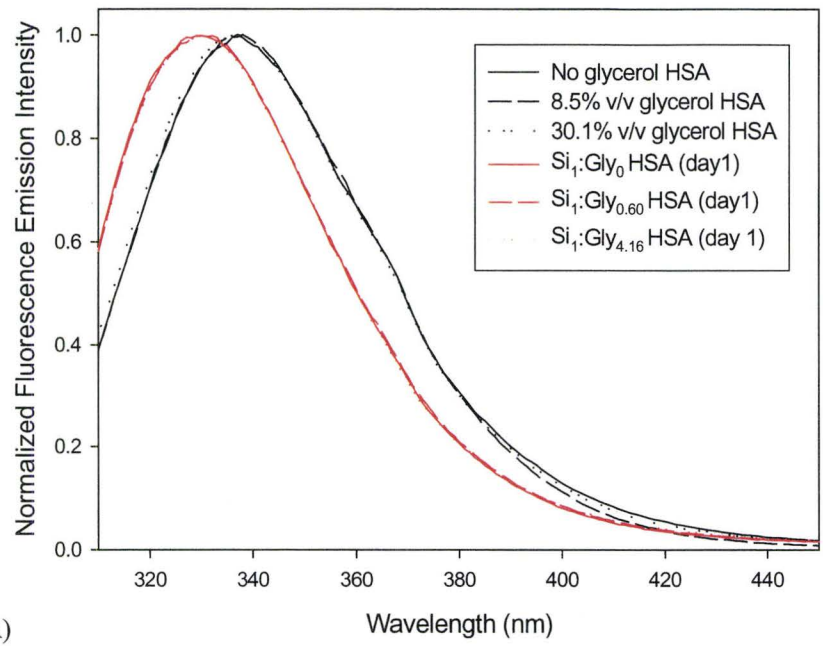

(A)

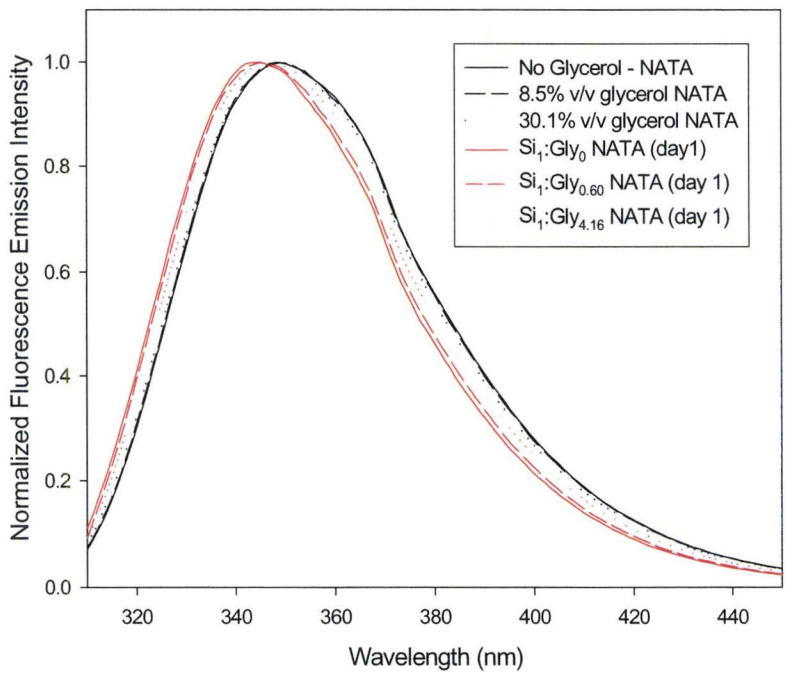

(B)

Figure 4.1: Solution (non-glycerated and glycerated) and Entrapped (undoped and doped sol-gel materials) Emission Spectra of HSA (A) and NATA (B)

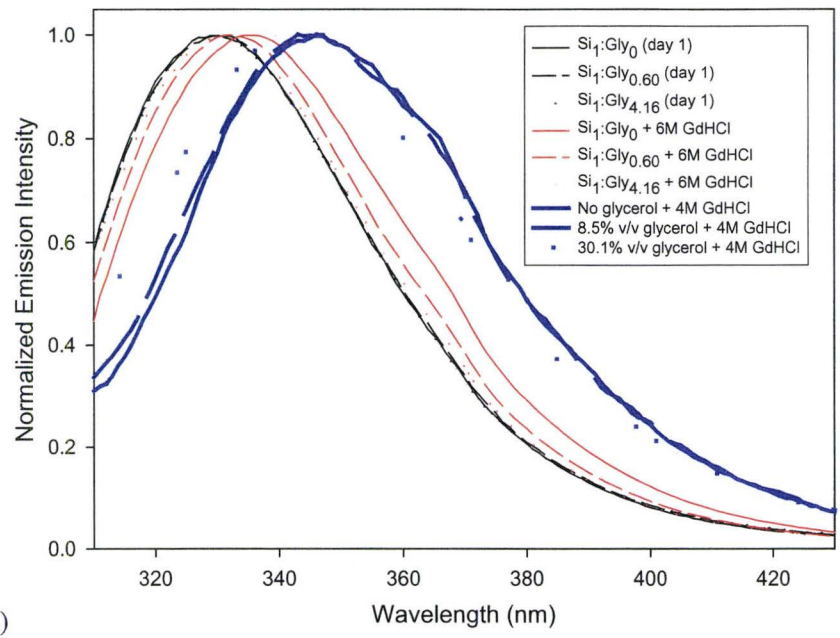

(A)

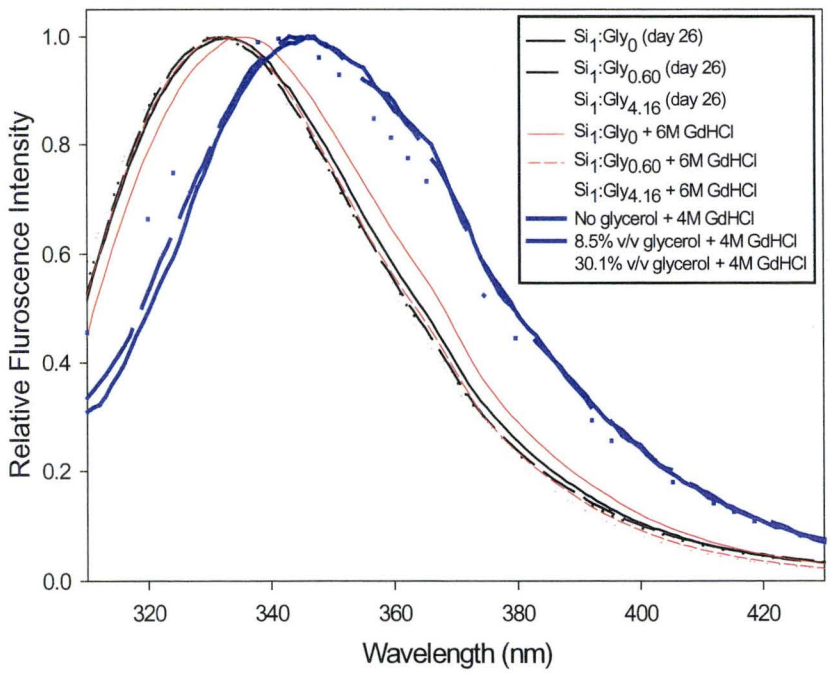

(B)

Figure 4.2: Spectral Emission Shift of entrapped HSA for day 1 (A) and day 26 (B) of aging

Figure 4.2.B, day 26 of aging, shows a slight red shift in the entrapped HSA emission spectra indicative of slight denaturation for the Si_1:$Gly_{0.60}$ and Si_1:$Gly_{4.16}$. These spectra were compared to chemically denatured samples shown in Figure 4.2.A. Once again, the entrapped samples do not show spectra as red-shifted as those in solution which could imply restricted unfolding.

4.3.2. Thermal Denaturation Studies of HSA in Solution and Entrapped:

Thermal denaturation experiments of HSA in solution were performed using normalized fluorescence intensity and 8_{em} measurements, as shown in Figure 4.3B. The temperature of unfolding, T_m, of HSA in solution increases with increasing percent volume of glycerol present (i.e., it takes a higher temperature to unfold HSA) as shown in Figure 4.3.A. The solution samples were degassed prior to thermal denaturation, to remove O_2, which increased the Tm (temperature of unfolding) as shown in Figure 4.3.A below. However, when examining Figure 4.3.B, the emission maximum for the HSA in 77%v/v glycerated solution is considerably blue-shifted which could be a solvent effect due to the increased glycerol doping as compared to the intermediate value of 30 % v/v glycerol. As shown in Figure 4.3B, samples show an initial blue-shift (N (native) $\rightarrow$ E (expanded transition) followed by a red-shift (E (expanded) $\rightarrow$ I (denatured intermediate) due to partial unfolding of domain II. In solution the protein is not initially in expanded form, therefore glycerol does not induce denaturation.

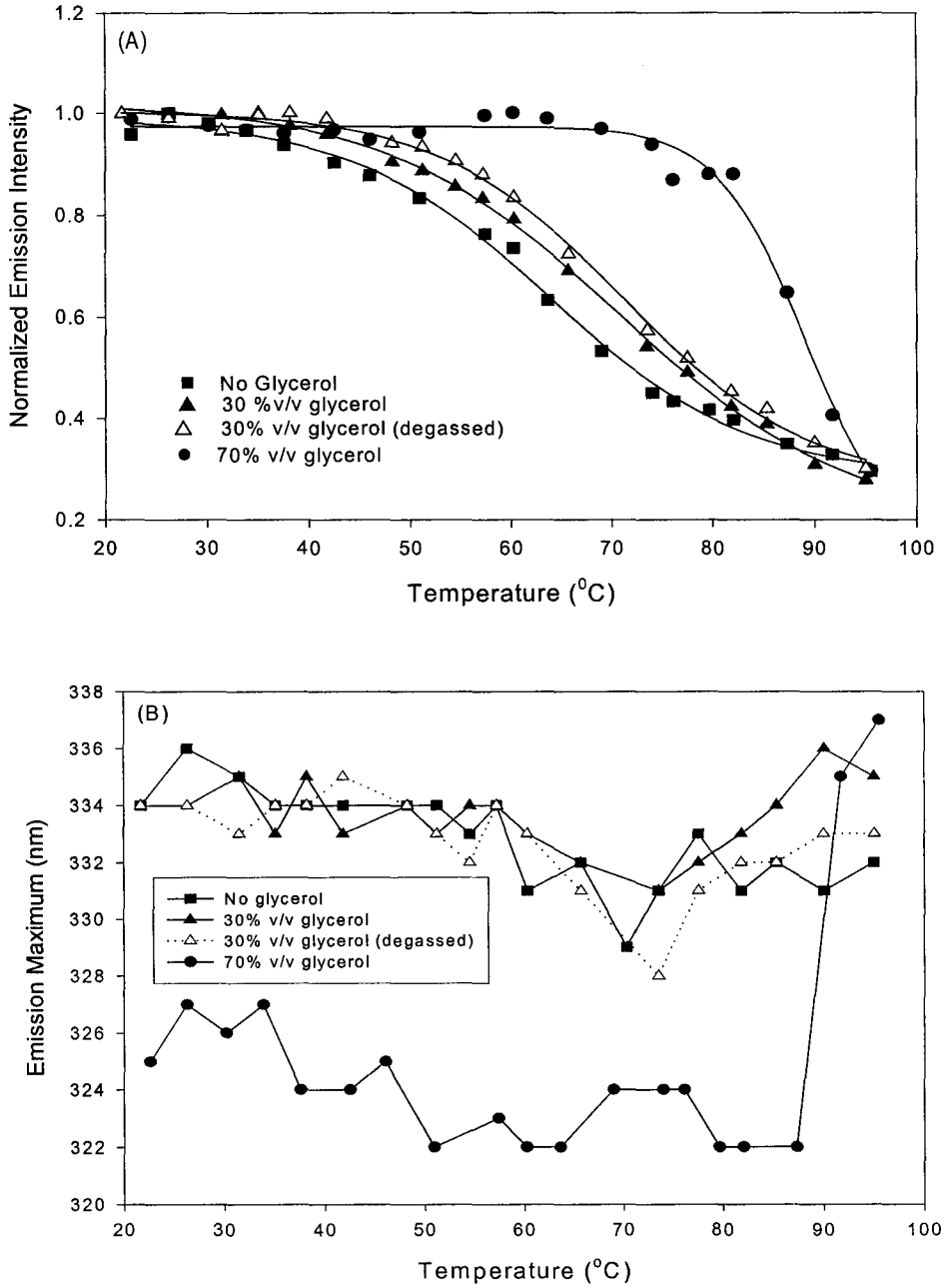

Figure 4.3: Panel A: Unfolding curves from thermal denaturation of free HSA in non-glycerated buffer (■), in (▲) 30% v/v glycerol-doped buffer (not degassed), in (△) 30% v/v glycerol doped buffer (degassed) and (●) 70 % v/v of glycerol-doped solution
Panel B: Emission Maximum wavelength of non-glycerol and % v/v glycerol-doped solutions monitored as a function of temperature

Thermal denaturation of entrapped HSA in varying glycerol-loaded sol-gels was also examined. However, intensity-based thermal denaturation curves of entrapped HSA were difficult to obtain because of photobleaching and photo-oxidation effects, since samples were not degassed. The emission maximum of the tryptophan signal, however, is immune to these effects and may give some insight into whether the protein is being stabilized within the sol-gel. Figure 4.4 shows the emission maximum (in nm) as a function of temperature for the different sol-gel materials used in the entrapment of HSA.

TEOS-based sol-gels are initially in a blue-shifted state and remain blue-shifted, which could signify the HSA protein adopting a partially unfolded intermediate state. There was no large change in the emission wavelength which could suggest that the HSA had adsorbed to the silica.[16] On the other hand, even though the glycerol-doped sol-gel material started off blue-shifted they maintained a more native like HSA emission; it was only at temperatures greater than 80 °C is red-shift observed (indicating the protein beginning to denature). By adding glycerol we obtained larger pores and perhaps less adsorption of HSA to the silica matrix; however a red shift is still observed therefore this could imply that the protein was conformationally more flexible. More importantly, there is no initial blue-shift in the spectra; rather the spectra are already blue-shifted relative to solution. Therefore, it is apparent that the entrapped protein is likely in an expanded state upon entrapment, but can further unfold at elevated temperatures in the presence of glycerol.

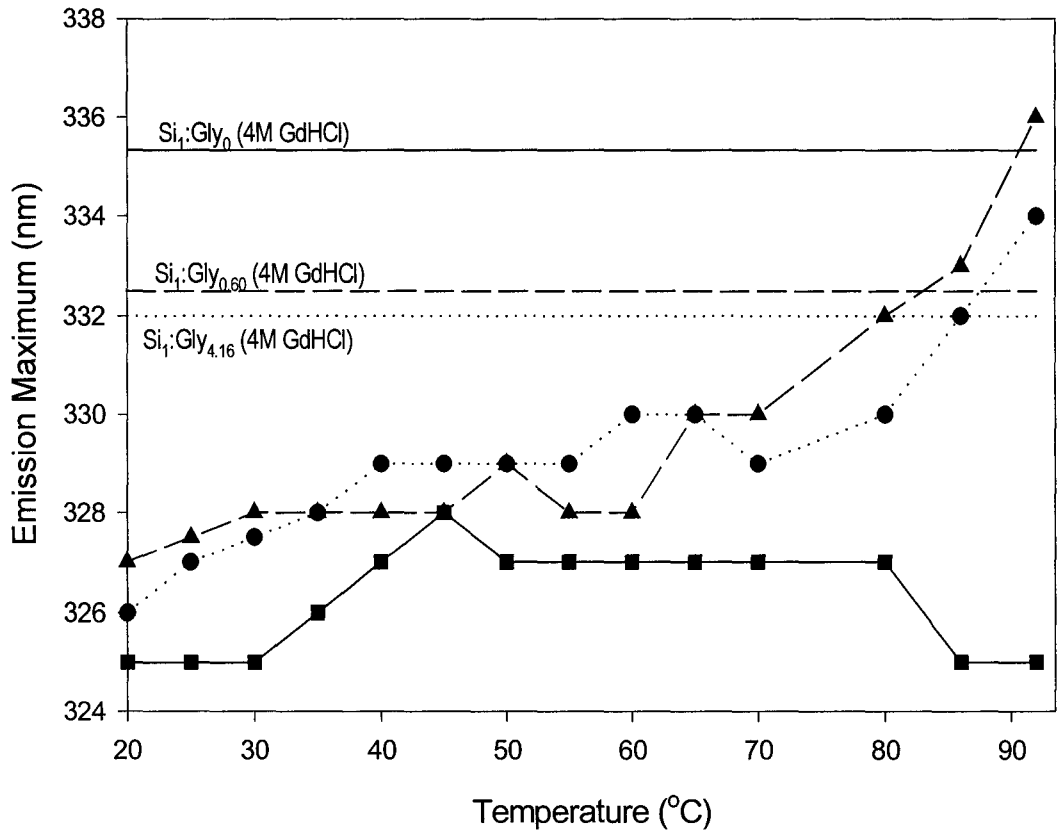

Figure 4.4: Monitoring the effects on increasing temperature on the emission maximum of entrapped HSA (day 30) to probe the relative stability of protein (where ■ $Si_1:Gly_0$, ▲$Si_1:Gly_{0.60}$ and ● $Si_1:Gly_{4.16}$) The horizontal lines are entrapped HSA in TEOS-based and glycerol-doped sol-gels in the presence of 4.0 M GdHCl.

4.3.3. Chemical Denaturation Studies of HSA in Solution and Entrapped:

Figure 4.5.A. shows the integrated emission intensity at different levels of denaturant for HSA in solution. Denaturation of HSA with GdHCl was monitored by changes in integrated fluorescence intensity and emission wavelength. The intensity data indicated that the protein denatured between 1.8 -2.0 M for the non-glycerated solution. There was an increase in denaturant concentration, required to unfold the protein, with increasing glycerated percent volume in solution as shown in Figure 4.5.A. From Figure 4.5.B. the emission maximum of HSA as a function of chemical denaturant GdHCl added. The spectral shifts of entrapped HSA show only a slight shift in the emission spectra as compared to solution as shown in Figure 4.6.

The chemical denaturant GdHCl was added at 6.0 M to the sol-gel blocks however GdHCl added did not interact with the HSA as it does in solution in which the spectra are significantly red-shifted indicating that HSA had denatured. The 6.0 M GdHCl was added to the sol-gels after entrapment. The smaller red-shift of the emission intensity for the encapsulated protein suggests that either not all of the protein was accessible to GdHCl (due to the presence of other solvent), or that the interaction of GdHCl with the entrapped protein was not able to produce as large a conformation change as was possible in solution. To further investigate the denaturing effect of GdHCl on entrapped HSA a titration should be performed. However, due to time constraints GdHCl titrations were not performed, as it takes 24 hr of equilibration time for each GdHCl concentration.

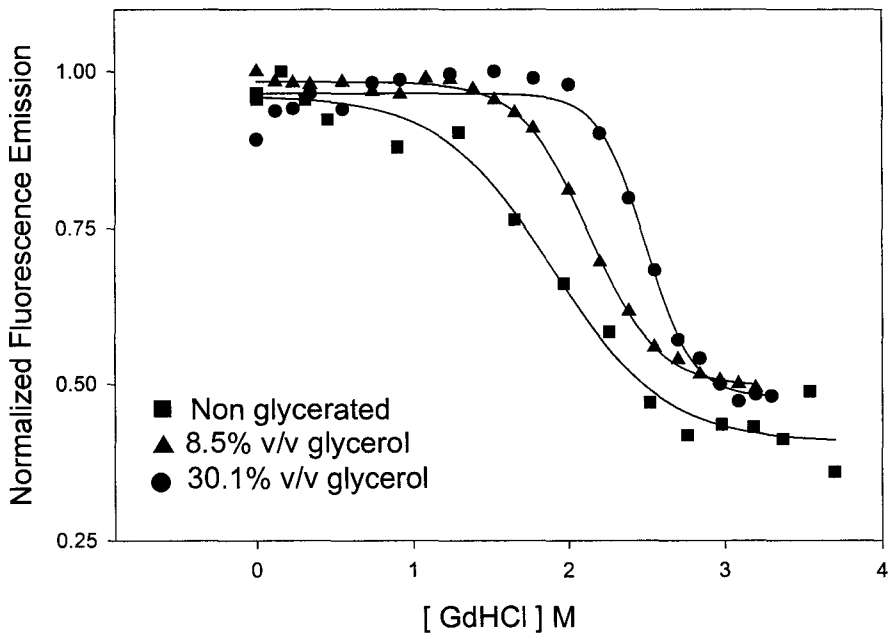

(A)

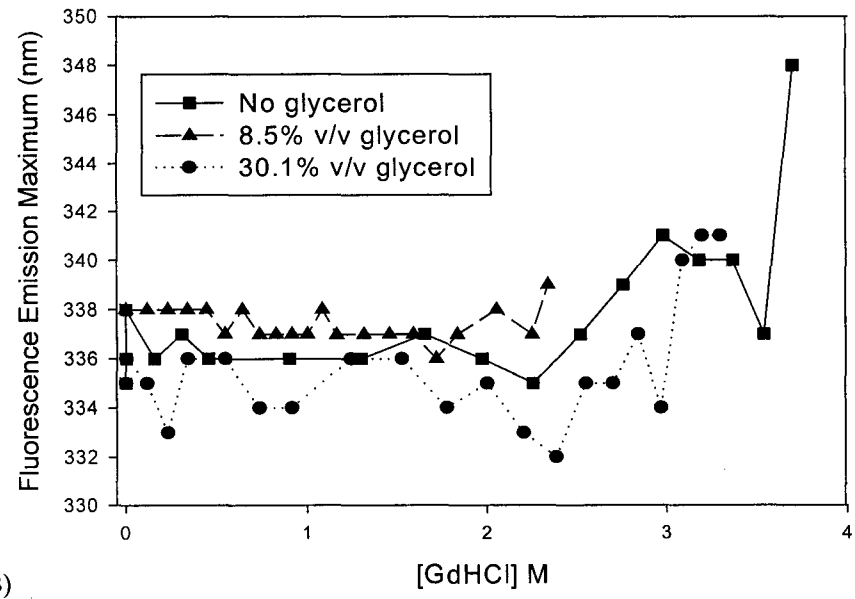

(B)

Figure 4.5: Panel A shows the chemical denaturation curves of HSA in the absence (■) and presence of Glycerol (▲ 8.5% v/v and ● 30.1 % v/v glycerol-doped solutions). Panel (B) shows the λ_{max} as function of increased [GdHCl]

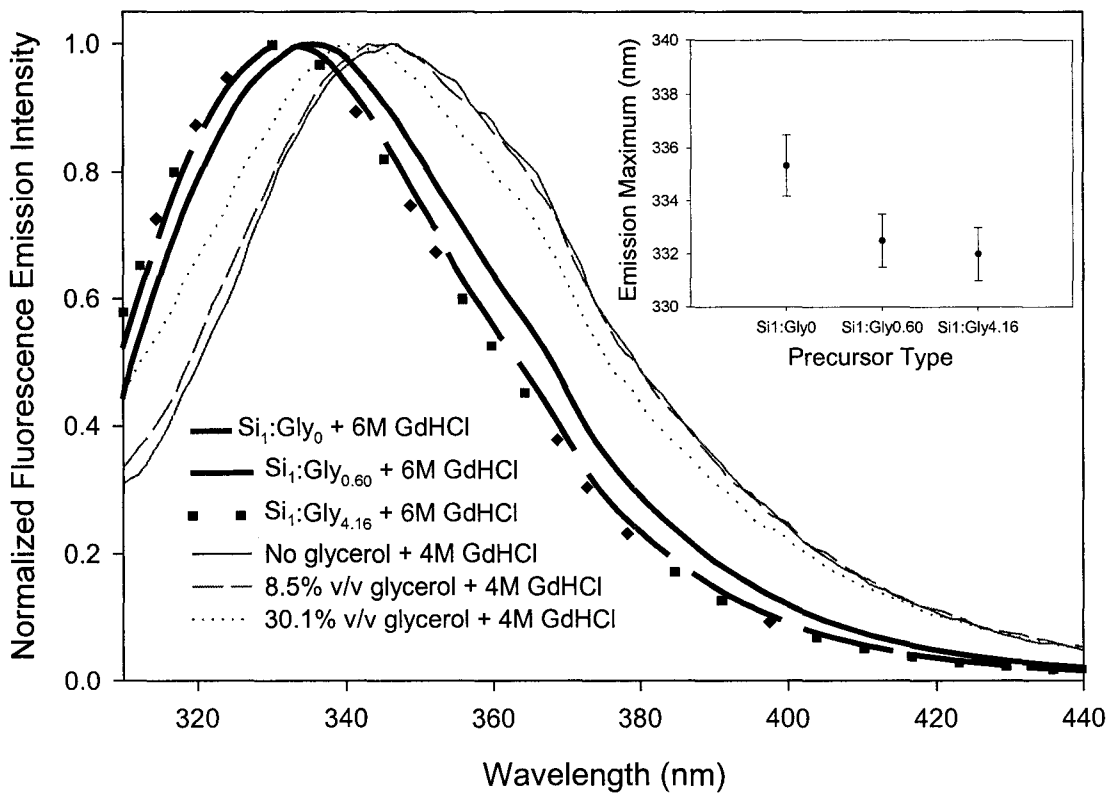

Figure 4.6: Entrapped HSA in the presence of 6.0 M GdHCl as compared to corresponding solutions with varying levels of % v/v glycerol in the presence of 4.0 M GdHCl

4.3.4. Solution Salicylate Binding Studies:

Salicylate binding studies provide information on the relationship between protein structure and function. This study was performed in solution to monitor whether and to what degree the presence of glycerol affects the binding ability of salicylate to HSA prior to entrapment. This study shows that glycerol does not hinder the proteins binding ability to salicylate. Rather the protein exhibits slightly improved binding when glycerol is present rather than absent, as shown in Figure 4.7. Therefore, this leads to the conclusion that HSA is not in an expanded or denatured state in solution. The better binding ability of HSA in glycerated as opposed to non-glycerated solutions may be a spectroscopic artifact based on changes in R_o in Gly:H_2O solutions, or it may be the case that the K_d value of the protein may have changed.

Salicylate binding studies in sol-gel derived materials were not done due to problems encountered with glass scattering artifacts and length of time for salicylate to diffuse into the sol-gel and interact with HSA (the equilibration time for binding).

4.3.5. Quenching of Free and Entrapped HSA - Accessibility Studies:

Quenching of HSA was performed using a neutral quencher, like acrylamide because it closely mimics the behaviour of both neutral substrates used in enzyme kinetic studies in Chapter 3. The accessibility of HSA in solution and entrapped within the varying sol-gel material doped with varying glycerol levels have been examined and are shown in Table 4.1. This part of the study was aimed at determining if glycerol had any

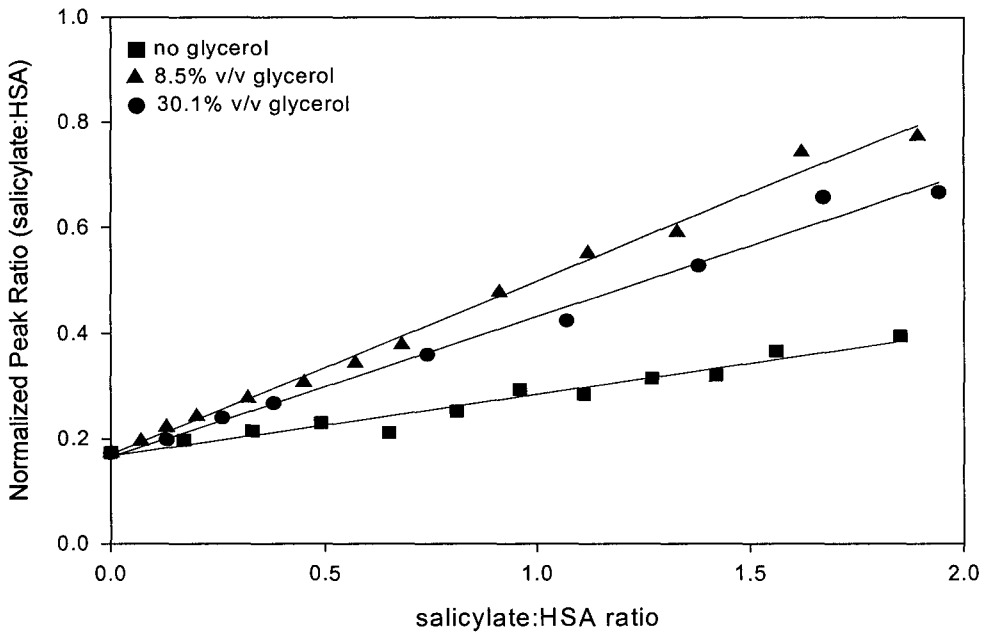

Figure 4.7: Salicylate Binding of free HSA in non-glycerated (■), 8.5% v/v (▲) and 30.1% v/v (●) glycerated solution

Table 4.1: Acrylamide Quenching of Free and Entrapped HSA in the absence and presence of glycerol dopant

Percent Volume Glycerol	K_{sv} (M^{-1})	k_q (M^{-1} s^{-1})	τ_o (ns)	R^2	f	D(cm^2/s)
No Glycerol	4.00 ± 0.07	(7.48 ± 0.16)x 10^8	5.35 ± 0.02	0.99	1.0	2.8 x 10^{-6}
8.5 % v/v Glycerol	3.76 ± 0.03	(6.75 ± 0.09) x 10^8	5.57 ± 0.03	0.99	1.0	2.5 x 10^{-6}
30.1% v/v Glycerol	1.17 ± 0.02	(1.98 ± 0.04) x 10^8	5.78 ± 0.02	0.99	1.0	7.5 x 10^{-7}
Si_1:Gly_0	0.58 ± 0.03	(5.80 ± 0.34) x 10^7	4.87 ± 0.03	0.96	0.6	2.2 x 10^{-7}
Si_1:$Gly_{0.60}$	0.32 ± 0.03	(6.42 ± 0.56) x 10^7	4.94 ± 0.04	0.96	1.0	2.4 x 10^{-7}
Si_1:$Gly_{4.16}$	0.17 ± 0.01	(3.40 ± 0.21) x 10^7	5.03 ± 0.01	0.98	1.0	1.3 x 10^{-7}

direct effect on the quenching of the HSA emission response and the possible protein environment which exists within the sol-gel, as illustrated in Figure 4.8.[43]

The single tryptophan fluorescence of the HSA molecule is quenched in the presence of acrylamide.[44,45] The emission spectra show a gradual decrease in fluorescence intensity with increased concentration of acrylamide (figure not shown). Two types of quenching contribute to the decrease in fluorescence intensity, they are: static and dynamic quenching.

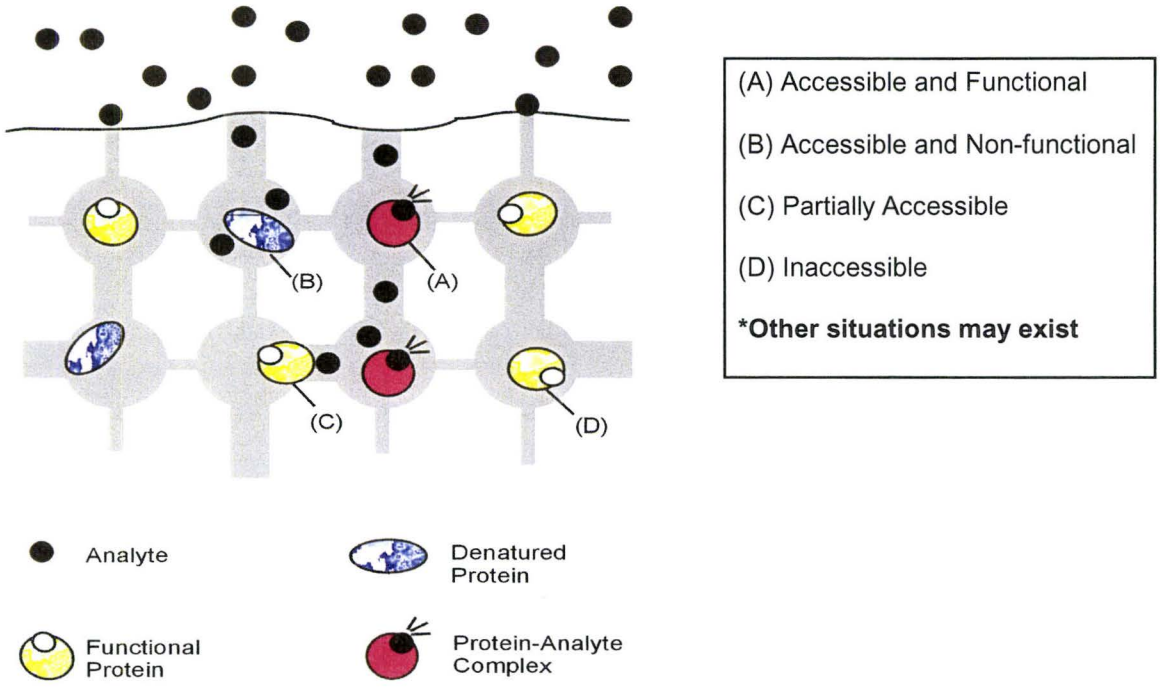

Figure 4.8: Possible Environment Encountered by the Entrapped Protein

At higher η, which correspond to increased levels of glycerol doping, the contribution from diffusional quenching decreases, while static stays the same, as shown in Figure 4.9 below. Punyiczki and Rosenberg show that the steady-state quenching of tryptophan in HSA by acrylamide as being dominated by static quenching. They state that glycerol (along with polyethylene glycol) aids in the formation of ground-state complexes between the quencher and fluorophore. Accordingly only 25% of the total quenching observed is due to collisional quenching.[46]

In solution studies, as the concentration of glycerol increased, the k_q, the rate at which the quencher collides with the fluorophore, decreases. This is in keeping with

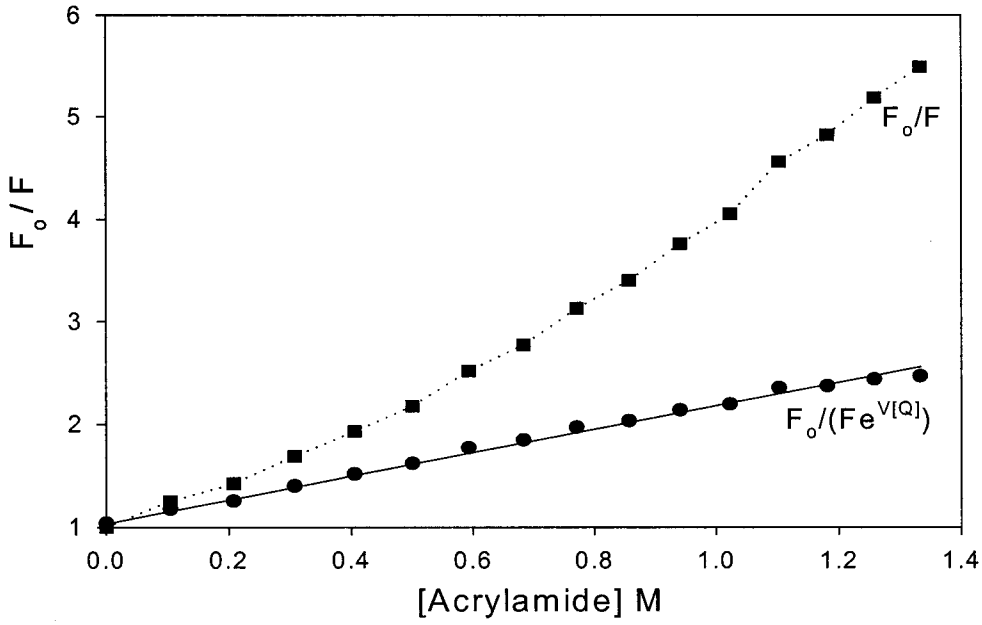

Figure 4.9: Upward curvature of the Stern-Volmer is indicative of Static Quenching as shown for acrylamide quenching of free HSA in presence 30.1% v/v glycerol dopant (where ■ uncorrected effects of static quenching, ● volume of interaction corrected plot)

viscosity studies, which show that with higher concentration of glycerol there is a corresponding increase in viscosity. Therefore, the rate of diffusion of the quencher to the fluorophore takes longer which results in lower k_q values.

For quenching experiments in sol-gel lifetimes were obtained at varying levels of quencher concentration to circumvent the effects of static quenching and only look at collisional quenching interaction of the intrinisic fluorophore with the neutral quencher, results shown in Figure 4.10.

For HSA entrapped in TEOS-based materials and glycerol-doped sol-gels there is a corresponding decrease in the bimolecular quenching constant. This is the result of two factors; first, the entrapment process itself results in a decrease of the k_q value; second, the glycerol-doped material is more viscous and will also have an added effect towards the decrease in the k_q value. An interesting point to note is that the quencher diffuses faster in Si_1:$Gly_{0.60}$ than the TEOS-based material. Since diffusion is higher, in Si_1:$Gly_{0.60}$ than for the TEOS-based sol-gels, the pores must be larger, and therefore there is less restriction to analyte movement. The accessibility of HSA in glycerol-doped glasses is 100% (f = 1.0), therefore all of the protein is accessible to the analyte. However, for TEOS-based glasses only 60% of the HSA is accessible to analyte. In terms of relating k_q to enzyme k_{cat}, the lower k_q vs. solution (ca. 10-fold) correlates relatively well with decreases in k_{cat} upon entrapment. Therefore, the porous nature of the sol-gel creates a tortuous path and restricts mass transport. This finding would be in agreement with Chapter 2 results which state with increased glycerol doping there is a corresponding increase in pore size.

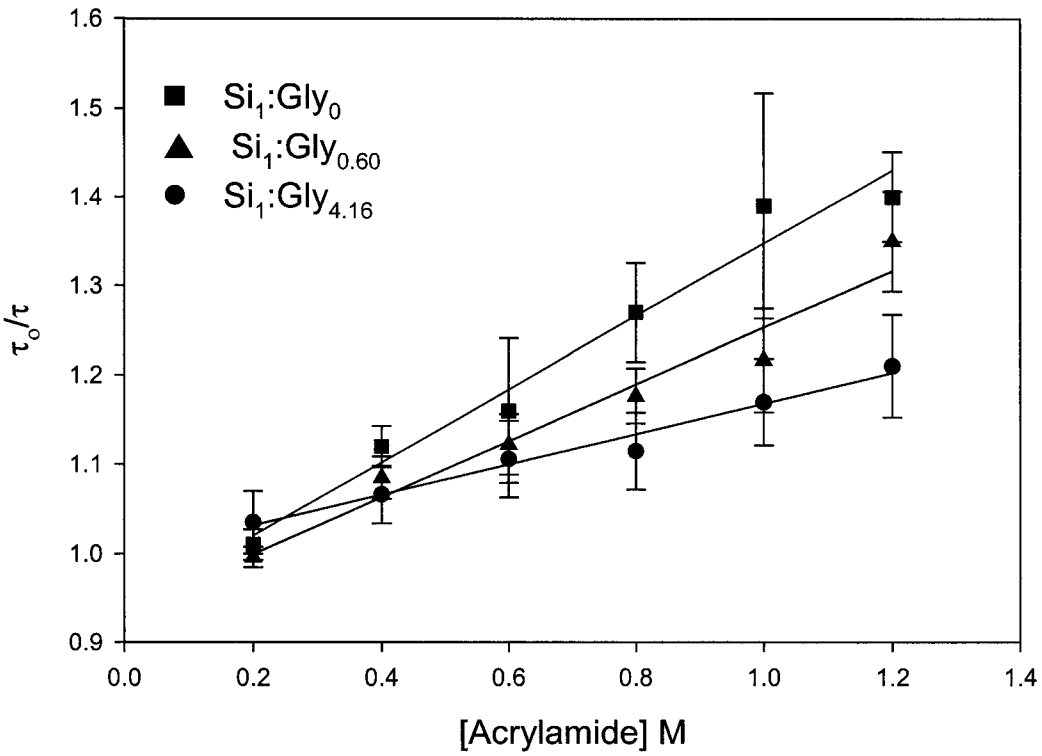

Figure 4.10: Lifetime quenching acrylamide quenching of entrapped HSA in TEOS-based (■) and glycerol-doped (▲) Si1:Gly0.60 and (●) Si1:Gly4.16 sol-gel materials (note: lifetime measurements were used for quenching studies to avoid static quenching and ascertain the degree of accessibility of HSA to acrylamide)

4.3.6. Lifetime Fluorescence Measurements of HSA in Solution and Entrapped:

Time-resolved fluorescence offers numerous opportunities for a detailed understanding of protein structure. The fluorescence properties of the tryptophan residue within the biomolecule could potentially provide information on the 'local' structure and environment. Conformational changes in protein often result in changes in the intensity decay due to altered interactions with nearby groups. HSA displayed a triple exponential lifetime decay, likely due to different rotamers of Trp in HSA.[27] The residual and autocorrelation plots indicated that it was possible to fit the decay of tryptophan fluorescence in HSA to three decay components for all samples, in agreement with previous time-resolved fluorescence studies of HSA.[27,47,48] The good fits obtained for the three component decay model indicated that the collection and fitting of time-resolved tryptophan emission decays data for the entrapped proteins could be done reliably with no background interference from the silica matrix. In the case of a single tryptophan protein, HSA, one can imagine that different conformations may bring the residue closer to or further from a quenching group. Under these conditions, only a fraction of the protein population would be fluorescent and this fraction would display a different decay time than the native protein. Figure 4.11 shows the changes in the fractional contributions of the three globally linked decay times for entrapped HSA as a function of aging time and condition.

Figure 4.11 shows the changes in the fractional contributions of the three globally linked decay times for entrapped HSA as a function of aging time and sol-gel material

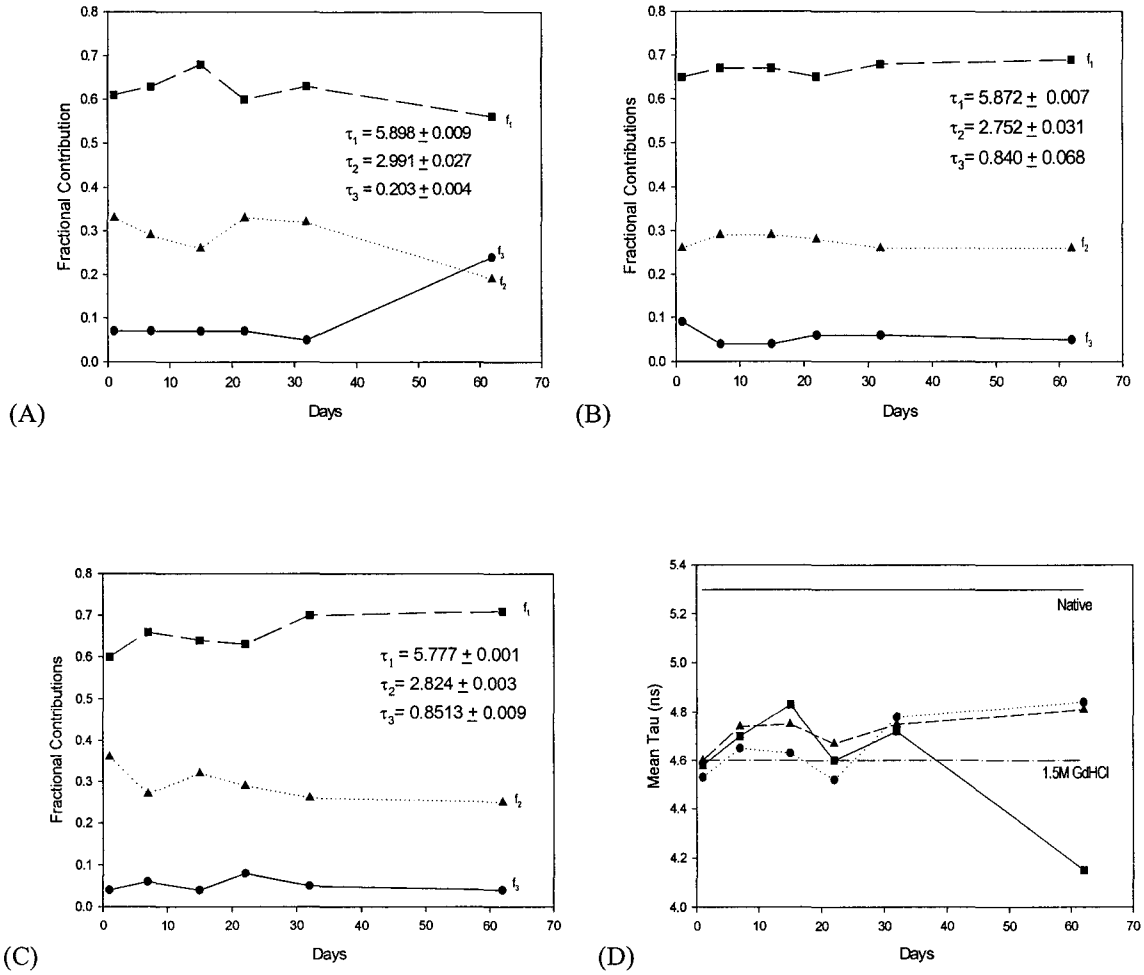

Figure 4.11: Fractional Contributions and Mean Lifetimes as Function of Sol-gel Material and Aging Time. Plot (A) is representative of Si_1:Gly_0; (B) shows Si_1:$Gly_{0.60}$ and (C) illustrates Si_1:$Gly_{4.16}$. Graph (D) shows the Mean Lifetime as Function of Aging Time and Sol-gel Material (where (■) Si_1:Gly_0, (▲) Si_1:$Gly_{0.60}$ and (●) Si_1:$Gly_{4.16}$).

formed. For TEOS-based samples, a significant decrease in the fractional contribution of the long lifetime component, f_1, is shown along with correlated increases in the intermediate, f_2, and shorter, f_3, lifetime components. Also, a lower mean lifetime value is shown in Figure 4.11 for the TEOS-based material. This begins to occur in TEOS-based materials (Si_1:Gly_0) near day 30 and is visible by day 62. Glycerol-doped materials on the other hand show no decrease in f_1, in fact the fractional components remain relatively constant after day 30 as the sol-gel entrapped HSA continues to age up to day 62. These results are consistent with the protein adopting an expanded form in dry-aged materials.

4.3.7. Conformation and Dynamics:

Figure 4.12A shows the maximum emission wavelengths and 4.12B shows the steady-state rotational correlation times for free and entrapped HSA as a function of aging time. Figure 4.12 shows the effects of immediate entrapment on HSA within the various sol-gel materials. HSA in solution has a λ_{em} = 335 nm, $\langle\tau\rangle$ = 5.28 ns, ϕ_{SS} = 4.12 ns. These results suggested that the protein within dry-aged Si_1:Gly_0 and glycerol doped sol-gels (Si_1:$Gly_{0.60}$ and Si_1:$Gly_{4.16}$) experienced an enivironment more close to that of HSA in solution exposed to 1.5M GdHCl (λ_{em} = 330 nm, $\langle\tau\rangle$ = 4.60 ns, ϕ_{SS} = 3.44 ns). Also, the viscosity increases (η) upon entrapment and therefore slower rotation is

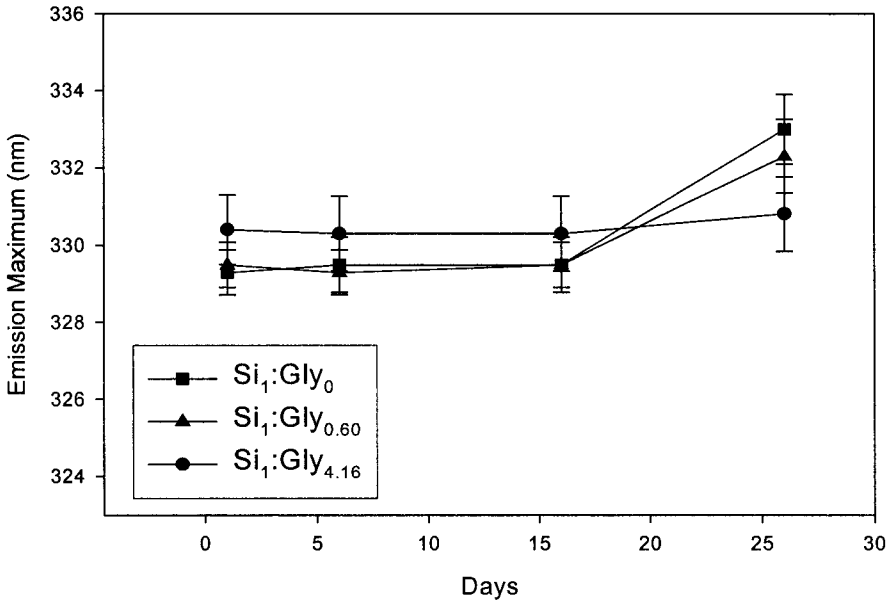

(A)

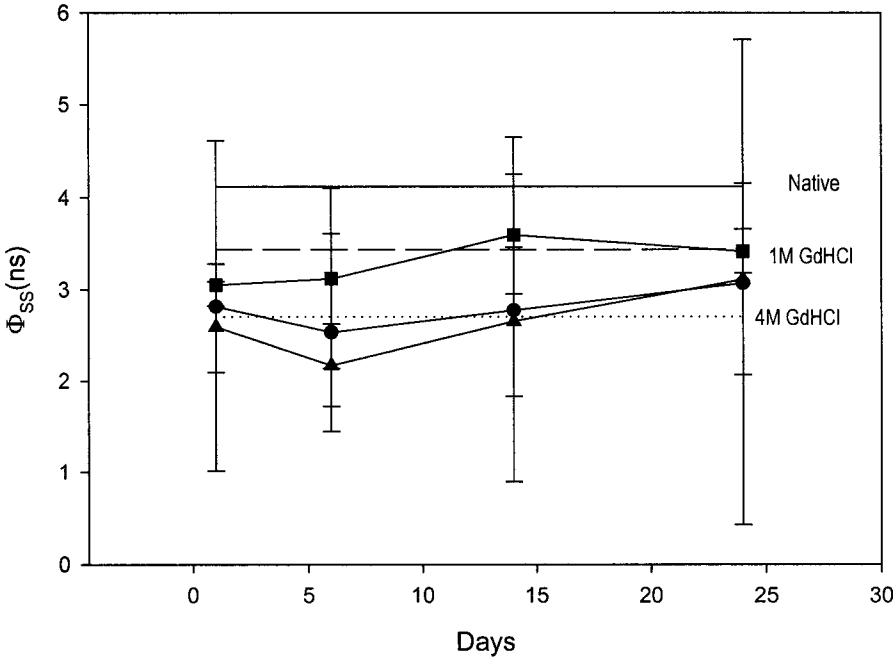

(B)

Figure 4.12: Plot (A) Emission Maximum versus Aging Time and (B) Steady-state rotational correlation times (Φ_{SS}) versus Aging Time (where (■) Si_1:Gly_0,(▲)Si_1:$Gly_{0.60}$ (●) Si_1:$Gly_{4.16}$)

observed. Upon entrapment due to the presence both EtOH and glycerol the protein exists in an intermediate state. However, with aging and the disappearance of ethyl alcohol and retention of water by glycerol the protein adopts a less strained form. Initially, the HSA entrapped in TEOS-based material has a steady-correlation time closer to that of the native protein. However with aging, the loss of EtOH enables the protein entrapped within Si_1:$Gly_{0.60}$ and Si_1:$Gly_{4.16}$ to adopt a conformation similar the TEOS-based material, and their rotational correlation times increase, meanwhile the Si_1:Gly_0 ϕ_{SS} starts to decline by day 26. But, ϕ_{SS} is very low relative to that expected for protein tumbling, therefore ϕ_{TR} (time-resolved) anisotropy is needed to sort out behaviour of HSA when entrapped.

4.3.8. Time-Resolved Anisotropy of Solution and Entrapped HSA:

To further explore protein dynamics, time-resolved anisotropy decay data was obtained for HSA in solution and in each type of glass that had been aged for ~1 month, as shown in Table 4.2. In all cases, the data for the entrapped protein could be fit relatively well to a hindered rotor model with two rotational components, reflecting local and segmental rotational motions for an adsorbed protein. Fitting to three or more components did not improve the statistics of the fits, and generally resulted in two of the three recovered rotational reorientation times having equivalent values. HSA in solution did not display hindered rotation ($r_\infty \approx 0$). Previous finding by our group on the rotational motions of HSA suggest that one or two rotational reorientation times of 20 ns (global motion) and 0.44 ns (local motion), with the relative weighting of these motions

being 2:1. The value obtained is different from previous findings, this may be due to the viscous nature of the glycerol dopant added which affects the global motion of the protein (as a result only segmental and local motion are most likely observed).[16,27]

Table 4.2: HSA in Solution with varying Glycerol Dopant and Entrapped in Various Sol-gel Materials

Sample	ϕ_1(ns)[a]	ϕ_2(ns)	β_1[b]	β_2	r_4[c]	r_o	r_4/r_o	SSR[d]
Solution								
Native	8.16		1.00		0.0349	0.1606	0.217	7.989×10^{-6}
8.5% v/v glycerol	10.50	0.52	0.30	0.60	0.0853	0.2185	0.390	1.768×10^{-6}
30.1% v/v glycerol	8.50	0.10	0.22	0.78	0.1195	0.3986	0.300	1.133×10^{-6}
Entrapped								
Day 1 Si_1:Gly_0	8.56	0.17	0.05	0.95	0.1664	0.3467	0.480	1.768×10^{-6}
Day 1 Si_1:$Gly_{0.60}$	14.30	0.27	0.15	0.85	0.0857	0.3411	0.249	8.666×10^{-6}
Day 1 Si_1:$Gly_{4.16}$	10.36	0.45	0.31	0.09	0.1638	0.3981	0.411	1.133×10^{-6}
Day 30 Si_1:Gly_0	8.68	0.64	0.39	0.61	0.1555	0.1785	0.871	4.034×10^{-7}
Day 30 Si_1:$Gly_{0.60}$	7.35	0.62	0.37	0.63	0.1402	0.1849	0.758	3.348×10^{-7}
Day 30 Si_1:$Gly_{4.16}$	6.75	0.52	0.23	0.77	0.1072	0.1615	0.664	4.034×10^{-7}
Day 37 Si_1:Gly_0	6.82	0.32	0.27	0.73	0.1371	0.2171	0.632	8.091×10^{-7}
Day 37 Si_1:$Gly_{0.60}$	6.00	0.23	0.11	0.89	0.1067	0.2062	0.527	6.413×10^{-7}
Day 37 Si_1:$Gly_{4.16}$	6.52	0.18	0.19	0.81	0.1200	0.2308	0.520	1.443×10^{-5}

Upon entrapment of HSA, the most striking change in the anisotropy decay was the high value of the residual anisotropy ($r_4 > 0.11$ in all cases). This large residual anisotropy value is consistent with adsorption of the probe onto the surface of the glass, causing a restriction in the global rotational motion of the protein or the motion is too slow to see on 40 ns timescale. A second unexpected result was that the value of the longer rotational reorientation time *decreased* to between 5.6 ns and 10.5 ns, and the proportion of the short rotational component increased, consistent with greater mobility in the region of Trp-214. Also, for the percent composition of the relative fractional components, the ϕ_1 component, the global motion, has lower percent fraction contribution to the total anisotropy decay than the ϕ_2 component, local/segmental motion of entrapped HSA. This could be explained by having HSA adopt an expanded conformation which results in an increase in the segmental/local, ϕ_2, component. This is displayed by both glycerol-doped and non-glycerol-doped sol-gel materials.

4.3.9. Protein-Silica Interactions (probed using Melittin and RNASeT1):

The two other biomolecules studied were choosen because they had no domains, and therefore no segmental motion. Another reason was because both contain a single tryptophan amino acid in order to determine the degree of protein-silica interactions. RNASeT1 has a buried tryptophan and therefore we are more likely to see the global motion of the entire biomolecule.[27,28,29] On the other had, Melittin is a polypeptide in which two types of motion could be observed (one was the segmental motion of the fluorophore with repect to polypeptide backbone and the other was the rotation of the

fluorophore).[27,30] Also both biomolecules were smaller in size and therefore the tumbling motions of the both RNASeT1 and Melittin could be more easily observed. HSA rotational motions of the entire molecule were too large to be monitored with glycerol being present. A nother reason for select RNASeT1 and Melittin was because of their charge at neutral pH. RNASeT1 had an isoelectric point (pI) of 2.9, and at neutral pH 7.0, which gives a negative charge.[49] Melittin on the other hand, has a pI 11.2 and at pH 7.0 is positively charged.[27]

In these studies both biomolecules exhibit an increase in the steady-state fluorescence upon entrapment regardless of the type of glass used as shown in Table 4.3. All of the data collected was done in at least triplicate and all of the steady-state anisotropies were blank subtracted to account for any scattering effects arising from the sol-gel block. For the Melittin samples there is an increase in the steady-state anisotropy with increase level of glycerol doping. Therefore, the increase in glycerol doping results in an increase in the viscosity and a corresponding increase in the steady-state anisotropy. Another interesting trend is that sol-gels Si_1:Gly_0 and Si_1:$Gly_{0.60}$ exhibit similar steady-state anisotropy. For RNASeT1 the glycerol-doped solutions show an increase in the steady-state anisotropy signifying a more rigid environment. Also, RNASeT1 data show an increase in the steady-state anisotropy upon entrapment however by day 30 there is a decrease in the steady-state anisotropy signifying a less rigid, more mobility of RNASeT1 sample similar to those in solution.

Table 4.3: Melittin and RNASeT1 Steady-State Anisotropy

Days	Sample	Melittin	**RNASeT1**
	Non-glycerated	0.0360 ± 0.003	**0.092 ± 0.014**
	8.5%v/v glycerol	0.0390 ± 0.001	**0.110 ± 0.008**
	30.1% v/v glycerol	0.0544 ± 0.001	**0.134 ± 0.018**
1 or 2	Si_1:Gly_0	0.045 ± 0.005	**0.137 ± 0.012**
	Si_1:$Gly_{0.60}$	0.044 ± 0.004	**0.135 ± 0.011**
	Si_1:$Gly_{4.16}$	0.054 ± 0.012	**0.148 ± 0.001**
15	Si_1:Gly_0	0.043 ± 0.005	**0.144 ± 0.013**
	Si_1:$Gly_{0.60}$	0.055 ± 0.029	**0.115 ± 0.005**
	Si_1:$Gly_{4.16}$	0.071 ± 0.028	**0.152 ± 0.003**
22	Si_1:Gly_0	0.043 ± 0.008	**0.128 ± 0.008**
	Si_1:$Gly_{0.60}$	0.041 ± 0.005	**0.154 ± 0.058**
	Si_1:$Gly_{4.16}$	0.071 ± 0.003	**0.143 ± 0.003**
30	Si_1:Gly_0	0.062 ± 0.017	**0.109 ± 0.026**
	Si_1:$Gly_{0.60}$	0.069 ± 0.024	**0.104 ± 0.027**
	Si_1:$Gly_{4.16}$	0.103 ± 0.024	**0.097 ± 0.037**

Therefore, in order to obtain more information about the effects that glycerol imparts on the biomolecule under investigation (either RNASeT1 or Melittin) in solution and when entrapped, time-resolved data of tryptophan fluorescence must be obtained.

4.4. Conclusions

By means of the examination of the various fluorescence techniques employed, it is clear that glycerol-doped HSA solution studies display an increase in stability (as

illustrated through an increase in the T_M of unfolding and an increase in the [GdHCl] required to denature the protein). Salicylate binding studies showed that glycerol does not alter the binding ability of HSA, as compared to non-glycerol-doped studies. Upon entrapment in TEOS-derived and glycerol-doped sol-gels HSA experienced a blue shift in their emission maximum. Also, quenching studies of sol-gel entrapped revealed that the HSA was fully accessible in the glycerated sol-gels and that the TEOS-based glasses were only 60% accessible to the analyte. Also, the lifetime data of TEOS-based sol-gels shows a lower mean lifetime value, consistent with the protein adopting a partially expanded form, however this was not observed for the glycerol-doped glasses. Inorder, to determine whether or not glycerol-doped bioglasses are likely to be amenable to commercial applications, further studies need to be done both on HSA, RNASeT1 and Melittin. On the basis of these findings, it is clear that the development of new sol-gel processing methods are needed which display increased longevity and protein stability and must be examined more thoroughly in order to clearly determine the effects the "second-generation" glasses impart upon the biomolecule under investigation.

4.5. References:

1. Braun, S.; Shtelzer, S.; Rappoport, S.; Avnir, D. and M. Ottolenghi. *Journal of Non-Crystalline Solids.* **1992**, *147*, 739.

2. Avnir, D.; Braun, S.; Lev, O.; Ottolenghi, M. *Chemistry of Materials.* **1994**, *6*, 1605.

3. Bakul, D. C.; Dunn, B.; Valentine, J. S. and J. I Zink. *Analytical Chemistry.* **1994**, *66*, 1120A.

4. Bhatia, R. B.; Gupta, A. K.; Singh, A. K.; and J. C. Brinker. *Chemistry of Materials.* **2000**, *12*, 2434.

5. Braun, S.; Rapport, S.; Zusman, R.; Avnir, D. and M. Ottolenghi. *Material Letters.* **1990**, *10*, 1.

6. Dave, B. C.; Soyez, H.; Miller, J. M.; Dunn, B.; Valentine, J. S. and J. I. Zink. *Chemistry Materials.* **1995**, *7*, 1431.

7. Flora, K. K.; Brennan, J. D.; Baker, G. A.; Doody, M. A.; and F. V. Bright. *Biophysical. Journal.* **1998**, *75*, 1084.

8. Demchenko, A. P.; Gryczynski, I; Gryczynski, Z; Wiczk, W; Malak, H. and M. Fishman. *Biophysical Chemistry.* **1993**, *48*, 39.

9. Flora, K. K; Dabrowski, M. A; Musson, S. P; and J.D. Brennan. *Canadian Journal of Chemistry.* **1999**, *77*, 1617.

10. Ellerby, L. M.; Nishida, C. R.; Nishida, F.; Yamanaka, S. A.; Dunn, B.; Valentine, J. S. and J. I. Zink. *Science* **1992**, *225*, 1113.

11. Zheng, L; Hogue, C. W. V. and J. D. Brennan. *Biophysical Chemistry.* **1998**. *71*, 1084.

12. Zheng, L.; Reid, W. R.; Brennan, J. D. *Analytical Chemistry.* **1997**, *69,* 3940.

13. Zheng, L.; and J. D. Brennan. *Analyst*, **1998**, *123*, 1735.

14. Edmiston, P. L.; Wambolt, C. L.; Smith, M. K. and S. S. Saavedra. Journal of *International Science.* **1994**, *163*, 395.

15. Jordan, J. D; Dunbar, R. A; and F. V. Bright. *Anaytical Chemistry.* **1995**, *67*, 2436.

16. Flora, K. K. and J. D. Brennan. *Chemistry of Materials*. **2001**, *13*, 4170.

17. Eftink, M. R. *Biophysical Journal*. **1994**, *66*, 482.

18. Carter, D. C; and J. X. Ho. *Advancements in Protein Chemistry*. **1994**, *45*, 153.

19. Min He, X. and D. C. Carter. *Nature*. **1992**, *358*, 209.

21. Pico, G. A. *Biochemistry and Molecular Biology International*. **1995**, *36*, 1017.

22. Pico, G. A. *Biochemstry and Molecular Biology International*. **1996**, *38*, 1.

23. Wetzel, R.; Becker, M.; Behlke, J.; White, H.; Bohn, S.; Ebert, B.; Hamaann, H.; Krumbiegel, J. and G. Lasiman. *European Journal of Biochemistry*. **1980**, *104*, 469.

24. Lee, J. Y.; and M. J. Hirose. *Journal of Biological Chemistry*. **1992**, *267*, 14753.

25. Farruggia, B.; Gabriela, G.; D'Angelo, C.; Pico, G. *International Journal of Macromolecules*. **1997**, *20*, 43.

26. Wambolt, C. L. and S. S. Saavedra. *Journal of Sol-Gel Science and Technology*. **1996**, *7*, 53.

27. Lakowicz, J. R. *Principles of Fluorescence Spectroscopy*, 2nd Ed.; Kluwer Academic/Plenum Press: New York, 1999.

28. Chen, L. X. Q.; Longworth, J. W. and G. R. Fleming. *Biophysical Journal*. **1987**, *51*, 865.

29. Gryczynski, I.; Eftink, M.; and J. R. Lackowicz. *Biochimica et Biophysica Acta*. **1988**, *954*, 244.

30. John, E. and F. Jahnig. *Biophysical Journal*. **1988**, *54*, 817.

31. Worthington for Melittin.

32. Worthington for RNASeT1.

33. Brennan, J. D.; Flora, K. K.; Bendiak, G. N.; Baker, G. A.; Kane, M.;. Pandey, S.; and F. V. Bright. *Journal of Physical Chemistry B*. **2000**, *104*, 10100.

34. James, D. R.; Siemiarczuk, A.; Ware, W. R. *Rev. Sci. Instrum*. **1992**, *63*, 1710.

35. O'Connor, D. V.; and D. Phillips. *Time-Correlated Single Photon Counting*; Academic Press: Orlando, **1984**.

36. Flora, K. K and J. D. Brennan. *Analyst.* **1999**, *124*, 1455.

37. Eftink, M. R; and C. A. Ghiron. *Biochemistry*, **1976**, *15*, 672.

38. Eftink, M. R.and C. A. Ghiron. *Biochemistry*, **1977**, *16*, 5546.

39. Gekko, K. and S. N. Timasheff. *Biochemistry.* **1981**, *20*, 4667.

40. Timasheff, S. N. and T. Arakawa. *Journal of Crystal Growth.* **1988**, *90*, 39.

41. Priev, A.; Almagor, A.; Yedgar, S.; and B. Gavish. *Biochemistry.* **1996**, *35*, 2061.

42. Eggers, D. K. and J. S. Valentine. *Journal of Molecular Biology.* **2001**, *314*, 911.

43. Brennan, J. D. *Applied Spectroscopy.* **1999**, *53*, 106A.

44. Punyiczki, M.; Norman, J. A.; and A. Rosenberg. *Biophysical Chemistry.* **1993**, *47*, 9.

45. Chang, G. G. and H. J. Lee. *Journal of Biochemical and Biophysical Methods.* **1984**, *9*, 351.

46. Punyiczki, M. and A. Rosenberg. *Biophysical Chemistry.* **1992**. *42*, 93.

47. Dahms, T. E. S. and A. G. Szabo. *Biophysical Journal.* **1995**, *69*, 569.

48. Willis, K. J; Neugebauer, W.; Sikorska, M. and A. G. Szabo. *Biophysical Journal.* **1994**, *66*, 1623.

49. Verrall, R. E. et.al. *Biochemistry.* **1985**, *24*, 5517.

Chapter 5

Reagentless pH-Based Biosensing using a Fluorescently-Labelled Dextran Co-entrapped with a Hydrolytic Enzyme in Sol-Gel Derived Nanocomposite Films

We report on the development of reagentless fluorescence-based sensing films utilizing hydrolytic enzymes co-entrapped with polymers that are labelled with pH sensitive fluorophores. Aqueous solutions of a hydrophilic enzyme (urease) containing carboxy-seminaphtharhodafluor-1 (SNARF-1), either free or conjugated to a dextran polymer backbone, mixed with hydrolyzed alkoxysilane solutions and cast onto planar surfaces to form thin, biologically active sol-gel-derived films (*ca.* 500 nm thick). The films also contained various additives, such as methyltrimethoxysilane, dimethyldimethoxysilane, polyethylene glycol, glycerol or polyvinyl alcohol, to optimize the activity of the entrapped enzymes. The photostability, leaching, pK_a and pH response of the entrapped probe were characterized, as was the performance of the entrapped enzyme, and an optimal set of processing conditions was obtained for each different sensing film. In general, the results indicated that SNARF-labelled dextran was insensitive to leaching and photobleaching. Furthermore, it was observed that the pK_a and pH response of this probe was insensitive to preparation conditions. The performance of the urease only moderately dependent on the type and level of additive, and in all cases it was possible to obtain active enzyme with good performance characteristics. Reagentless sensing films for urea are demonstrated based on the detection of enzyme-mediated pH changes from films coated onto planar substrates.

5.1. Introduction

In the past few years, several reports have appeared describing biosensors based on biorecognition elements that were entrapped into sol-gel processed glasses derived from tetraethylorthosilicate (TEOS) or tetramethylorthosilicate (TMOS).[1,2,3,4,5,6,7,8,9,10,11,12,13,14,15,16,17,18] The encapsulation protocol generally involved hydrolysis of the alkoxysilane precursors using acidic or basic catalysts, followed by the addition of a buffer solution containing the protein of interest to promote gelation. In most cases, low temperature aging over a period of several days or weeks resulted in a durable, optically clear material that was suitable for optical sensor development.[19]

The development of fluorescence-based biosensors generally relies on the ability to place both a biorecognition element and a fluorescent reporter group in close proximity to an inorganic transducer. A key advantage of sol-gel-derived matrixes is the ability to entrap multiple species within a confined space. Recently, several reports have described the successful entrapment of multi-enzyme systems within a single sol-gel derived matrix. Examples include the co-immobilization of glucose oxidase and horseradish peroxidase for glucose sensing,[20] the entrapment of a three-enzyme system[21] for catalysis of reactions to form CO_2 from methanol, and the entrapment of a six enzyme mixture produce a multi-step biosynthesis of α(2,6) sialyl - *N*-acetyllactosamine from *N*-acetyllactosamine and *N*-acetylmannosamine.[22] In each of these cases, the ability to co-immobilize multiple species with good control over the spatial distribution of the various dopants resulted in an increase in the rate of product formation, and thus better overall performance.

A second advantage of sol-gel processed materials is the ability to tune the material properties so as to optimize the performance of the entrapped biomolecules.[23,24,25,26,27] Examples include the entrapment of atrazine chlorohydrolase into methyltrimethoxysilane-based materials,[28] entrapment of lipase and human serum albumin in organically modified silicates (ORMOSILS),[29] co-immobilization of glucose oxidase and horseradish peroxidase in the presence of a graft copolymer of polyvinylimidazole and polyvinylpyridine[30,31] and the entrapment of acetylcholinesterase and butyrylcholinesterase in the presence of polyethylene glycol.[32] In each case, the addition of organosilane precursors or polymers resulted in improved function for the entrapped protein as compared to that obtained in unmodified glasses, with typical activity enhancements being on the order of 4 - 20 fold.[23,24,25,26,27,28]

In this study, we have employed sol-gel processing methods to develop a reagentless biosensor for urea based on the co-entrapment of urease and a pH sensitive fluorescent probe into submicron thick silica films. The basic products that are generated by the urease catalyzed reaction are detected *via* changes in the emission of the pH sensitive dye, resulting in a sensing film that requires the addition of no extra reagents (aside from the analyte) to generate a signal. The hydrophilic enzyme (urease) was examined to allow us to investigate the effects of organosilane precursors and polymer additives on enzyme performance, and to see if optimal compositions could be obtained for this type of enzyme. The reactions catalyzed by urease, and the resultant products, are shown below:

$$H_2NCNH_2 + 3H_2O \xrightarrow{\text{urease}} CO_2 + 2NH_4^+ + 2OH^- \quad (1)$$

The detection of pH shifts resulting from product formation was accomplished using the pH sensitive fluorescent probe seminaphtharhodafluor-1 (SNARF-1), whose structure is shown in Figure 5.1. This probe was used in the free form, or as bound to a high molecular weight dextran backbone to determine if this modification could prevent leaching.[33]

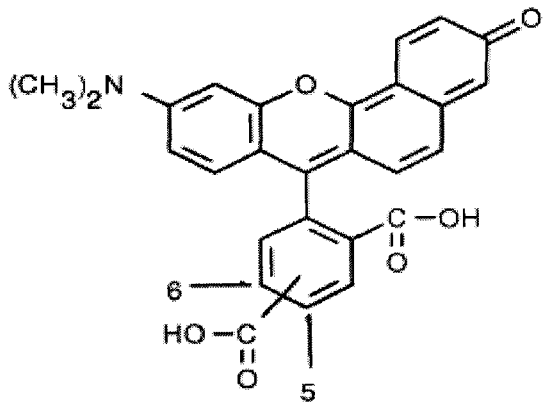

Figure 5.1: Structure of Seminaptharhodafluor-1 (SNARF-1)

SNARF-1 reports pH by monitoring the change in the ratio of intensities at two emission wavelengths as a function of pH as shown in Figure 5.2.[34] Overall, our results show that the film composition has significant effects on both the pH sensitive dye and the entrapped urease. However, careful choice of organosilane precursors, polymer additives, and the pH sensitive dye allows one to optimize the activity of entrapped enzyme the overall sensitivity of the sensing films.

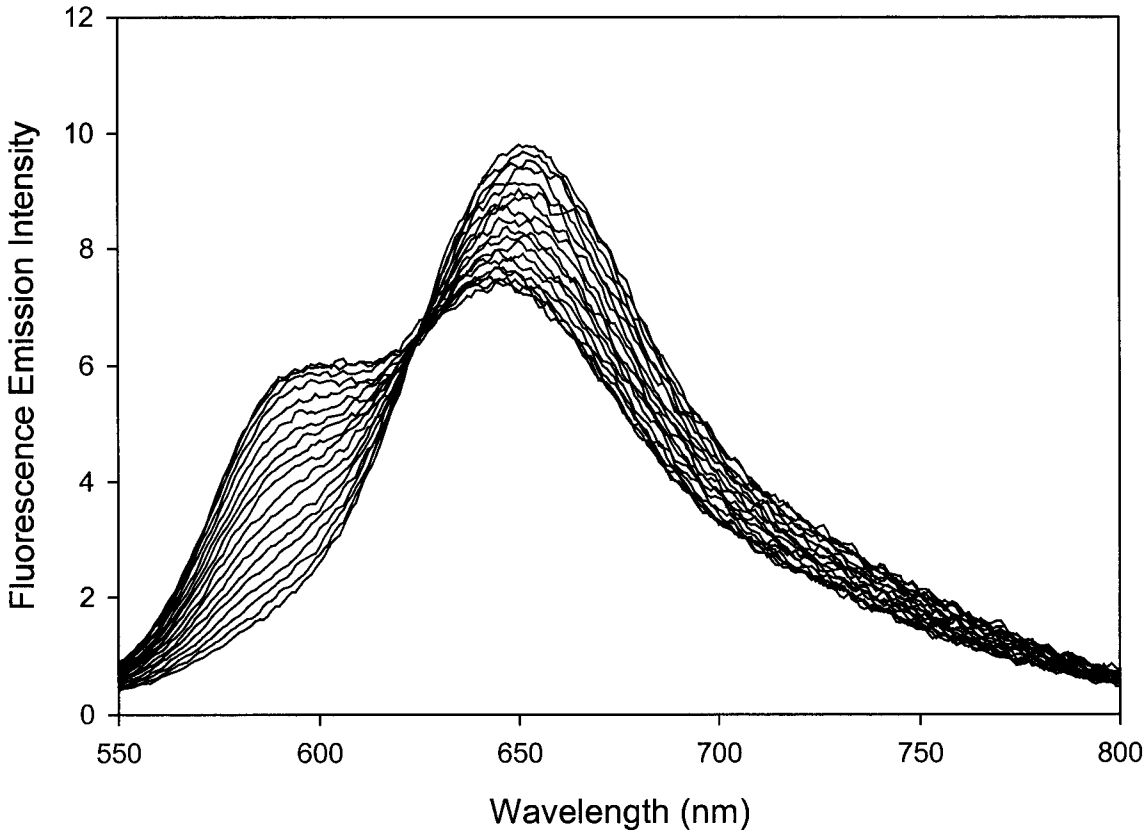

Figure 5.2: The Ratiometric Response of Seminaptharhodafluor-1 (SNARF-1) as a function of the production of ammonium carbonate during urease catalyzed hydrolysis of urea.

5.2. Experimental

5.2.1. Chemicals

Tetraethylorthosilicate (TEOS, 98%), methyltriethoxysilane (MTES, 98%), dimethyldimethoxysilane (DMDMS, 98%), polyvinyl alcohol (PVA, MW 9000-13,000, 87% hydrolyzed) and polyethylene glycol (PEG 400 or 600) were purchased from Aldrich (Oakville, ON) and were used without further purification. Urease (E.C. 3.5.1.5, type IX from Jack Beans, 50,000 units.g^{-1} solid) and urea were from Sigma (Oakville, ON). Seminaphtharhodafluor-1 (SNARF-1), and SNARF-dextran (SD, MW 70,000), were obtained from Molecular Probes (Eugene, Oregon). Glass microscope slides (cut to dimensions of 7 mm x 25 mm) were obtained from Fisher Scientific (Toronto, ON). All water was purified by reverse osmosis and deionized using a 4-stage Milli-Q water purification system. All other chemicals and solvents used were of analytical grade and were used without further purification.

5.2.2 Procedures

5.2.2.1. Preparation of Sol-Gel Derived Films:

Solutions containing 20% (mol:mol) MTES or 10% (mol:mol) DMDMS in TEOS were hydrolyzed using a H_2O:Si molar ratio of 4:1 under acid-catalyzed conditions, as described elsewhere.[32] After sonication, varying volumes of glycerol were added, at 41°C over an hour with continual stirring to prepare solutions with glycerol:TEOS mole

ratios, ranging from 0.08:1 to 4.16:1. A volume of 0.1 mL of the hydrolyzed silane solution was added to an equivalent volume of a buffer solution (10 mM Tris, 100 mM KCl, pH 7.0) that contained 10 – 50 μM of the appropriate fluorophore or fluorophore-dextran conjugate, and *ca.* 2.0 mg/mL of the appropriate enzyme, if present. In some cases, the buffer solution also contained 3% (w/v) of PEG 400, PEG 600 or PVA. The contents were mixed for one minute (using a vortex mixer) and 70 μL of the solution was transferred onto a glass slide that was previously cleaned by soaking in 1.0 M KOH for 24 hours, followed by rinsing with copious amount of distilled, deionized water drying under a stream of N_2. The slide was spun at 2000 rpm for 1 minute to produce a thin film. The films were then aged in air at 4 °C for at least 12 hours before testing. The thickness of the films was determined using an alpha-step 500 surface profilometer. All samples were prepared and tested in triplicate.

5.2.2.2. Fluorescence Spectroscopy:

Silane coated glass slides were mounted in a teflon holder in a 1 cm^2 polymethacrylate cuvette at an angle of 45° with respect to the excitation beam, such that the excitation radiation was reflected away from the emission PMT.[18] The coated slides were present in a Tris buffer solution maintained at a temperature of 20 ± 0.2°C, using an SLM 8100 spectrofluorimeter described elsewhere.[18] Samples containing SNARF were excited at 510 nm with emission collected from 550 nm to 800 nm. All spectra were collected in 1 nm increments at a rate of 3 nm/sec and were corrected for wavelength-dependent anomalies in the emission monochromator throughput and PMT response.

5.2.2.3. Leaching and Photobleaching Studies:

Fluorophore-doped films were incubated in cuvettes containing 2.0 mL of a buffer solution for 12 hours. The emission spectra of these solutions were then collected to examine probe leaching. Photobleaching studies were done using samples that showed no leaching, to eliminate contributions to intensity decreases resulting from loss of the probe. The samples were continuously irradiated at their maximum excitation wavelength and the fluorescence intensity at the emission wavelength maximum was monitored for 15 minutes. The total loss of intensity after 15 minutes of irradiation is reported.

5.2.2.4. pH Response Studies:

The pH response of the free and entrapped fluorophore was tested by placing the sample into solutions containing 0.1 M Tris buffer adjusted to pH values ranging from 4.0 to 10.5. Fluorophore-doped films were equilibrated for 10 minutes before a scan was collected (note: longer equilibration times did not alter the results). For SNARF, the ratio of emission maxima at 588 nm and 620 nm, obtained by integrating a 20 nm window centered on each peak, was plotted against pH. Alternatively, the emission intensity was collected simultaneously at 588 nm and 620 nm (T-format detection for SNARF) as a function of time for response time studies.

5.2.2.5. Reagentless Sensing:

Silane-coated slides containing SNARF-dextran and the appropriate enzyme were suspended from the top of a cuvette containing 1.5 mL of buffer. The sample was excited at 510 nm and emission was detected by obtaining a full emission spectrum, or by simultaneously monitoring the emission intensity at 588 nm and 620 nm using T-format detection. Once a constant signal was obtained, the appropriate substrate solution was added to the cuvette to obtain a final substrate concentration of 50 – 300 mM urea. The emission ratio was measured as a function of time and the slope of the response curve was plotted against substrate concentration to generate a concentration-response curve.

5.3. Results and Discussion

5.3.1. Optimization of Signals from Entrapped Probes

Three key factors determine the utility of entrapped fluorophores for optical pH sensing. These are the signal-to-noise level for detection of the probe in the thin films, the retention of the probe within the films (which relates to the stability of intensity-based signals), and the photostability of the probe, which can alter intensity-based signals. Entrapment of various levels of SNARF-dextran (SD) into thin films revealed that the limits-of-detection for the probe was ~1.0 μM. In order to produce high quality emission spectra, we typically used μM SD in all samples. At these levels, the signal-to-noise ratios were ~ 100:1, respectively (using 4 nm bandpasses on both the excitation and emission monochromators). This concentration level was also selected so that the

emission signal was at least a factor of 50 higher than the background, eliminating the need for subtraction of blanks.

Table 5.1 shows the extent of leaching and photobleaching for free and dextran-linked versions of SNARF. It is clear that the dispersed probe leached extensively from TEOS-derived films, even with polymer doping, with as much as 30% of the entrapped probe leaching from the films after 12 hours. These results suggest that the probe was located in the solvent phase of the film, and thus was free to diffuse throughout the matrix. On the other hand, incorporation of organosilanes markedly reduced the extent of leaching of the probe, consistent with the hydrophobic probes associating with the alkyl chains present at the pore surfaces. This result clearly demonstrates that leaching of probes can be controlled relatively well by incorporation of hydrophobic groups into the polar silica glasses, in agreement with previous studies by Collinson et al.[35] and MacCraith and co-workers.[36]

Films that contained dextran-linked SNARF showed no leaching whatsoever, regardless of the film composition, provided that the films were aged for a minimum of 12 hours before testing to allow the films to fully dry.[37,38,39] These results are in agreement with previous studies by Bright and coworkers,[35] but are contrary to recent results reported by Saavedra et al.[40] The latter results suggested that significant leaching of Fluorescein-dextran (70,000 MW) occurred from bulk glasses derived from TMOS. However, these glasses were aged for only 48 hrs, and thus would be expected to have a relatively open pore structure.[41] In contrast, our films are almost completely dry after 12 hrs of aging,[42] and therefore are likely to have a more highly cross-linked structure

that would result in full retention of the probe. Overall, the attachment of the probe to a high molecular weight backbone of neutral charge proved to be an effective means to eliminate leaching of the probe from thin films, and thus provided a stable intensity-based signal. Furthermore, this method did not require the incorporation of hydrophobic species (although this was still possible), meaning that a wider range of glass compositions could be employed for sensor development. Thus, fluorescently-labelled dextran species were used for all further studies.

The data in Table 5.1 indicates the photostability of the probe was a more serious problem; SNARF-dextran showed substantial photobleaching over a period of 15 minutes. The incorporation of organosilanes or polymers into the films did not alter the extent of photobleaching, within error. This result suggested that the major cause of photodegradation was likely the inability of the probe to diffuse within the matrix, coupled with the fact that the films were not deoxygenated, potentially leading to photo-oxidation.[18] One potential method to overcome this difficulty is to use a pulsed excitation source in conjunction with gated detection. However, such instrumentation was not utilized in the present study since the ability to detect pH changes by monitoring a ratio of intensities for the two emission peaks of SNARF removed any deviations that were related to degradation of the probe.

5.3.2. Analytical Behavior of Entrapped pH-Sensitive Fluorescent Probe

The use of an entrapped optical probe for sensing of pH changes has been examined extensively, and it has been noted that entrapment can in many cases alter the pK_a of the

Table 5.1: Properties of entrapped SNARF probe. All values are given after aging the films for 24 hours in sealed cuvettes, unless otherwise stated.

Sample	% Leaching after 12 hrs[a] (S/SD)	% Photo-bleaching (SD)[b,c]	pK_a (± 0.2) (SD)	Change in Signal (%) (SD)[d]	Analytical Range (ΔpH) (SD)[e]	Response Time (s)[f] (SD)
Solution	-	9	7.2	1.43	3.9	5
TEOS	30/0	6	7.5	0.97	4.1	95
20% MTES	1/0	5	7.5	0.78	3.0	73
10% DMDMS	4/0	3	7.8	0.53	3.4	76
TEOS-PEG 600[c]	12/0	3	7.8	0.87	3.8	84
20% MTES-PEG 600	2/0	7	8.1	0.77	2.8	96
10% DMDMS-PEG 600	4/0	3	7.4	0.39	3.2	30
TEOS-PVA[d]	13/0	5	8.2	0.78	3.6	86
20% MTES-PVA	2/0	5	8.1	0.75	3.0	51
10% DMDMS-PVA	3/0	2	8.0	0.43	3.6	111

a) S = SNARF, SD =SNARF-dextran, typical relative standard deviation (RSD) for leaching data is ± 10%, b) photobleaching was done only for dextran linked probes to avoid contributions from leaching, c) values refer to photobleaching after 15 minutes irradiation time d) the first number gives the changes in emission ratio for SD, e) the limit of detection for the upper and lower pH values was determined using a S/N ratio of 3, and the number reported is the difference in these values, the RSD for SD samples is ± 0.2, RSD, f) typical errors are on the order of ± 10s.

probe,[35,42] the sensitivity of the probe to pH changes[35] and the analytical range for pH sensing.[43] Figure 5.3 shows typical pH response profile for SNARF-dextran in solution and in sol-gel-derived films prepared from pure TEOS (which typically gave good response characteristics) and from DMDMS containing 3% (v/v) PVA (as an example of a sample with relatively poor response characteristics).

As shown in Figure 5.3, SNARF showed a decrease in the intensity of the peak at 588 nm (acidic form) and an increase in the intensity of the peak at 640 nm (basic form) as pH increased, resulting in the ratio (I_{588}/I_{640}) decreasing as pH became more basic. Incorporation of the probe into sol-gel derived thin films caused the apparent pK_a (obtained by determining the inflection point in the pH-based titration curves) to increase by up to 1.0 pH unit as compared to the solution pK_a of 7.8. This result suggests that the probe sensed a more acidic environment within the glass. The shift in the pK_a value to more basic pH values may reflect the association of the positively charged probe with the negatively charged silicate surface, leading to protonation of the probe. It should be noted that the pK_a is still fairly close to the physiologically relevant pH value (pH 7.4), making it useful for enzyme-based studies.

The data in Table 5.1 also reveal that entrapment causes SNARF to have lower sensitivity to pH, as judged by the smaller change in the emission ratio over the pH range from 4.5 to 10.0. For example, the probe is 33% less sensitive when entrapped in a TEOS-derived glass than in solution, while the probe loses over 75% of its sensitivity to pH shifts when entrapped in DMDMS-PVA glasses.

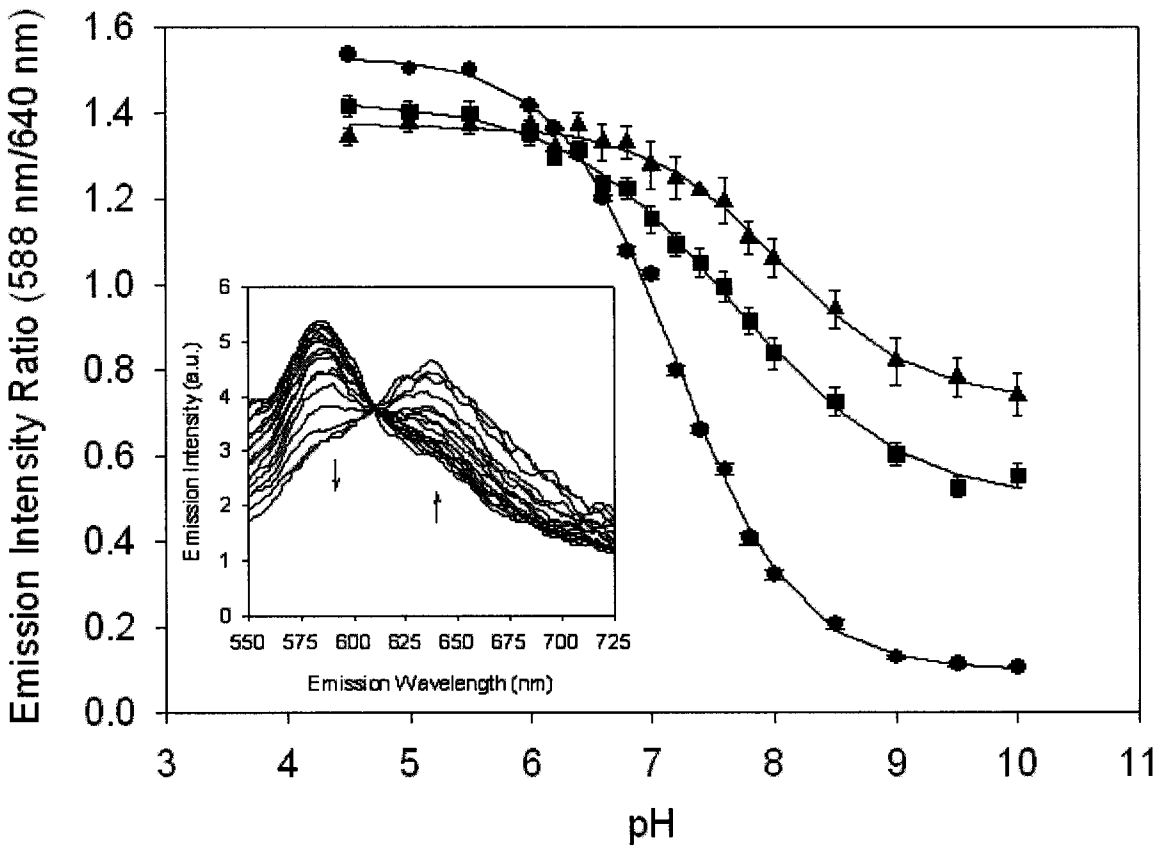

Figure 5.3: Typical pH response profiles for SNARF-dextran in solution (●) and in sol-gel derived films prepared from pure TEOS (■) and from DMDMS containing 3% (v/v) PVA (▲). The error bars for SD in solution are within the symbols. The lines are intended only as a guide for the eye. The inset figures show the spectra obtained from TEOS derived films, the arrows show the direction of the peak intensity changes on shifting the pH to more basic conditions.

In general, the probe within the TEOS-derived samples was the most sensitive to pH changes, followed by probe within MTES and then DMDMS. Addition of polymers tended to produce slight decreases in the sensitivity of the entrapped SNARF to pH, perhaps reflecting polymer-probe interactions that produced photophysical changes in the probe (i.e., alterations in quantum yield of the basic and/or acidic forms). SNARF entrapped within TEOS-derived samples also showed that largest analytical ranges, followed by DMDMS and MTES. Addition of polymer had no statistically significant effect on the analytical ranges for the three types of films. Overall, the data show that the addition of organosilane species alters the pH response behaviour of the probe significantly, while addition of polymers tends to have a smaller overall effect. The results suggest that TEOS-based films are best for pH sensing when using SNARF as the pH-sensitive dopant as shown in Table 5.1.

Perhaps most important for pH sensing was the relative error of the pH measurement. For SNARF, there was typical variation of a few percent in the emission ratio for a given pH value (note the small error bars on the SD titration curves). Hence, the use of changes in peak ratios to monitor shifts in pH appears to produces a more robust signal and thus a more reliable sensing strategy.

Figure 5.4 shows the pH response obtained upon addition of acid or base to SNARF-dextran entrapped in TEOS-derived films containing 3% PVA. These films were chosen as they showed reasonable sensitivity to pH changes, and, as shown below, good responses from entrapped enzymes. In general, the response times were quite rapid for all samples (< 2 min, see Table 5.1), as expected given that the films were on the order of

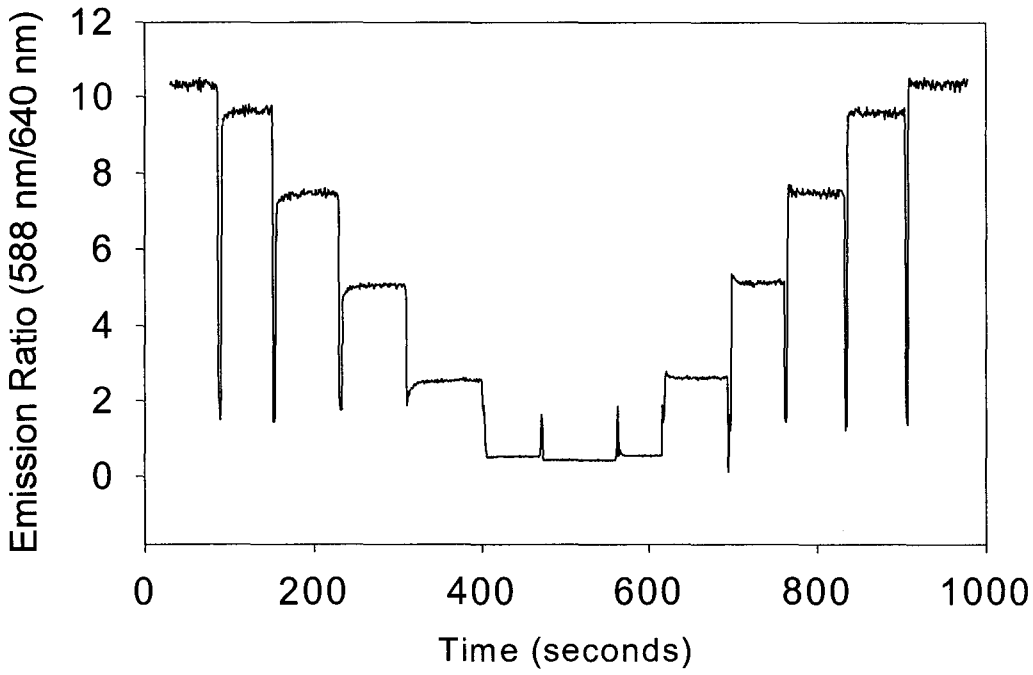

Figure 5.4: pH response as a function of time during addition of acid or base to SNARF-dextran in TEOS derived films. The response refers to the successive addition of six 10 μL aliquots of 0.1 M NaOH (0-500 s), resulting in decreases in the emission ratio, or 0.1 M HCl (500-1000 s), resulting in increases in the emission ratio. Note: the dips in intensity shown are due to closing of the shutters in the instrument during addition of reagents, and are not part of the actual response of the probe.

500 nm thick. However, it was noted that the response was fastest in the more polar films (TEOS < MTES < DMDMS), and that the addition of PEG improved response times while PVA had no effect on response times relative to undoped films.

The ratio of emission intensities for entrapped SNARF-dextran as a function of pH as revealed in Figure 5.4 shows the ratio of emission intensities for entrapped SNARF-dextran decreased with increasing pH. It must be noted that the gain on the detectors for peaks at 588 nm and 640 nm was adjusted to expand the range of peak ratios from 0 – 10. The pH-dependent responses are consistent with those obtained from solution based studies. The pH response was fully reversible, and was sensitive to small changes in pH while being immune to changes in emission intensity resulting from photodegradation of the probe. The signals obtained from SNARF-dextran were completely reversible, and the films could be cycled through numerous pH shifts with no degradation in performance. The reproducibility in the response with pH is excellent, with the relative standard deviation of the response being on the order of 1% or less.

5.3.3. Reagentless sensing using Enzymes Co-entrapped with SNARF-dextran

5.3.3.1. Effect of Film Composition on Enzyme Performance

Urease was co-immobilized with SNARF-dextran and was used to monitor the activity of the entrapped biomolecule. Knowing the SNARF-dextran is a pH sensitive probe it monitored the generation of the products carbamate and ammonia. However, carbamate is unstable and spontaneously decomposes to yield a second molecule of ammonia and carbonic acid.[44] Figure 5.5 shows the relative activity of urease in the presence of

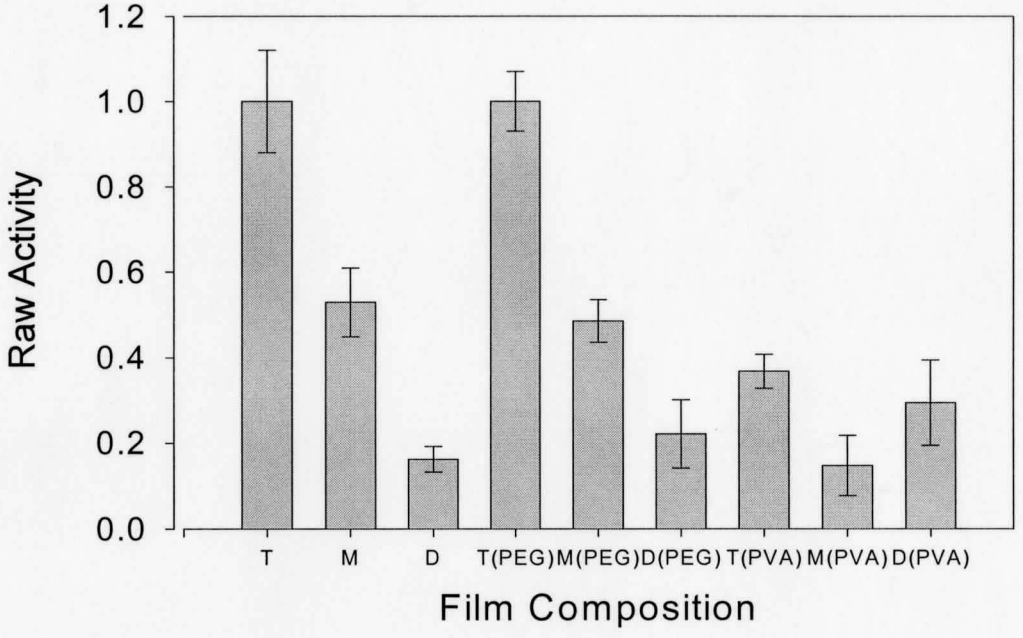

(A) Uncorrected Relative Activity

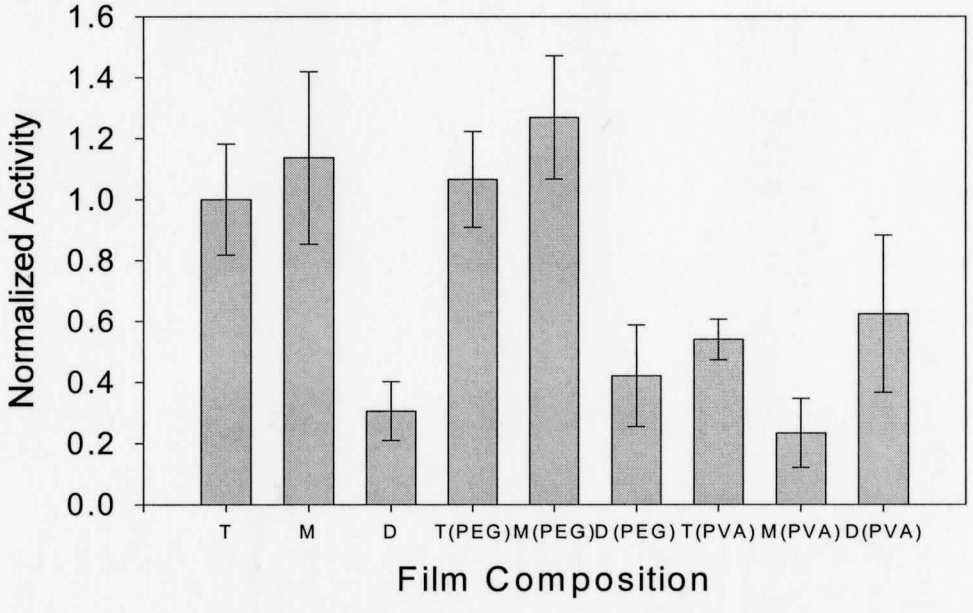

(B) Corrected Activity (Film Thickness (amount of enzyme present) and SNARF-dex response to various film compositions.

Figure 5.5: Relative activity of the urease as a function of film composition.

saturating levels of urea for each of the nine different films compositions, as measured using SNARF-dextran that was entrapped in each of the films. Panel A shows actual measured data, while panel B shows activity data that has been corrected for both film thickness (to account for differences in amount of enzyme present) and for probe sensitivity to shifts in pH to provide insights into how additives alter enzyme performance. In this case, the enzyme showed maximum activity in the more polar TEOS-derived films, as might be expected given that the enzyme is water soluble and the analyte is polar. Addition of organosilane precursors lowered the measured activity markedly, regardless of whether there was any polymer additives incorporated into the film. Panel B shows the direct effect of film composition on enzyme behaviour, after accounting for differences in pH sensitivity and amount of enzyme. These results indicate that the inclusion of MTES does not alter the apparent enzyme activity; rather it is the lower pH sensitivity of SNARF-dextran and the decrease in film thickness that produces the lower overall measured activity in such films. The results also show that PEG has no statistically significant effect on the enzyme behaviour, regardless of which organosilane is used to form the film. On the other hand, both DMDMS and PVA are somewhat deleterious to enzyme function (or they reduce the penetration of urea into the film). Overall, the results clearly show that tuning of the film properties is essential for optimizing the sensitivity of the sensing film to the analyte of interest. In general, more polar films are most suitable for polar analytes and soluble proteins.

5.3.3.2. Reagentless Sensing Using Urease Coated Slides

Figure 5.6 shows the calibration plot for the response of SD entrapped in a urease-doped TEOS-glycerol-doped film as a function of urea concentration. The ratio of basic (640 nm) over acidic (588 nm) peak intensities is reported in this case so that the signal increases with concentration of substrate. In this case, the signal is initially linear (over the range from 0 – ~20 mM urea), and then begins to show a non-linear response beyond ~30 mM urea, likely owing to saturation of the enzyme with the substrate. The changes in emission ratio per unit time were obtained by recording the slope during only the first minute after the addition of substrate, (at which point the slope was stable), providing a relatively rapid response. Based on the calibration plot, a limit-of-detection on the order of 1 mM is obtained for urea, with a dynamic range of ~30 mM. These values are in agreement with those obtained using other electrochemical[45] and optical[46] sensors for urea.

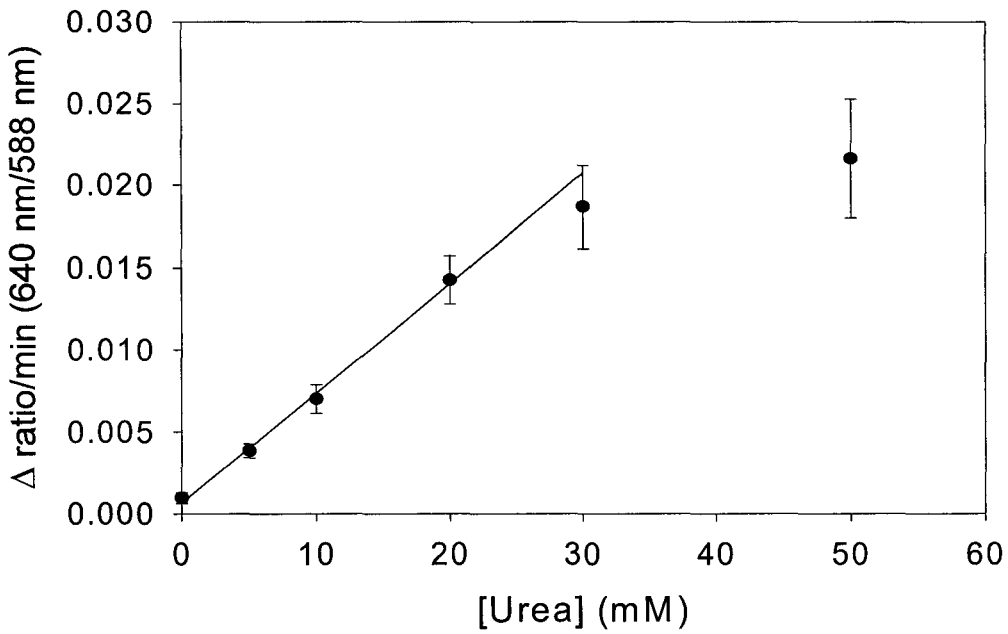

Figure 5.6: Calibration plot for a TEOS-glycerol based film containing urease and SNARF-dextran upon addition of varying concentrations of urea.

5.4. Conclusions

Reagentless fluorescence-based sensing films that are suitable for the determination of pH, urea or concentration have been developed based on co-entrapment of a fluorescently-labelled polymer and a hydrolytic enzyme in a sol-gel-derived glass. It was determined that linkage of the fluorophore to a high molecular weight polymer backbone completely eliminated leaching, while use of a ratiometric signal from a dual-emission probe eliminated signal variations arising from photodegradation of the probe. Together, these improvements led to a highly stable and reproducible fluorescence signal that, in optimal cases, was capable of measuring a pH change of as little as 0.10 units over the range from 6.5 to 9.5 in under one minute. The sensitivity to pH could be adjusted by varying either silane precursors or polymer additives, although optimal pH sensitivity was obtained from TEOS derived films without polymer present.

The addition of a hydrolytic enzyme (urease) to the matrix resulted in the production of biologically selective films, which were used for biosensing of urea based on the detection of basic products related to the enzyme-substrate reactions. The ability to co-immobilize the pH indicator along with the protein led to rapid response times while avoiding the possibility of altering the protein behaviour as a result of covalent attachment of the probe. An important finding from this work was that the overall performance of the entrapped enzyme could be optimized to a significant degree by addition of both organosilane precursors and polymer dopants. Results clearly show that substantial tuning of the response can be achieved by carefully adjusting the sol-gel immobilization protocols to suit the particular biomolecule and analyte of interest.

While the new biofilms show promise for reagentless sensing applications, more work is needed to both understand and optimize the signal. Firstly, the enzyme behaviour in the films must be more carefully examined, and factors such as the Michealis constant and turnover number must be measured to better understand how the various additives altered enzyme performance. Furthermore, the accessibility of the enzyme must be determined (via quenching studies) to verify if the higher sensitivity is due to improved enzyme activity or enhanced accessibility. Finally, methods must be developed to account for drifts in pH that are not related to enzyme-substrate reactions, including the use of multi-analyte sensing configurations with one sensor for pH, and the other for analyte.

5.5. References

1. Narang, U.; Jordan, J. D. ; Bright, F. V.; and P.N. Prasad. *Journal of Physical Chemistry*. **1994**, *98*, 8101.

2. Lundgren, J. S.; and F. V. Bright. *Analytical Chemistry*. **1996**, *68*, 3377.

3. Jordan, J. D.; Dunbar, R. A.; and F. V. Bright. *Analytical Chemistry*. **1995**, *67*, 2436.

4. Wang, R.; Narang, U.; Prasad, P. N.; and F. V. Bright. *Analytical Chemistry*. **1993**, *65*, 2671.

5. Narang, U.; Prasad, P. N; Bright, F. V; Ramanathan, K; Kumar, N. D; Malhotra, B.D.; Kamalasanan, M. N.; and S. Chandra. *Analytical Chemistry*. **1994**, *66*, 3139.

6. Ellerby, L. M.; Nishida, C. R.; Nishida, F.; Yamanaka, S. A.; Dunn, B.; Valentine, J. S.; and J. I. Zink. *Science*, **1992**, *225*, 1113.

7. Wu, S.; Ellerby, L. M.; Cohan, J. S.; Dunn, B.; El-Sayed, M. A; Valentine, J. S; and J. I. Zink. *Chemistry of Materials*. **1993**, *5*, 115.

8. Miller, J. M.; Dunn, B.; Valentine, J. S.; and J. I. Zink. *Journal of Non-Crystalline Solids*. **1996**, *220*, 279.

9. Yamanaka, S. A.; Dunn, B.; Valentine, J. S.; and J. I. Zink. *Journal of the American Chemical Society*. **1995**, *117*, 9095.

10. Dave, B. C.; Soyez, H.; Miller, J. M.; Dunn, B.; Valentine, J. S.; and J. I. Zink. *Chemistry of Materials*. **1995**, *7*, 1431.

11. Yamanaka, S. A.; Nishida, F; Ellerby, L. M.; Nishida, C. R.; Dunn, B.; Valentine, J. S; and J. I. Zink. *Chemistry of Materials*. **1992**, *4*, 495.

12. Dave, B.; Dunn, B. C.; Valentine, J. S.; and J. I. Zink. *Analytical Chemistry*. **1994**, *66*, 1120A.

13. Braun, S.; Rappoport, S.; Zusman, R.; Avnir, D.; and M. Ottolenghi. *Material Letters*. **1990**, *10*, 1.

14. Braun, S.; Shtelzer, S.; Rappoport, S.; Avnir, D.; and M. Ottolenghi. *Journal of Non-Crystalline Solids*. **1992**, *147*, 739.

15. Avnir, D.; *Accounts of Chemical Research*. **1995**, *28*, 329.

16. Edmiston, P. L; Wambolt, C. L.; Smith, M. K.; and S. S. Saavedra. *Journal of Colloids International Science.* **1994**, *163*, 395.

17. Wambolt, C. L.; and S. S. Saavedra. *Journal of Sol-Gel Science and Technology.* **1996**, *7*, 53.

18. Zheng, L.; Reid, W. R.; and J. D. Brennan. *Analytical Chemistry.* **1997**, *69*, 3940.

19. Avnir, D.; Braun, S.; Lev, O.; and M. Ottolenghi. *Chemistry of Materials.* **1994**, *6*, 1605.

20. Coche-Guérente, L.; Cosnier, S.; and P. Labbé. *Chemistry of Materials.* **1997**, *9*, 1348.

21. Obert, R.; and Dave, B. C. *Journal of the American Chemical Society.* **1999**, *121*, 12192.

22. Gill, I.; and A. Ballesteros. *Journal of the American Chemical Society.* **1998**, *120*, 8587.

23. Chen, Q.; Kenausis, G. L; and A. Heller. *Journal of American Chemical Society.* **998**, *120*, 4582.

24. Heller, J. and A. Heller. *Journal of the American Chemical Society.* **1998**, *120*, 586.

25. Baker, G. A.; Jordan, J. A.; and F. V. Bright. *Journal of Sol-Gel Science and Technology.* **1998**, *11*, 43.

26. Baker, G. A.; Pandey, S.; Maziarz III, E. P.; and F. V. Bright. *Journal of Sol-Gel Science and Technology.* **1999**, *15*, 37.

27. Lesot, P.; Chapuis, S.; Bayle, J. P.; Tault, J.; Lafontaine, E.; Campero, A.; and P. Judeinstein. *Journal of Materials Chemistry.* **1998**, *8*, 147.

28. Kauffmann, C.; and Mandelbaum, R. T.; *Journal of Biotechnology.* **1998**, *62*, 169.

29. Brennan, J. D.; Hartman, J. S.; Ilnicki, E. I.; and M. Rakic. *Chemistry of Materials.* **1999**, *11*, 1853.

30. Wang, B.; Li, B.; Deng, Q.; and S. Dong. *Analytical Chemistry.* **1998**, *70*, 3170.

31. Wang, B.; Li, B.; Wang, Z.; Xu, G.; Wang, Q.; and S. Dong. *Analytical Chemistry.* **1999**, *71*, 1935.

32. Altstein, M.; Segev, G.; Aharonson, N.; Ben-Aziz, O.; Turniansky, A.; and D. Avnir. *Journal of Agricultural Food Chemistry.* **1998**, *46*, 3318.

33. Baker, G. A.; Watkins, A. N.; Pandey, S.; and F. V. Bright. *Analyst.* **1999**, *124*, 373.

34. Whitaker, J. E; Haugland, R. P; and F. G. Prendergast. *Analytical Biochemistry.* **1991**, *194*, 330.

35. Makote, R; and M. M. Collinson. *Analytica Chimica Acta.* **1999**, *394*, 195.

36. Butler, T. M.; MacCraith, B. D.; and C. McDonagh. *Journal of Non-Crystalline Solids.* **1998**, *224*, 249.

37. Huang, M. H; Dunn, B. S.; Soyez, H.; and J. I. Zink. *Langmuir.* **1998**, *14*, 7331.

38. Huang, M. H.; Dunn, B. S.; and J. I. Zink. *Journal of the American Chemical Society.* **2000**, *122*, 3739.

39. Chia, S.; Urano, J.; Fuyuhiko, T.; Dunn, B.; and J. I. Zink. *Journal of the American Chemical Society.* **2000**, *122*, 6488.

40. Skrkla, P. J.; Saavedra, S. S.; and N. R. Armstrong. *Applied Spectroscopy.* **1999**, *53*, 785.

41. Brinker, C. J.; and G. W. Scherer. *Sol-Gel Science: The Physics and Chemistry of Sol-Gel Processing.* Academic Press, San Diego, **1990**.

42. Dunn, B. and J. I. Zink. *Chemistry of Materials.* **1997**, *9*, 2280.

43. Lam, M. H. W.; Lee, D. Y. K.; Man, K. W.; and C. S. W. Lau. *Journal of Materials Chemistry.* **2000** *10*, 1825.

44. Hausinger, R. P. et al. *Protein Science.* **1995**, *4*, 2234.

45. Ogura, K.; Nakaoka, K.; Kakayama, M.; Kobayashi, M.; and A. Fujii. *Analytica Chimica Acta.* **1999**, *384*, 219.

46. Xie, X.; Suleiman, A. A; and G. G. Guilbault. *Talanta.* **1991**, *38*, 1197.

Chapter 6

Conclusion and Future Outlook

The addition of glycerol to hydrolyzed TEOS-based sols results in a polyglycerylsilane precursor solution in which the level of ethanol is reduced relative to undoped sols. Materials prepared from polyglycerylsilane sols were shown to have larger pores (meso and/or macropores), less shrinkage and reduced cracking relative to TEOS-based materials. Such materials remained optically clear and could be formed as bulk glasses or thin films, which should be suitable for optical sensor development.

The polyglycerylsilane sols were mixed with buffered solutions containing enzymes to produce silica materials containing the entrapped biomolecules urease or glucose oxidase / horseradish peroxidase. The entrapped enzymes displayed improved initial activity and better long-term stability in glycerol-doped silica relative to traditional TEOS-based materials. However, both K_M and k_{cat} values for the entrapped enzymes were significantly altered relative to solution values owing to limitations in mass transport of analytes through the mesoporous matrix. The results indicate that, at least with some enzymes, this technique may provide extended shelf-life for entrapped biomolecules.

To gain further insight into the effects of glycerol doping on the properties of entrapped proteins, both steady-state and time-resolved fluorescence of Trp 214 was used to examine the conformation, dynamics, accessibility, thermal/chemical stability and the degree of ligand binding of human serum albumin (HSA) in solution and after

entrapment of the protein in glycerol-doped TEOS-based materials. HSA entrapped in glycerol-doped materials showed improved thermal and chemical stability and the presence of glycerol (in solution) did not appear to alter the ability of HSA to bind to the ligand salicylate. These results are consistent with the well-known 'osmophobic effect' in which the protein becomes preferentially hydrated and thus retains a more native-like conformation. Entrapment of HSA, however, even in the presence of glycerol, appeared to result in conformational changes in the protein that were consistent with HSA adopting a more compacted state (due to osmophobic effect) or an expanded form. Quenching data showed that HSA within TEOS-derived and glycerol-doped silica was fully accessible to neutral analytes. However, entrapment also resulted in a significant decrease in the rate of diffusion of analytes through the matrix, as demonstrated by the lowering of the k_q value. The lower k_q values correlate well to the decreases in k_{cat} values for entrapped enzymes, and show that mass transport through the matrix must be further optimized to obtain improved enzyme performance.

The glycerol-doped materials were shown to be amenable to the formation of thin, protein-doped films that were suitable for the development of reagentless fluorescence-based sensing films. These films utilized the hydrolytic enzyme urease co-entrapped with a polymer that was labelled with the pH sensitive fluorophore SNARF. Reagentless sensing films of urea were developed based on the detection of enzyme-mediated pH changes from films coated onto planar substrates.

Overall, the inclusion of glycerol into TEOS-based materials resulted in improved performance for entrapped biomolecules when compared to the traditional TEOS-based

materials. Some drawbacks of these materials, however, remain to be overcome. For example, the material properties still need to be improved to further reduce cracking and shrinking of the silica matrix. The changes in the silica material and the behaviour of entrapped proteins as a function of aging must also be better controlled, as the aging of the material reduces the reproducibility of analytical responses from the entrapped enzymes. Furthermore, the glycerol can be washed out of the matrix, thus removing the beneficial effects of this additive. To overcome these problems, a number of improvements in sol-gel biocomposites are possible. Further developments of materials through the creation of permanently linked glycerol, sugars or polyelectrolytes (currently under investigation in our group) will result in a permanent modification of the silica matrix, and may allow for control of matrix electrostatics, reduction or elimination of analyte-matrix interactions, and an overall improvement in the activity and stability of entrapped biomolecules.